

April 22, 2013

Statistical mechanics of temporal and interacting networks

Kun Zhao
Northeastern University

Recommended Citation

Zhao, Kun, "Statistical mechanics of temporal and interacting networks" (2013). *Physics Dissertations*. Paper 34. <http://hdl.handle.net/2047/d20003046>

This work is available open access, hosted by Northeastern University.

Statistical Mechanics of Temporal and Interacting Networks

A dissertation presented

by

Kun Zhao

to

The Department of Physics

In partial fulfillment of the requirements for the degree of

Doctor of Philosophy

in the field of

Physics

Northeastern University

Boston, Massachusetts

April 22, 2013

Statistical Mechanics of Temporal and Interacting Networks

by

Kun Zhao

ABSTRACT OF DISSERTATION

Submitted in partial fulfillment of the requirements
for the degree of Doctor of Philosophy in Physics
in the College of Science of
Northeastern University
April 22, 2013

Abstract

In the last ten years important breakthroughs in the understanding of the topology of complexity have been made in the framework of network science. Indeed it has been found that many networks belong to the universality classes called small-world networks or scale-free networks. Moreover it was found that the complex architecture of real world networks strongly affects the critical phenomena defined on these structures. Nevertheless the main focus of the research has been the characterization of single and static networks.

Recently, temporal networks and interacting networks have attracted large interest. Indeed many networks are interacting or formed by a multilayer structure. Example of these networks are found in social networks where an individual might be at the same time part of different social networks, in economic and financial networks, in physiology or in infrastructure systems. Moreover, many networks are temporal, i.e. the links appear and disappear on the fast time scale. Examples of these networks are social networks of contacts such as face-to-face interactions or mobile-phone communication, the time-dependent correlations in the brain activity and etc. Understanding the evolution of temporal and multilayer networks and characterizing critical phenomena in these systems is crucial if we want to describe, predict and control the dynamics of complex system.

In this thesis, we investigate several statistical mechanics models of temporal and interacting networks, to shed light on the dynamics of this new generation of complex networks. First, we investigate a model of temporal social networks aimed at characterizing human social interactions such as face-to-face interactions and phone-call communication. Indeed thanks to the availability of data on these interactions, we are now in the position to compare the proposed model to the real data finding good agreement.

Second, we investigate the entropy of temporal networks and growing networks , to provide a new framework to quantify the information encoded in these networks and to answer a fundamental problem in network science: how complex are temporal and growing networks.

Finally, we consider two examples of critical phenomena in interacting networks. In particular , on one side we investigate the percolation of interacting networks by introducing antagonistic interactions. On the other side, we investigate a model of political election based on the percolation of antagonistic networks . The aim of this research is to show how antagonistic interactions change the physics of critical phenomena on interacting networks.

We believe that the work presented in these thesis offers the possibility to appreciate the large variability of problems that can be addressed in the new framework of temporal and interacting networks.

Dedicated to my parents, and my wife

Acknowledgements

First of all, I would like to express my deep gratitude to my advisor Prof. Ginestra Bianconi, for her enduring guidance and tremendous help in my research and the writing of this thesis.

I am indebted to my parents for raising me and supporting me in all my life. I am also indebted to my wife Ching Ting Ren for loving me, encouraging me and giving me the momentum towards my PhD in the last four years.

I would like to thank all of my collaborators: Dr. Alain Barrat, Juliette Stehlé, Dr. Márton Karsai, Dr. Simone Severini and Dr. Andrea Baronchelli.

I would like to thank my committee members Prof. Albert-László Barabási, Prof. Alessandro Vespignani and Prof. Armen Stepanyants, for their useful suggestion for my dissertation.

I am also grateful to all my friends and colleagues with whom I have a enjoyable time during my PhD study: Arda Halu, Zheng Ma, Qing Jin, Kien Nguyen, Younggil Song, Ziyao Zhou, Yung-Jui Wang, Xiang Cui, Ming Yan, Heng Ji and Kenan Song.

Contents

Abstract	ii
Dedication	v
Acknowledgements	vi
Table of Contents	vii
List of Figures	x
List of Tables	xvi
1 Introduction	1
1.1 Brief overview of complex networks	2
1.1.1 Structural Characteristics of networks	3
1.1.1.1 Degree distribution	3
1.1.1.2 Clustering Coefficient	4
1.1.1.3 Giant component	4
1.1.2 Basic generating network models	4
1.1.2.1 Classical random network model	4
1.1.2.2 Small-world network model	4
1.1.2.3 BA model	5
1.1.2.4 Configuration model	5
1.2 Temporal networks and social networks	6
1.3 Entropy of complex networks	7
1.4 Percolation of complex networks	8
1.5 Outline	10
2 Model of Temporal Social Networks	11
2.1 Background	11
2.2 Temporal social networks and the distribution of duration of contacts . .	13
2.2.1 Evidence of distribution of human face-to-face interactions	14
2.2.2 Evidence of distribution of mobile phone communication	15
2.3 Model of social interaction	17
2.4 Model of face-to-face interactions	19
2.4.1 Pairwise interactions	20
2.4.2 Formation of groups of any size	25
2.4.3 Heterogeneous model	32

2.5	Model of phone-call communication	35
2.6	Conclusion	41
3	Entropy of Temporal Networks and Growing Networks	42
3.1	Background	42
3.1.1	Entropy measures of social networks and human social behaviors	43
3.1.2	Entropy measures of complex networks	43
3.1.3	Motivation	44
3.2	Entropy of temporal social networks	44
3.2.1	Definition	45
3.2.2	Entropy of phone-call communication	46
3.2.3	Analysis of the entropy of a large dataset of mobile phone communication	46
3.2.4	Entropy modulated by the adaptability of human behavior	48
3.2.5	Remarks	48
3.3	Entropy of growing networks	50
3.3.1	Gibbs entropy of networks with a given degree distribution	51
3.3.2	Entropy rate of growing trees	53
3.3.2.1	Growing network models	54
3.3.2.2	Entropy rate	55
3.3.2.3	Maximal and minimal bound to the entropy rate of growing network trees	55
3.3.3	Growing trees with stationary degree distribution	56
3.3.3.1	The entropy rate of the BA model	57
3.3.3.2	The entropy rate of the growing network model with initial attractiveness	58
3.3.3.3	The entropy rate of the Bianconi-Barabási fitness model	60
3.3.3.4	Entropy rate for growing network models with structural phase transitions	61
3.3.4	Remarks	63
4	Percolation on Interacting Networks	64
4.1	Background	64
4.2	Review of percolation on single networks and interdependent networks	65
4.2.1	Percolation on single network	65
4.2.2	Percolation on two interdependent networks	67
4.2.2.1	Two Poisson networks with equal average degree	67
4.2.2.2	Two Poisson networks with different average degree	69
4.2.3	Antagonistic interactions and antagonistic networks	70
4.3	Percolation on two antagonistic networks	70
4.3.1	The stability of solution	71
4.3.2	Two Poisson networks	72
4.3.3	Two scale-free networks	74
4.3.4	A Poisson network and a scale-free network	75
4.4	Percolation on interdependent networks with a fraction q of antagonistic nodes	78
4.4.1	Two Poisson networks	80
4.4.2	The phase diagram as a function of q	84

4.5	A model of political election	86
4.5.1	Parties as antagonistic social networks	88
4.5.2	Dynamics of the model	88
4.5.3	Phase diagram	90
4.5.4	Committed agents	92
4.6	Conclusion	93
5	Summary	95
A	Solution to the model of face-to-face interactions	98
A.1	Self-consistent solution of the pairwise model	98
A.2	Self-consistent solution of the general model	100
A.3	Self-consistent solution of the heterogeneous model for $\lambda = 1$	104
B	Solution to the model of cellphone communication	107
B.1	Dynamical social network for pairwise communication	107
B.2	General solution to the model	108
B.3	Stationary solution with specific $f_1(t_0, t)$ and $f_2(t_0, t)$	109
B.3.1	Case $0 < \beta < 1$	110
B.4	Comparisons with quenched simulations	112
B.4.1	Case $\beta = 0$	112
B.4.2	Case $\beta = 1$	113
B.5	Solution of the mean-field model on a fully connected network	114
C	Calculations of the entropy of temporal social networks	115
C.1	Entropy of the temporal social networks of pairwise communication	115
C.2	Entropy of the null model	117
C.3	Measurement of the entropy of a typical week-day of cell-phone communication from the data	118
	Bibliography	121

List of Figures

2.1	Probability distribution of the duration of human face-to-face interaction. A) Probability distribution of duration of contacts between any two given persons. Strikingly, the distributions show a similar long-tail behavior independently of the setting or context where the experiment took place or the detection range considered. The data correspond to respectively 8700, 17000 and 600000 contact events registered at the ISI, SFHH and 25C3 deployments. B) Probability distribution of the duration of a triangle. The number of triangles registered are 89, 1700 and 600000 for the ISI, SFHH and 25C3 deployments. C) Probability distribution of the time intervals between the beginning of consecutive contacts AB and AC. This figure is from [1].	14
2.2	(A) Distribution of duration of phone-calls between two users with weight w . The data depend on the typical scale $\tau^*(w)$ of duration of the phone-call. (B) Distribution of duration of phone-calls for people of different age. (C) Distribution of duration of phone-calls for users of different gender. The distributions shown in the panel (B) and (C) do not significantly depend on the attributes of the nodes.	16
2.3	Distribution of duration of phone-calls for people with different types of contract. No significant change is observed that modifies the functional form of the distribution.	17
2.4	Distribution of non-interaction times in the phone-call data. The distribution strongly depends on circadian rhythms. The distribution of rescaled time depends strongly on the connectivity of each node. Nodes with higher connectivity k are typically non-interacting for a shorter typical time scale $\tau^*(k)$	19
2.5	Phase diagram of the pairwise model of face-to-face interactions. The white area indicates the stationary regime in which the transition rate is constant. The colored (gray) area indicates the non-stationary phase.	22
2.6	Evolution of the transition rate $\pi_{21}(t)$ in the different phase regions of the pairwise model of face-to-face interactions. The simulation is performed with $N = 1000$ agents for a number of time steps $T_{max} = N \times 10^5$, and averaged over 10 realizations. The simulations are performed in the stationary region with parameter values $b_1 = b_2 = 0.7$ (circles) and in the non-stationary region with parameter values $b_1 = 0.3, b_2 = 0.7$ (squares) and $b_1 = b_2 = 0.1$ (triangles). The lines indicate the analytical predictions Eqs. (2.7)-(2.8).	22

- 2.7 Probability distribution of the durations of contacts $P_2(\tau)$ and of the inter-contact durations $P_1(\tau)$ in the stationary region, for the pairwise model. The data is reported for a simulation with $N = 1000$ agents, run for $T_{max} = N \times 10^5$ elementary time steps, with parameter values $b_1 = 0.6$, $b_2 = 0.8$. The data is averaged over 10 realizations. 23
- 2.8 Probability distribution of the durations of contacts $P_2(\tau)$ and of the inter-contact durations $P_1(\tau)$ in the non-stationary region of the pairwise model, with $b_1 < 0.5$ and $b_2 < 0.5$. In this region we observe some deviations of the probabilities $P_2(\tau)$ and $P_1(\tau)$ from the power-law behavior for large durations. The data are reported for a simulation with $N = 1000$ agents run for $T_{max} = N \times 10^5$ elementary time steps, with parameter values $b_1 = b_2 = 0.1$. The data are averaged over 10 realizations. 24
- 2.9 Phase diagram of the general model of face-to-face interactions with formation of groups of arbitrary size. The region behind the green surface corresponds to the stationary phase [i.e., Region (I), with $\lambda > 0.5$, $b_2 > 0.5$ and $b_1 > \frac{2\lambda-1}{3\lambda-1}$]. The region in front of the green surface and above the blue one [Region (II)] corresponds to a non-stationary system with decaying transition rates. Strong finite size effects with a temporary formation of a large cluster are observed in the region below the blue surface [i.e., Region (III) with $\lambda < 0.5$]. 27
- 2.10 Transition rate $\pi_{21}(t)$ for the model of face-to-face interactions in the presence of groups of any size, for different parameters λ , b_1 , b_2 corresponding to the different regions of the phase diagram. The straight lines correspond to the analytical predictions. The simulation is performed with $N = 1000$ agents for a number of time steps $T_{max} = N \times 10^4$. The data are averaged over 10 realizations. 28
- 2.11 Distribution $P_n(\tau)$ of durations of groups of size n in the stationary region for the model of face-to-face interactions. The simulation is performed with $N = 1000$ agents for a number of time steps $T_{max} = N \times 10^5$. The parameter used are $b_1 = b_2 = 0.7$, $\lambda = 0.8$. The data are averaged over 10 realizations. The dashed lines correspond to the analytical predictions Eqs. (2.18). 28
- 2.12 Distribution of time intervals between successive contacts of an individual for the model of face-to-face interactions with $\lambda = 0.8$, $b_1 = 0.7$ and $b_2 = 0.3$ and 0.9 . The simulation is performed with $N = 10^4$ for a number of time steps $T_{max} = N \times 10^5$. The data are averaged over 10 realizations. 29
- 2.13 Average coordination number $\langle n \rangle$ vs λ for the model of face-to-face interactions with $b_1 = b_2 = 0.7$. The simulation is performed with $N = 2000$ agents for a number of time steps $T_{max} = N \times 10^3$. $\langle n \rangle$ is computed in the final state over 30 realizations. The solid line indicates the theoretical prediction given by Eq. (2.19). 29
- 2.14 Distribution $P_n(\tau)$ of durations of groups of size 1 for the model of face-to-face interactions in the non-stationary region, i.e. Region (II). The simulation is performed with $N = 1000$ agents for a number of time steps $T_{max} = N \times 10^5$. The parameter used are $b_1 = 0.3$ and $b_2 = 0.7$, $\lambda = 0.8$. The data are averaged over 10 realizations. The dashed lines correspond to the analytical predictions Eqs. (2.18). 30

- 2.15 Average coordination number $\langle n \rangle$ for the model of face-to-face interactions as a function of time in Region (II) of the phase diagram for different values of the parameters λ , b_1 and b_2 . The data is in very good agreement with the theoretical expectations given by Eqs. (2.20) – (2.21). The simulations are performed with $N = 1000$ agents for a number of time steps $T_{max} = N \times 10^4$. The data are averaged over 10 realizations. 30
- 2.16 Average coordination number $\langle n \rangle$ for the model of face-to-face interactions with $\lambda = 0.2$, $b_1 = b_2 = 0.7$. The simulations of a single realization are performed with $N = 250$ and $N = 500$ agents, respectively, for a number of time steps $T_{max} = N \times 10^5$ 32
- 2.17 Distributions of times spent in state 0 and 1 for the heterogeneous model. The simulation is performed with $N = 10^4$ for a number of time steps $T_{max} = N \times 10^5$. The data are averaged over 10 realizations. The symbols represent the simulation results (circles for $n = 1$ and squares for $n = 2$). The dashed lines represent our analytical prediction. In order to improve the readability of the figure we have multiplied $P_2(\tau)$ by a factor of 10^{-1} . 35
- 2.18 Distribution $P_2^\eta(\tau)$ of contact durations of individuals with sociability η in the pairwise heterogeneous model. The simulations are performed with $N = 1000$ agents and $T_{max} = N \times 10^5$ time steps. The data are averaged over 10 realizations. The data decays as a power-law $P_2^\eta(\tau) \propto \tau^{-\xi(\eta)}$, and we report the exponents $\xi(\eta)$ as a function of η in the inset. 36
- 2.19 Distribution $P_n(\tau)$ of the durations of groups of size n in the heterogeneous model with formation of groups of any size. The data are shown for simulations of $N = 1000$ agents performed over $T_{max} = N \times 10^5$ time steps and $\lambda = 0.8$, averaged over 10 realizations. 36
- 2.20 $\langle n \rangle - 1$ as a function of λ for the heterogeneous case where where $\langle n \rangle$ is the average coordination number. The solid line indicates the best fit with $\langle n \rangle \propto (\lambda - 0.5)^{-\delta}$ with $\delta = 0.996$ in agreement with the exponent -1 within the statistical uncertainty. The data correspond to simulations of $N = 500$ agents performed over $T_{max} = N \times 10^3$ time steps. The data are averaged over 10 realizations. 37
- 3.1 The dynamical social networks are composed by different dynamically changing groups of interacting agents. In panel (A) we allow only for groups of size one or two as it typically happens in mobile phone communication. In panel (B) we allow for groups of any size as in face-to-face interactions. 46
- 3.2 Mean-field evaluation of the entropy of the dynamical social networks of phone calls communication in a typical week-day. In the nights the social dynamical network is more predictable. 47
- 3.3 Entropy S of the phone-call communication model defined in Chapter 2 normalized with the entropy S_R of a null model in which the expected average duration of phone-calls is the same but the distribution of duration of phone-calls and non-interaction time are Poisson distributed. The network size is $N = 2000$ the degree distribution of the network is exponential with average $\langle k \rangle = 6$, the weight distribution is $p(w) = Cw^{-2}$ and $g(w)$ is taken to be $g(w) = b_2/w$ with $b_2 = 0.05$. The value of S/S_R is depending on the two parameters β, b_1 . For every value of b_1 the normalized entropy is smaller for $\beta \rightarrow 1$ 49

3.4	The entropy rate H calculated for the growing network model with initial attractiveness [2] as a function of a and evaluated by Eq. (3.36) using a maximal degree equal to $K = 10^7$	59
3.5	The value of Δ calculated for the growing network model with initial attractiveness [2] as a function of a evaluated for networks of $N = 50000$ nodes and over 20 realizations of the process.	60
3.6	The entropy rate H is evaluated for the Kapiivsky-Redner model [3, 4] (panel A), for the "Bose-Einstein condensation in complex networks" of Bianconi-Barabási with $g(\epsilon) = 2\epsilon$, and $\epsilon \in (0, 1)$, ($\kappa = 1$) [5] (panel B) and for the aging model [6] of Dorogovtsev-Mendes (panel C). The data are averaged over N_{run} different realizations of the network. We took $N_{run} = 100$ for simulations with $N = 10^4$ and $N_{run} = 30$ otherwise. Above the structural phase transition indicated with the solid line, the entropy rate H strongly depends on N	62
4.1	Plot of the function $g(S)$ for different values of average connectivity z . At $z = z_c = 2.455 \dots$ a new non-trivial solution of the function $g(S) = 0$ indicates the onset of a first-order phase transition.	68
4.2	Phase diagram of two interdependent Poisson networks with average degree z_A and z_B respectively. In region I we have $S = 0$, in region II we have $S > 0$ and the critical line indicates the points where the first-order transition occurs.	69
4.3	Solution scenarios by plotting $S_B(S_A)$ (blue line) and $S_A(S_B)$ (red line) in Eqs. (4.20) with different Z_A and Z_B . (a) $Z_A \leq 1$, $Z_B \leq 1$. (b) $Z_A = 2$, $Z_B = 0.8$. (c) $Z_A = 2$, $Z_B = 1.2$. (d) $Z_A = 2$, $Z_B = 1.3863$. (e) $Z_A = Z_B = 2$. (f) $Z_A = 2$, $Z_B = 6$. The color dots in the figure represent the valid solutions for Eqs. (4.20).	74
4.4	Phase diagram of two antagonistic Poisson networks with average degree z_A and z_B respectively. In region I the only stable solution is the trivial solution $S_A = S_B = 0$. In region II-A we have only one stable solution $S_A > 0, S_B = 0$, Symmetrically in region II-B we have only one stable solution $S_A = 0, S_B > 0$. On the contrary in region III we have two stable solutions $S_A > 0, S_B = 0$ and $S_A = 0, S_B > 0$ and we observe a bistability of the percolation steady state solution.	75
4.5	Panels (a) and (b) show the hysteresis loop for the percolation problem on two antagonistic Poisson networks with $z_B = 1.5$. Panels (c) and (d) show the hysteresis loop for the percolation problem on two antagonistic networks of different topology: a Poisson network of average degree $z_A = 1.8$ and a scale-free networks with power-law exponent γ_B , minimal degree $m = 1$ and maximal degree $K = 100$. The hysteresis loop is performed using the method explained in the main text. The value of the parameter ϵ used in this figure is $\epsilon = 10^{-3}$	76
4.6	The phase diagram of the percolation process in two antagonistic scale-free networks with power-law exponents γ_A, γ_B . The minimal degree of the two networks is $m = 1$ and the maximal degree K . Panel (a) show the effective phase diagram with $K = 100$, the panel (b) show the phase diagram in the limit of an infinite network $K = \infty$	77

4.7	Phase diagram of the percolation process on a Poisson network with average degree $\langle k \rangle_A = z_A$ interacting with a scale-free network of power-law exponent γ_B , minimal degree $m = 1$ and maximal degree K . The panel on the left show the effective phase diagram for $K = 100$ and the panel on the right show the effective phase diagram for $K = \infty$	78
4.8	Phase diagram two Poisson interdependent networks with a fraction $q = 0.3$ of antagonistic interactions.	80
4.9	Phase diagram two Poisson interdependent networks with a fraction $q = 0.45$ of antagonistic interactions.	81
4.10	Phase diagram two Poisson interdependent networks with a fraction $q = 0.6$ of antagonistic interactions.	82
4.11	Phase diagram two Poisson interdependent networks with a fraction $q = 0.8$ of antagonistic interactions.	84
4.12	Hysteresis loop for $q = 0.3$. The hysteresis loop is performed using the method explained in the main text. The value of the parameter ϵ used in this figure is $\epsilon = 10^{-3}$. In panel (a) and (b) $z_B = 4.0$. In panel (c) and (d) $z_B = 2.8$	86
4.13	Hysteresis loop for $q = 0.8$. The hysteresis loop is performed using the method explained in the main text. The value of the parameter ϵ used in this figure is $\epsilon = 10^{-3}$. In panel (a) and (b) $z_B = 5.7$. In panel (c) and (d) $z_B = 4.5$	87
4.14	The two competing political parties are represented by two networks. Each agent is represented in both networks but can either be active (green node) in only one of the two or inactive (red node) in both networks. Moreover the activity of neighbor nodes influence the opinion of any given node.	89
4.15	(Panel A) The size of the largest connected component S_A in network A at the end of the simulated annealing calculation as a function of the average connectivity of the two networks: z_A and z_B respectively. The data is simulated for two networks for $N = 500$ nodes and averaged 60 times. The simulated annealing algorithm is independent of initial conditions. The white line represent the boundary between the region in which network A is percolating and the region in which network A is not percolating. (Panel B) The schematic representation of the different phases of the proposed model. In region I none of the networks is percolating, in region II network B is percolating in region III network A is percolating in region IV both networks are percolating.	90
4.16	We represent the fraction of nodes in the giant component S_A of network A and in the giant component S_B of network B in different regions of the phase space. In region II ($z_A = 1.5, z_B = 4$) the giant component in network A (S_A) disappears in the thermodynamic limit while in region IV ($z_A = 2.5, z_B = 4$) it remains constant. The giant component in network B remains constant in the thermodynamic limit both in region II and region IV. Each data point is simulated for the two networks for N nodes and averaged 200 times.	91

- 4.17 The contour plot for the difference between the total number of votes m_A in party A (total number of agents active in network A) and the total number of votes m_B in party B (total number of agents active in network B). The data is simulated for two networks for $N = 500$ nodes and averaged 90 times. It is clear that the larger the difference in average connectivity of the two networks, the larger the advantage of the more connected political party. 92
- 4.18 We represent the role of a fraction f of committed agents in reverting the outcome of the election. In particular we plot the histogram of the difference between the fraction of agents m_B/N voting for party B and the fraction of agents m_A/N voting for party A for a fraction f_A of committed agents to party A, with $f_A = 0$ and $f_A = 0.1$ and average connectivities of the networks $z_A = 2.5, z_B = 4$. The histogram is performed for 1000 realizations of two networks of size $N = 1000$. In the inset we show the average number of agents in network A (m_A) and agents in network B (m_B) as a function of the fraction of committed agents f_A . A small fraction of agents ($f_A \simeq 0.1$) is sufficient to reverse the outcome of the elections. The data in the inset is simulated for two networks for $N = 1000$ nodes and averaged 10 times. 93
- B.1 Data collapse of the simulation of the proposed model for cell phone communication. In the panel (A) we plot the probability $P_2^w(\tau)$ that in the model a pair of agents with strenght w are interacting for a period τ and in the panel (B) we plot the probability $P_1^k(\tau)$ that in the model an agents of degree k is non-interacting for a period τ The simulation data on a quenched networks are compared with the analytical predictions (solid lines) in the annealed approximation. The collapses data of $P_2^w(\tau)$ is described by Weibull distribution in agreement with the empirical results found in the mobile phone data. 112

List of Tables

2.1	Typical times $\tau^*(w)$ used in the data collapse of Figure 2.2.	16
2.2	Typical times $\tau^*(k)$ used in the data collapse of Figure 2.4.	16
3.1	The configuration of networks with degree sequence $\{1,1,1,1,5\}$ (on top, $\mathcal{N}[\{k_i\}] = 1$) and $\{1,2,2,2,3\}$ (on bottom, $\mathcal{N}[\{k_i\}] = 6$).	51
4.1	Stable phases in the different regions of the phase diagram of the percolation problem on two antagonistic Poisson networks (Figure 4.4).	75
4.2	Stable phases in the different regions of the phase diagram of the percolation on two antagonistic scale-free networks (Figure 4.6).	77
4.3	Stable phases in the phase diagram for the percolation on two antagonistic networks: a Poisson network (network A) and a scale-free network (network B). (Figure 4.7)	78
4.4	Stable phases in the different regions of the phase diagram of the percolation on two antagonistic Poisson networks with a fraction $q = 0.3$ of antagonistic nodes (Figure 4.8)	79
4.5	Stable phases in the different regions of the phase diagram of the percolation on two antagonistic Poisson networks with a fraction $q = 0.45$ of antagonistic nodes (Figure 4.9).	81
4.6	Stable phases in the different regions of the phase diagram of the percolation on two antagonistic Poisson networks with a fraction $q = 0.6$ of antagonistic nodes (Figure 4.10)	81
4.7	Stable phases in the different regions of the phase diagram of the percolation on two antagonistic Poisson networks with a fraction $q = 0.8$ of antagonistic nodes (Figure 4.11).	85

Chapter 1

Introduction

Complex networks describe a large variety of technological, social and biological systems [7–14]. Therefore network science is now established as a new interdisciplinary research field. In this context the role of physicists, using the powerful tools of statistical mechanics, has been extremely important [7–13]. Universal structural properties, such as the small-world property and the scale-free degree distribution, have been observed in a large variety of systems from the Internet to the protein interactions in the cell. Moreover, dynamical processes defined on networks show a rich interplay between network structure and dynamics [12, 14]. Recently, the scientific community has demonstrated significant interest in temporal networks and interacting networks.

In temporal networks [15] links are continuously created and annihilated. Human social interactions such as face-to-face interactions or mobile-phone mediated interactions are prominent examples of temporal networks. Recently, thanks to the advancement in technology, new extensive data on social interactions has been collected. In order to explain new fundamental observations made on the data, such as the bursty behavior of human social interactions [16], new models need to be formulated. These models will shed light on the basic mechanisms beyond social network dynamics and can be also useful to test new hypothesis on a well-defined setting.

Interacting networks [17, 18] describe interconnected infrastructures, economic networks, social networks, and biological networks. Recently, it has been shown that interacting and interdependent networks are more fragile than single networks. Moreover it has been shown that in this case the percolation transition can be first-order. Yet, understanding how robust are interacting networks and how cascading failures might spread in the system are topics of intense scientific debate.

In this thesis, we investigate statistical mechanics of temporal and interacting networks, to echo the increasing interest in this field and to answer some new relevant questions raising in this context. In this chapter, we first review some basic notations of complex networks. After that, we discuss some latest results on statistical mechanics of temporal networks and interacting networks. Finally we give the outline of the thesis.

1.1 Brief overview of complex networks

A complex network is a complex system that can be represented as a set of nodes and links (also called vertices and edges). Mathematically, a network G , also called a graph in graph theory, is defined by a pair of sets $G = (V, E)$, where V is a set of nodes and E is a set of links. It is also convenient to define a network by adjacency matrix. For a undirected network of N nodes, the adjacency matrix $A = \{a_{ij} = 0, 1\}$ is a $N \times N$ matrix in which the index i and j represent the label of nodes. The matrix element $a_{ij} = 1$ if a link is present between node i and j , otherwise $a_{ij} = 0$. For undirected networks the adjacency matrix A is symmetric where $a_{ij} = a_{ji}$. For weighted networks in which links are associated with a specific weight, the adjacency element a_{ij} can be any non-negative real number representing the weight of the link. In the rest of this thesis we will mostly deal with undirect networks. Therefore a network in this thesis usually refers to a undiected network unless there is an explicit notation. From the point of statistical mechanics, random networks under specified constraints (e.g. fixed average degree) can be treated as a statistical ensemble, where each member is a particular configuration satisfying the constraints.

The study of complex networks has been a part of graph theory in mathematics for a long time. The history of graph theory goes back to the 18th century when the notable problem of the Seven Bridges of Königsberg was raised and solved by Leonhard Euler. The Königsberg problem was to find a path crossing each of the seven bridges in the city once and only once, which is also called Eulerian path. Over centuries the framework of graph theory has been well developed by mathematicians. Nevertheless, before 1950s most of the studies in graph theory have focused on regular graphs which is defined as purely abstract representations in mathematics. Little attention was paid to the organization principle of graphs in nature. In 1959, the model of random graphs was first studied by Paul Erdős and Alfred Rényi, which is considered a significant landmark in modern graph theory. The Erdős-Rényi random graph model is the first model introducing the element of stochasticity in networks. The basic assumption of this model is that links are generated by connecting node pairs in equal probability, i.e. the generation of links between node pairs is completely random.

Networks have also been studied extensively in sociology. The study of networks in sociology is mostly based on the means of questionnaires or survey, asking participants to elaborate their interactions with others. Such responses can be used to reconstruct a social network in which nodes represent individuals and links represent the interactions among them. The first attempt was given by Jacob Moreno in 1953, who introduced the sociograms to describe relationships among children [19]. Structural properties of social networks such as average path length and community centrality have also been studied by experiments in social science. One of the most well-known work is the "six degrees of separation" experiment conducted by Stanley Milgram in 1967 [20]. In Milgram's experiment, a group of people were asked to send a package to a final person who they did not know, through a friend or acquaintance who they thought would forward the package closer to the final person. This experiment recorded a median of five intermediate acquaintance between the original sender and the final recipient, which first experimentally demonstrated the small-world property in human society. Nowadays, modern technologies such as mobile sensors, communication devices and communication softwares over Internet have been applied to gather data on human social networks.

In late 1990s, two significant works initiated a new era for complex networks. The first was the small-world network model proposed by Duncan Watts and Steven Strogatz in 1998 [21]. The small-world network model generates a network by randomly rewiring a fraction of links of a regular graph, and exhibits a combination of short average path length and high clustering coefficient. The second was the Barabási-Albert (BA) model proposed by Albert-László Barabási and Albert Réka in 1999 which explains the scale-free property of networks [22]. These two works attracted tremendous interest from various fields and established complex networks as a new interdisciplinary science.

In this session, we briefly review some classical models and structural characteristics of complex networks as an introduction of the thesis. We refer interested readers to [7–9, 11, 13] for a detailed review of complex networks.

1.1.1 Structural Characteristics of networks

In this subsection we briefly recall some important structural characteristics of networks.

1.1.1.1 Degree distribution

Degree distribution is the first significant structural characteristics of networks. The degree of a node in a network, sometimes called connectivity, is the number of links the

node has, or the number of neighbors the node has. The degree distribution $P(k)$ of a network is then defined to be the fraction of nodes in the network with degree k .

1.1.1.2 Clustering Coefficient

Clustering coefficient is a quantity that measures the tendency of nodes to form clusters. The clustering coefficient C_i of node i in a network is defined as $C_i = \frac{2E_i}{k_i(k_i-1)}$, where k_i is the degree of i and E_i is the number of links between the neighbors of i . The average clustering coefficient of a network $C = \frac{\sum_i C_i}{N}$ is the average over the clustering coefficient of all individual nodes.

1.1.1.3 Giant component

The giant component is an important structural property of a network. Let us define a connected component of a network as a subset of mutually reachable nodes of the network. A giant component is defined as the connected component that contains an extensive number of nodes in the limit $N \rightarrow \infty$, i.e. a giant component contains a constant fraction of nodes of an infinite network.

1.1.2 Basic generating network models

In this subsection, we briefly review some important generating network models: random network model, BA model, scale-free network model and configuration model.

1.1.2.1 Classical random network model

The most important classical random network model is the Erdős-Rényi model. An Erdős-Rényi random network $G(N, M)$ is generated by randomly placing M links between N nodes. A variation of Erdős-Rényi model is the Gilbert model, which generates a random network $G(N, p)$ by making links present between nodes with probability p . The degree distribution of these two classical random network model is poissonian, i.e. $P(k) = e^{-\langle k \rangle} \langle k \rangle^k / k!$ where $\langle k \rangle$ is the average degree of the network.

1.1.2.2 Small-world network model

The small-world network model generates a network interpolating between a regular graph and a random graph. The basic idea of small-world network model is to randomly

rewire a fraction the links of a regular graph. The original model proposed by Watts and Strogatz is constructed in one-dimension as follows: Starting with a ring of N nodes, each link of the ring is rewired with probability p excluding the situation with self-links and double links. The advantage of small-world model is that it can generate a network with both short average path length, namely the small-world property, and high clustering coefficient.

1.1.2.3 BA model

A number of models have been proposed to explain the widely observed scale-free degree distribution of networks. The most important one is the Barabási-Albert model (BA model) based on preferential attachment [22]. The BA model describes a growing network evolving according to the following algorithm: Starting with a small connected network with n_0 nodes and m_0 links, at each step a new node with degree m is added to the system and the other end of each link is connected to another existing node of the network with probability proportional to the degree of that node. A network generated by the BA model has scale-free degree distribution $P(k) \propto k^{-3}$. There are a number of variants of the BA network model with different mechanism of preferential attachment and growing process, such as Bianconi-Barabási model [23], Krapivsky-Redner model [3, 4], Dorogovtsev-Mendes model [6], and etc. A more detailed review of these growing network models is given in Chapter 3.

1.1.2.4 Configuration model

The configuration model [24] proposed by Béla Bóllabas is a generalization of random graph model and is widely used to generate uncorrelated networks with arbitrary degree distribution. The construction of the model is proposed as follows: (i) Generate N stubs (a stub is a node attached by links with the other end open) following specific degree distribution. The sum of the degree sequence must be even. (ii) Randomly connect the links of stub in pairs. The network generated by the configuration may have loops and multiple links. Fortunately it has been shown that the effect of loops can be neglected in the large network limit $N \rightarrow \infty$, as long as the network has nodes with degree smaller than the so-called structural cutoff.

1.2 Temporal networks and social networks

In the last decade, large attention has been devoted to static networks and dynamical processes defined on them. Nevertheless, most natural and artificial networks have significant temporal structures in which nodes and links appear and disappear on various time-scales. For example, the links representing social relationships in social networks are aggregations of successive contacts or communication events, which are constantly created or terminated between pairs of individuals. The temporal evolution of networks may lead to notable consequences for the dynamical processes defined on them. The traditional models of static networks are not capable of capturing the temporal properties of these networks. Therefore, the scientific community has recently focused the attention on temporal networks.

Temporal networks, also called time-varying graphs in some literature, can be described by various representations. Generally, one can define a temporal network by a discrete sequence of graphs. Each graph of the sequence represents the structure of a temporal network at the corresponding time step [25]. In most circumstances, the number of nodes in the system is constant and only the variation of links, e.g. the contacts between individuals in a social network, form the temporal network. It is convenient to define such temporal network by sequences of time intervals [15]. In particular, considering a graph $G = (V, E)$, one can define a sequence of time intervals for each link $e \in E$, i.e. $T_e = \{(t_1, t'_1), \dots, (t_n, t'_n)\}$ where the parentheses indicate the periods of activity, the unprimed times mark the beginning of the interval and the primed quantities mark the end [15].

Social networks are probably one of the most important examples of temporal networks. Social networks evolve on many different timescales. Social relationships in static representation are indeed aggregations of dynamical sequences of fast social interactions such as face-to-face interactions, phone calls or email exchanges over a certain period of time. Therefore social relationships are continuously changing, possibly in a way correlated with the dynamical processes taking place during social interactions. In this context, an important topic of investigation is to model the dynamics of social interactions, e.g. the community formation [26–28] in social networks and the evolution of adaptive dynamics of opinions and social ties through schematic models in which links can disappear or be rewired at random [29–35].

Recently, new technologies have made possible the access to data sets that give new insights into such link internal dynamics, characterized by sequences of events of different durations. Traces of human behavior are often unwittingly recorded in a variety of contexts such as financial transactions, phone calls, mobility patterns, purchases using

credit cards, etc. Data have been gathered and analyzed about the mobility patterns inside a city [36], between cities [37], as well as at the country and at worldwide levels [38–41]. At a more detailed level, mobile devices such as cell phones make it possible to investigate individual mobility patterns and their predictability [42, 43]. Mobile devices and wearable sensors using Bluetooth and Wifi technologies give access to proximity patterns of pairs of individuals [44–48], and even face-to-face presence can be resolved with high spatial and temporal resolution [1, 49–51]. Finally, on-line interactions occurring between individuals can be monitored by logging instant messaging or email exchange [16, 52–57].

The combination of these technological advances and of heterogeneous data sources allows researchers to gather longitudinal data that have been traditionally scarce in social network analysis [58, 59]. Analysis of such data sets has clearly shown the bursty nature of many human and social activities, revealing the inadequacy of many traditional frameworks that posit Poisson distributed processes. In particular, the durations of “contacts” between individuals, as defined by the proximity of these individuals, display broad distributions, as well as the time intervals between successive contacts [1, 44, 48, 49, 51, 60]. Burstiness of interactions has strong consequences on dynamical processes [25, 51, 61–64], and should therefore be correctly taken into account when modeling the interaction networks. New frameworks are therefore needed, which integrate the bursty character of human interactions and behaviors into dynamic network models.

1.3 Entropy of complex networks

Entropy is one of the most important concepts in statistical mechanics, and quantifies the number of possible microscopic states of a system in equilibrium (the Boltzmann’s definition). Various forms of entropy have been proposed in the context of statistical mechanics. The most general one is the Gibbs entropy given by $S = -k_B \sum p_i \log p_i$ where k_B is the Boltzmann constant and p_i is the probability of microscopic state. An extension of the Gibbs entropy to quantum mechanics is the Von Neumann entropy. In information theory entropy also plays a key role, which measures the uncertainty of random variable. The most well-known definition is the Shannon entropy. For a discrete random variable X with n possible values $\{x_1, \dots, x_n\}$, the Shannon entropy is given by $S = -\sum P(x_i) \log P(x_i)$ where $P(x_i)$ represents the probability of a specific value x_i . Shannon entropy is widely used in communication theory and coding theory, e.g. data compression and signal transmission. It has been shown that the entropy in statistical mechanics and the entropy in information theory are closely related.

A complex network is a complex system incorporating abundant information on its topology, structural characteristics and dynamics taking place on it. A fundamental problem of complex networks is: how complex is a complex network? To solve this problem, we need a new theory to measure and quantify the information encoded in complex networks. In this context, attention has been attracted to the entropy of complex networks.

The history of network entropy can go back to the concept of graph entropy. The classical graph entropy has various definitions and most of them are based on the topological structures of a graph, e.g. the symmetries, the chromatic structure and vertex-degree inequity [65]. Another significant attempt to perform entropy measure on a graph is the Körner graph entropy [66], which characterizes how much information can be communicated in a setting where pairs of symbols may be confused. For more details of graph entropy, we refer interested readers to [65, 67, 68].

Recently, entropy measures of complex networks have been investigated in the framework of statistical mechanics. One successful approach is the definition of Gibbs entropy on complex networks by Ginestra Bianconi [69–71]. The approach is based on the microcanonical network ensemble which is a set of all possible networks that satisfy some specific constraints such as fixed number of links, given degree sequence and community structure. The Gibbs entropy is simply the logarithm of the number of networks in the ensemble, which can be evaluated by efficient calculation schemes such as path-integral and cavity method [69, 70, 72]. Other entropy measures in the context of complex networks such as Von Newman entropy or Shannon entropy have been studied as well [73]. The entropy of complex networks provides a way to quantify the complexity of networks and has potential to play an important role in solving inference problems of networks.

1.4 Percolation of complex networks

Percolation is one of the most important critical phenomena. A network is percolating when it contains a giant component in the thermodynamic limit, i.e. $N \rightarrow \infty$, where N indicates the total number of nodes in the network.

In the last decade, percolation of single and non-interacting networks have been studied extensively. Here we review some well-known results. Most of these results are based on configuration model and can be obtained by the method of generating functions [74] which is a powerful tool in handling percolation problem.

The classical percolation problem of random networks is to study the emergence of the giant component in a network. A general condition for the phase transition at which the

giant component first appears is given by $\langle k^2 \rangle > 2\langle k \rangle$, which is called the Molloy-Reed condition [75]. It has been known that such phase transition is continuous and second-order. For an Erdős-Rényi (ER) network, the condition is simply given by $\langle k \rangle > 1$. For a purely scale-free network with degree distribution $P(k) \propto k^{-\gamma}$ where γ is the scaling component and $k \in [m, M]$, the situation is more interesting and depending on the degree cutoff m and M . For instance, when $m = 1$ and $M \rightarrow \infty$, the condition is given by $\gamma > 3.478\dots$, i.e. there is no giant component in the network if $\gamma > 3.478\dots$. When $m \geq 2$, a giant component exists for every γ and the phase transition does not exist in this case.

An important variant of the percolation of networks is the model of random failures or breakdown of networks [76]. This model is aimed to study the robustness of networks under random failures due to random error or external attack. In this model, a random fraction $1 - p$ of nodes (including the links attached to them) are removed from the network. The percolation problem is to study the emergence of the giant component in the remaining network. If a giant component still exists after the removal, the network is robust. Generally, for a random network with degree distribution $P(k)$, the critical fraction p_c for percolation is given by $p_c = \frac{1}{\kappa - 1}$ where $\kappa = \langle k^2 \rangle / \langle k \rangle$. The size of giant component S near the critical fraction p_c follows a scaling law $S \propto (p - p_c)^\beta$ where β is a scaling component. In particular for ER networks we have $p_c = 1/\langle k \rangle$ and $\beta = 1/2$. For a purely scale-free network with degree distribution $P(k) \propto k^{-\gamma}$ and $k \in [m, M]$, it has been shown that the percolation properties are depending on the scaling exponent γ and the degree cutoff m and M . In fact, for $\gamma \leq 3$, when $M \rightarrow \infty$ the critical p_c vanishes and the percolation transition does not exist. For a finite system in which $M < \infty$, the critical p_c does not vanish but usually maintains at an extremely low value if $M \gg m$. In this case the network is very robust since the giant component sustains even that a large fraction of nodes are removed. For $3 < \gamma < 4$, the critical p_c exists and there is a second-order phase transition alike the ER network.

Recently, attention has been addressed to percolation of interacting networks. Most real networks do not live in isolation. In fact, they are coupled with other networks, and forming a network of networks. Buldyrev et al. [17] studied percolation problem for interdependent networks, where the functionality of a node in a network is dependent on the functionality of other nodes. Therefore, a failure of one node in a network may lead to a cascade of failures in the entire system. One can find various examples of interdependent networks in real systems. For instance, the sites of the Internet depend on the sites of the electrical-power network, and a failure of one site in the electrical-power network may lead to consequent failure of depending sites of the Internet. In particular, in [17] a system of two coupled interdependent networks A and B has been considered. In this case the nodes in each network are coupled one-to-one, i.e the node in network A

depends on the node in network B , and vice versa. The authors of [17] have considered an iterative process of cascading failures starting with randomly removing a fraction $1 - p$ of network A nodes and all the A-links that are connected to them. Due to the interdependence between the networks, the nodes in network B that depend on removed A-nodes are also removed together with the B-links that are connected to them. Finally the networks may break into independent connected components (or clusters). The nodes belonging to the giant component are considered remaining functional, while the nodes belonging to small clusters are considered non-functional. The most remarkable finding in this model is that, unlike the second-order transition occurring in percolation of single network, there exists a critical p_c at which the the fraction of functional component undergoes a first-order transition, i.e. the fraction of nodes in the functional component drops abruptly to zero when p goes below p_c . The model reveals that interdependent networks may be more fragile than a single network. A concise treatment of the model was presented by Son et al. [77], who related the percolation of interdependent networks to epidemic spreading. A detailed review of the percolation of interdependent networks based on epidemic spreading is given in Chapter 4. We also refer interested readers to [17, 78] for details of percolation of interdependent networks. One should note that, not all percolation of interdependent networks are discontinuous and some exceptions have been found recently [79].

Percolation of complex networks is a broad topic. There are a number of notable percolation models on complex networks, such as bootstrap percolation [80], k-core percolation [81], explosive percolation [82] and etc. We can not cover all aspects of this topic but we refer interested readers to [14] for a comprehensive review.

1.5 Outline

The thesis is organized as follows. In Chapter 2, we investigate the model of temporal social networks. In particular, we model social interactions as temporal networks reproducing the distribution of contact duration observed in the data. In Chapter 3, we investigate the entropy of temporal and growing networks providing a way to quantify the information encoded in their structure and dynamics. In Chapter 4, we investigate the percolation of interacting and anatagonistic networks by introducing antagonistic interactions between nodes of the coupled interacting networks. In Chapter 5 we give the summary of the thesis.

Chapter 2

Model of Temporal Social Networks

Temporal social networks describing human social interactions are characterized by heterogeneous duration of contacts, which can either follow a power-law distribution, such as in face-to-face interactions, or a Weibull distribution, such as in mobile-phone communication. In this chapter we propose a unified model of face-to-face interactions and mobile phone communication based on a reinforcement dynamics, which explains the data observed in these different types of social interaction. The chapter is based on the author's work [83–86]

2.1 Background

Complex networks theory [8, 9, 11, 12, 14, 87] has flourished thanks to the availability of new datasets on large complex systems, such as the Internet or the interaction networks inside the cell. In the last ten years attention has been focusing mainly on static or growing complex networks, with little emphasis on the rewiring of the links. The topology of these networks and their modular structure [28, 88–90] are able to affect the dynamics taking place on them [12, 14, 91, 92]. Only recently temporal networks [1, 15, 25, 51, 61, 64], dominated by the dynamics of rewirings, are starting to attract the attention of quantitative scientists working on complexity. One of the most beautiful examples of temporal networks are social interaction networks. Indeed, social networks [93, 94] are intrinsically dynamical and social interactions are continuously formed and dissolved. Recently we are gaining new insights into the structure and dynamics of these temporal social networks, thanks to the availability of a new generation of datasets recording the social interactions of the fast time scale. In fact, on one side we have

data on face-to-face interactions coming from mobile user devices technology [44, 45], or Radio-Frequency-Identification-Devices [1, 51], on the other side, we have extensive datasets on mobile-phone calls [63] and agent mobility [39, 42].

This new generation of data has changed drastically the way we look at social networks. In fact, the adaptability of social networks is well known and several models have been suggested for the dynamical formation of social ties and the emergence of connected societies [29–32]. Nevertheless, the strength and nature of a social tie remained difficult to quantify for several years despite the careful sociological description by Granovetter [93]. Only recently, with the availability of data on social interactions and their dynamics on the fast time scale, it has become possible to assign to each acquaintance the strength or weight of the social interaction quantified as the total amount of time spent together by two agents in a given time window [1].

The recent data revolution in social sciences is not restricted to data on social interaction but concerns all human activities [16, 56, 57, 95], from financial transaction to mobility. From these new data on human dynamics evidence is emerging that human activity is bursty and is not described by Poisson processes [16, 95]. Indeed, a universal pattern of bursty activities was observed in human dynamics such as broker activity, library loans or email correspondence. Social interactions are not an exception, and there is evidence that face-to-face interactions have a distribution of duration well approximated by a power-law [1, 60, 85, 96, 97] while they remain modulated by circadian rhythms [98]. The bursty activity of social networks has a significant impact on dynamical processes defined on networks [62, 99].

In this chapter we compare these observations with data coming from a large dataset of mobile-phone communication and show that human social interactions, when mediated by a technology, such as the mobile-phone communication, demonstrate the adaptability of human behavior. Indeed, the distribution of duration of calls does not follow any more a power-law distribution but has a characteristic scale defining the weight of the links, and is described by a Weibull distribution. At the same time, however, this distribution remains bursty and strongly deviates from a Poisson distribution. We will show that both the power-law distribution of durations of social interactions and the Weibull distribution of durations and social interactions observed respectively in face-to-face interaction datasets and in mobile-phone communication activity can be explained phenomenologically by a model with a reinforcement dynamics [83–85, 96, 100] responsible for the deviation from a pure Poisson process. In this model, *the longer two agents interact, the smaller is the probability that they split apart, and the longer an agent is non interacting, the less likely it is that he/she will start a new social interaction.* We observe

here that this framework is also necessary to explain the group formation in simple animals [101]. This suggests that the reinforcement dynamics of social interactions, much like the Hebbian dynamics, might have a neurobiological foundation. Furthermore, this is supported by the results on the bursty mobility of rodents [102] and on the recurrence patterns of words encountered in online conversations [103]. We have therefore found ways to quantify the adaptability of human behavior to different technologies. We observe here that this change of behavior corresponds to the very fast time dynamics of social interactions and it is not related to macroscopic change of personality consistently with the results of [104] on online social networks.

2.2 Temporal social networks and the distribution of duration of contacts

Human social dynamics is bursty, and the distribution of inter-event times follows a universal trend showing power-law tails. This is true for e-mail correspondence events, library loans, and broker activity. Social interactions are not an exception to this rule, and the distribution of inter-event time between face-to-face social interactions has power-law tails [16, 95]. Interestingly enough, social interactions have an additional ingredient with respect to other human activities. While sending an email can be considered an instantaneous event characterized by the instant in which the email is sent, social interactions have an intrinsic duration which is a proxy of the strength of a social tie. In fact, social interactions are the microscopic structure of social ties and a tie can be quantified as the total time two agents interact in a given time-window. New data on the fast time scale of social interactions have been now gathered with different methods which range from Bluetooth sensors [45], to the new generation of Radio-Frequency-Identification-Devices [1, 51]. In all these data there is evidence that face-to-face interactions have a duration that follows a distribution with a power-law tail. Moreover, there is also evidence that the inter-contact times have a distribution with fat tails.

If we want to characterize the universality of these distributions, a fundamental question may be raised: how do these distributions change when human agents are interfaced with a new technology? To answer this question, in this session we first report evidence of distribution of human face-to-face interactions. Then we analyze a cellphone dataset and report new evidence of distribution of mobile phone communication. We compare these two distributions and show human social behaviors are highly adaptive.

2.2.1 Evidence of distribution of human face-to-face interactions

Here we report a figure of Ref. [1] (Figure 2.1 of this chapter) in which the duration of contact in Radio-Frequency-Device experiments conducted by Sociopatterns experiments is clearly fat tailed and well approximated by a power-law (straight line on the log-log plot). In this figure the authors of Ref. [1] report the distribution of the duration of binary interactions and the distribution of duration of a the triangle of interacting agents. Moreover they report data for the distribution of inter-event time.

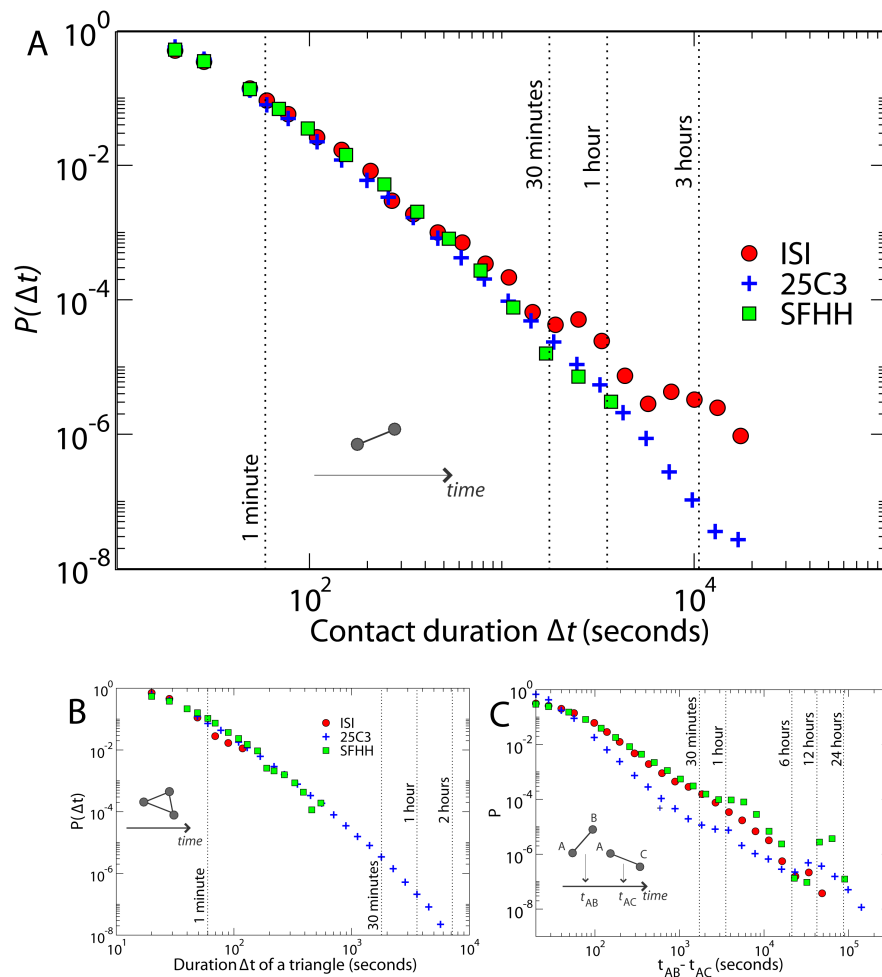


FIGURE 2.1: Probability distribution of the duration of human face-to-face interaction. A) Probability distribution of duration of contacts between any two given persons. Strikingly, the distributions show a similar long-tail behavior independently of the setting or context where the experiment took place or the detection range considered. The data correspond to respectively 8700, 17000 and 600000 contact events registered at the ISI, SFHH and 25C3 deployments. B) Probability distribution of the duration of a triangle. The number of triangles registered are 89, 1700 and 600000 for the ISI, SFHH and 25C3 deployments. C) Probability distribution of the time intervals between the beginning of consecutive contacts AB and AC. This figure is from [1].

2.2.2 Evidence of distribution of mobile phone communication

Here we analyze the call sequence of subscribers of a major European mobile service provider. In the dataset the users were anonymized and impossible to track. We consider calls between users who called each other mutually at least once during the examined period of 6 months in order to examine calls only reflecting trusted social interactions. The resulted event list consists of 633,986,311 calls between 6,243,322 users. We performed measurements for the distribution of call durations and non-interaction times of all the users for the entire 6 months time period. The distribution of phone call durations strongly deviates from a fat-tail distribution. In Figure 2.2 we report these distributions and show that they depend on the strength w of the interactions (total duration of contacts in the observed period) but do not depend on the age, gender or type of contract in a significant way. The distribution $P^w(\Delta t_{in})$ of duration of contacts within agents with strength w is well fitted by a Weibull distribution

$$\tau^*(w)P^w(\Delta t_{in}) = W_\beta \left(x = \frac{\Delta t}{\tau^*(w)} \right) = \frac{1}{x^\beta} e^{-\frac{1}{1-\beta} x^{1-\beta}}. \quad (2.1)$$

with $\beta = 0.47\dots$. The typical times of interactions between users $\tau^*(w)$ depend on the weight w of the social tie. In particular the values used for the data collapse of Figure 3 are listed in Table 2.1. These values are broadly distributed, and there is evidence that such heterogeneity might depend on the geographical distance between the users [105]. The Weibull distribution strongly deviates from a power-law distribution to the extent that it is characterized by a typical time scale $\tau(w)$, while power-law distribution does not have an associated characteristic scale. The origin of this significant change in the behavior of human interactions could be due to the consideration of the cost of the interactions (although we are not in the position to draw these conclusions (See Figure 2.3 in which we compare distribution of duration of calls for people with different type of contract) or might depend on the different nature of the communication. The duration of a phone call is quite short and is not affected significantly by the circadian rhythms of the population. On the contrary, the duration of non-interaction periods is strongly affected by the periodic daily or weekly rhythms. In Figure 2.4 we report the distribution of duration of non-interaction periods in the day periods between 7AM and 2AM next day. The typical times $\tau^*(k)$ used in Figure 5 are listed in Table 2.2. The distribution of non-interacting times is difficult to fit due to the noise derived by the dependence on circadian rhythms. In any case the non-interacting time distribution is clearly fat tail.

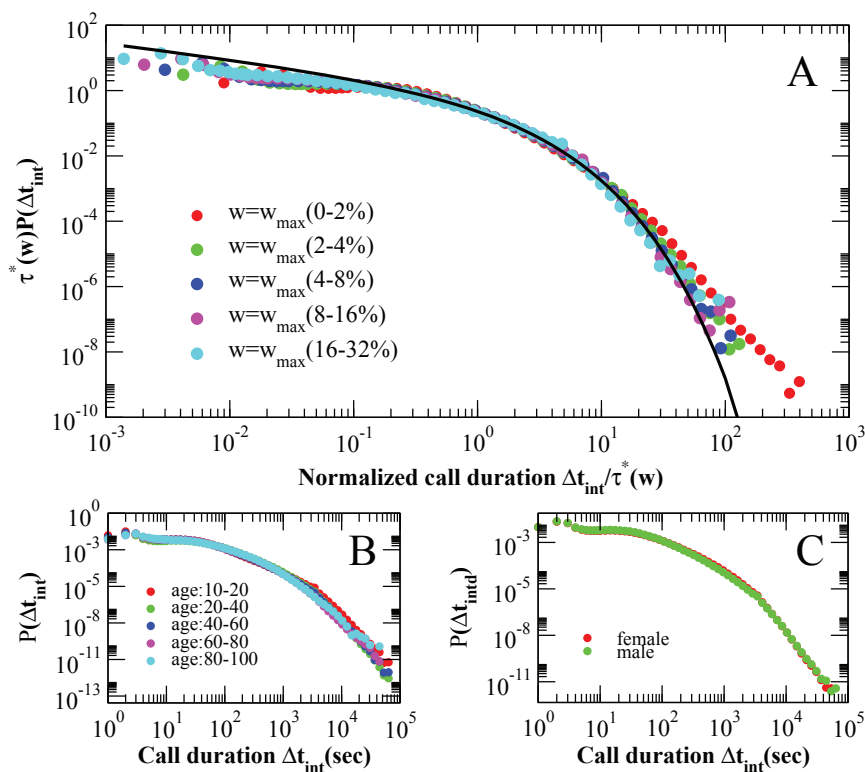


FIGURE 2.2: (A) Distribution of duration of phone-calls between two users with weight w . The data depend on the typical scale $\tau^*(w)$ of duration of the phone-call. (B) Distribution of duration of phone-calls for people of different age. (C) Distribution of duration of phone-calls for users of different gender. The distributions shown in the panel (B) and (C) do not significantly depend on the attributes of the nodes.

TABLE 2.1: Typical times $\tau^*(w)$ used in the data collapse of Figure 2.2.

Weight of the link	Typical time $\tau^*(w)$ in seconds (s)
(0-2%) w_{max}	111.6
(2-4%) w_{max}	237.8
(4-8%) w_{max}	334.4
(8-16%) w_{max}	492.0
(16-32%) w_{max}	718.8

TABLE 2.2: Typical times $\tau^*(k)$ used in the data collapse of Figure 2.4.

Connectivity	Typical time $\tau^*(k)$ in seconds (s)
k=1	158,594
k=2	118,047
k=4	69,741
k=8	39,082
k=16	22,824
k=32	13,451

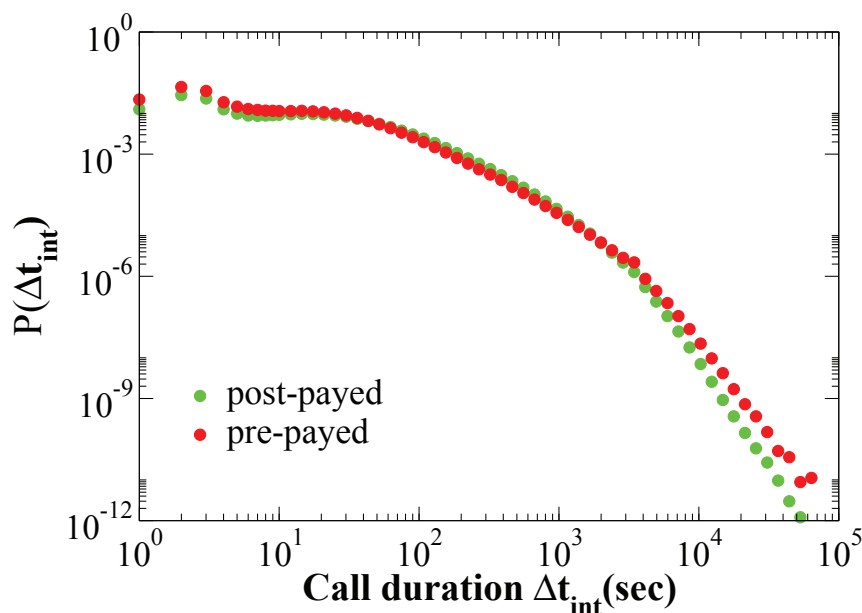


FIGURE 2.3: Distribution of duration of phone-calls for people with different types of contract. No significant change is observed that modifies the functional form of the distribution.

2.3 Model of social interaction

In the previous section we have showed evidence that the duration of social interactions is generally non-Poissonian. Indeed, both the power-law distribution observed for duration of face-to-face interactions and the Weibull distribution observed for duration of mobile-phone communication strongly deviate from an exponential. The same can be stated for the distribution of duration of non-interaction times, which strongly deviates from an exponential distribution both for face-to-face interactions and for mobile-phone communication. Indeed, the non-Poissonian distribution has been observed from the data on email correspondence. and two important models have been proposed to explain the bursty email correspondence. First, a queueing model of tasks with different priorities has been suggested to explain bursty interevent time. This model implies rational decision making and correlated activity patterns [16, 95]. This model gives rise to power-law distribution of inter event times. Second, a convolution of Poisson processes due to different activities during the circadian rhythms and weekly cycles have been suggested to explain bursty inter event time. These different and multiple Poisson processes are introducing a set of distinct characteristic time scales on human dynamics giving rise to fat tails of interevent times [57].

Nevertheless, to explain the data on duration of contacts in human social interaction we

cannot use any of the models proposed for bursty interevent time in email correspondence. In fact, on one side it is unlikely that the decision to continue a conversation depends on rational decision making. Moreover the queueing model [16, 95] cannot explain the observed stretched exponential distribution of duration of calls. On the other side, the duration of contacts it is not effected by circadian rhythms and weekly cycles which are responsible for bursty behavior in the model [57]. This implies that a new theoretical framework is needed to explain social interaction data. Therefore, in order to model the temporal social networks we have to abandon the generally considered assumption that social interactions are generated by a Poisson process. In this assumption the probability for two agents to start an interaction or to end an interaction is constant in time and not affected by the duration of the social interaction.

To build a model for human social interactions we have to consider a reinforcement dynamics, in which the probability to start an interaction depends on how long an individual has been non-interacting, and the probability to end an interaction depends on the duration of the interaction itself. Generally, to model the human social interactions, we can consider an agent-based system consisting of N agents that can dynamically interact with each other and give rise to interacting agent groups. In the following subsections we give more details on the dynamics of the models. We denote by the state n of the agent, the number of agents in his/her group (including itself). In particular we notice here that a state $n = 1$ for an agent, denotes the fact that the agent is non-interacting. A reinforcement dynamics for such system is defined in the following frame: (i) The longer an agent is interacting in a group the smaller is the probability that he/she will leave the group. (ii) The longer an agent is non-interacting the smaller is the probability that he/she will form or join a new group. (iii) The probability that an agent i change his/her state (value of n) is given by

$$f_n(t, t_i) = \frac{h(t)}{(\tau + 1)^\beta} \quad (2.2)$$

where $\tau := (t - t_i)/N$, N is the total number of agents in the model and t_i is the last time the agent i has changed his/her state, and β is a parameter of the model. The reinforcement mechanism is satisfied by any function $f_n(t, t_i)$ that is decreasing with τ but social-interaction data currently available are reproduced only for this particular choice $f_n(t, t_i)$.

The function $h(t)$ in Eq.(2.2) only depends on the actual time in which the decision is made. This function is able to modulate the activity during the day and throughout the weekly rhythms. For the modelling of the interaction data we will first assume that the function $h(t)$ is a constant in time. Moreover in the following subsections we will show that in order to obtain power-law distribution of duration of contacts and non-interaction

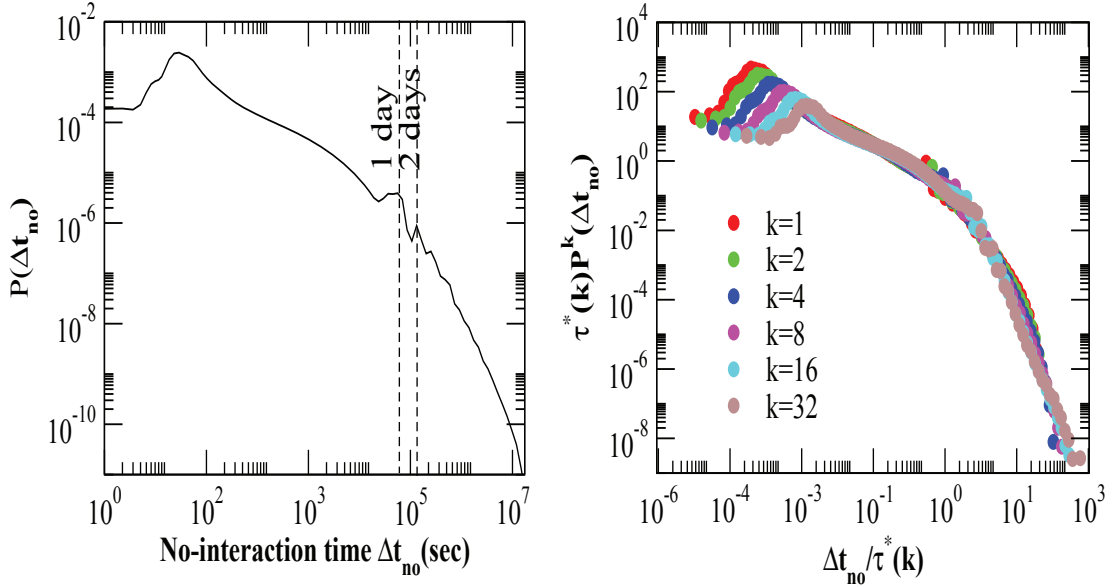


FIGURE 2.4: Distribution of non-interaction times in the phone-call data. The distribution strongly depends on circadian rhythms. The distribution of rescaled time depends strongly on the connectivity of each node. Nodes with higher connectivity k are typically non-interacting for a shorter typical time scale $\tau^*(k)$.

times (as it is observed in face-to-face interaction data) we have to take $\beta = 1$ while in order to obtain Weibull distribution of duration of contacts we have to take $\beta < 1$. Therefore, summarizing here the results of the following two sections, we can conclude with the following statement for the adaptability of human social interactions.

In the following, we discuss two specific cases, the model of face-to-face interactions and the model of phone-call communication, based on the framework given in this section.

2.4 Model of face-to-face interactions

Starting from given initial conditions, the stochastic dynamics of the model of face-to-face interactions at each time step t is implemented as the following algorithm:

- (1) An agent i is chosen randomly.
- (2) The agent i updates his/her state $n_i = n$ with probability $f_n(t, t_i)$.

If the state n_i is updated, the subsequent action of the agent proceeds with the following rules.

- (i) If the agent i is non-interacting ($n_i = 1$), he/she starts an interaction with another non-interacting agent j chosen with probability proportional to $f_1(t, t_j)$.

Therefore the coordination number of the agent i and of the agent j are updated ($n_i \rightarrow 2$ and $n_j \rightarrow 2$).

- (ii) If the agent i is interacting in a group ($n_i = n > 1$), with probability λ the agent leaves the group and with probability $1 - \lambda$ he/she introduces a non-interacting agent to the group. If the agent i leaves the group, his/her coordination number is updated ($n_i \rightarrow 1$) and also the coordination numbers of all the agents in the original group are updated ($n_r \rightarrow n - 1$, where r represent a generic agent in the original group). On the contrary, if the agent i introduces another isolated agent j to the group, the agent j is chosen with probability proportional to $f_1(t, t_j)$ and the coordination numbers of all the interacting agents are updated ($n_i \rightarrow n + 1$, $n_j \rightarrow n + 1$ and $n_r \rightarrow n + 1$ where r represents a generic agent in the group).

- (3) Time t is updated as $t \rightarrow t + 1/N$ (initially $t = 0$). The algorithm is repeated from (1) until $t = T_{max}$.

We have taken in the reinforcement dynamics with parameter $\beta = 1$ such that

$$f_n(t, t') = \frac{b_n}{1 + (t - t')/N}. \quad (2.3)$$

In Eq. (2.3), for simplicity, we take $b_n = b_2$ for every $n \geq 2$, indicating the fact the interacting agents change their state independently on the coordination number n .

We note that in this model we assume that everybody can interact with everybody so that the underline network model is fully connected. This seems to be a very reasonable assumption if we want to model face-to-face interactions in small conferences, which are venues designed to stimulate interactions between the participants. Nevertheless the model can be easily modified by embedding the agents in a social network so that interactions occur only between social acquaintances.

2.4.1 Pairwise interactions

We first consider a restricted version of the model, in which the agents can only interact in pairs. This set-up is obtained by setting $\lambda = 1$ and by considering initial conditions in which the agents interact at most in groups of size 2. In this case, each agent is thus assigned a variable $n_i = 1, 2$ indicating if the agent i is isolated ($n_i = 1$) or interacting with another agent ($n_i = 2$).

As in the analysis of empirical data, the most immediate quantities of interest concern the time spent by agents in each state, the duration of contacts between two agents, and

the time intervals between successive contacts of an agent. To gain insight into these temporal properties of the system, we can write rate equations for the evolution of the numbers $N_n(t, t')$ of agents in state $n = 1, 2$ at time t who have not changed state since time t' . In the mean-field approximation, and treating time and numbers as continuous variables, these equations are given by

$$\begin{aligned}\frac{\partial N_1(t, t')}{\partial t} &= -2\frac{N_1(t, t')}{N}f_1(t, t') + \pi_{21}(t)\delta_{tt'}, \\ \frac{\partial N_2(t, t')}{\partial t} &= -2\frac{N_2(t, t')}{N}f_2(t, t') + \pi_{12}(t)\delta_{tt'},\end{aligned}\quad (2.4)$$

where the transition rates $\pi_{n,m}(t)$ denote the average number of agents switching their states from n to m ($n \rightarrow m$) at time t . If the agents make their decisions according to the reinforcement dynamics described by the probabilities $f_n(t, t')$ given by Eq. (2.3), the dynamic equations (2.4) have a solution of the form

$$\begin{aligned}N_1(t, t') &= \pi_{21}(t') \left(1 + \frac{t-t'}{N}\right)^{-2b_1}, \\ N_2(t, t') &= \pi_{12}(t') \left(1 + \frac{t-t'}{N}\right)^{-2b_2}.\end{aligned}\quad (2.5)$$

Since the total number of isolated agents who change their state at time t is equal to $\pi_{12}(t)$ and the total number of interacting agents who change their state is equal to $\pi_{21}(t)$, it follows that $\pi_{21}(t)$ and $\pi_{12}(t)$ are given in terms of $N_1(t, t')$ and $N_2(t, t')$ by the relations

$$\begin{aligned}\pi_{21}(t) &= \frac{2}{N} \sum_{t'=1}^t f_2(t, t') N_2(t, t'), \\ \pi_{12}(t) &= \frac{2}{N} \sum_{t'=1}^t f_1(t, t') N_1(t, t').\end{aligned}\quad (2.6)$$

To solve the coupled set of equations (2.5) and (2.6), we assume self-consistently that $\pi_{21}(t)$ and $\pi_{12}(t)$ are either constant or decaying in time as power laws. Therefore, we assume

$$\begin{aligned}\pi_{21}(t) &= \tilde{\pi}_{21} \left(\frac{t}{N}\right)^{-\alpha_1}, \\ \pi_{12}(t) &= \tilde{\pi}_{12} \left(\frac{t}{N}\right)^{-\alpha_2}.\end{aligned}\quad (2.7)$$

To check the self-consistent assumption Eq. (2.7), we insert it in Eqs. (2.5) and (2.6) and compute the values of the parameters α_1 , α_2 , $\tilde{\pi}_{21}$ and $\tilde{\pi}_{12}$ that determine the solution in the asymptotic limit $t \rightarrow \infty$. If $\alpha_1 = \alpha_2 = 0$, we obtain a stationary solution in which

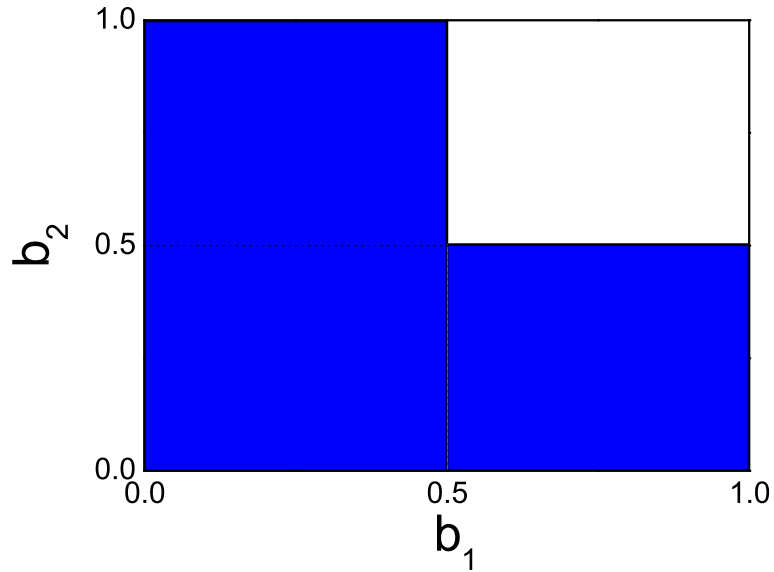


FIGURE 2.5: Phase diagram of the pairwise model of face-to-face interactions. The white area indicates the stationary regime in which the transition rate is constant. The colored (gray) area indicates the non-stationary phase.

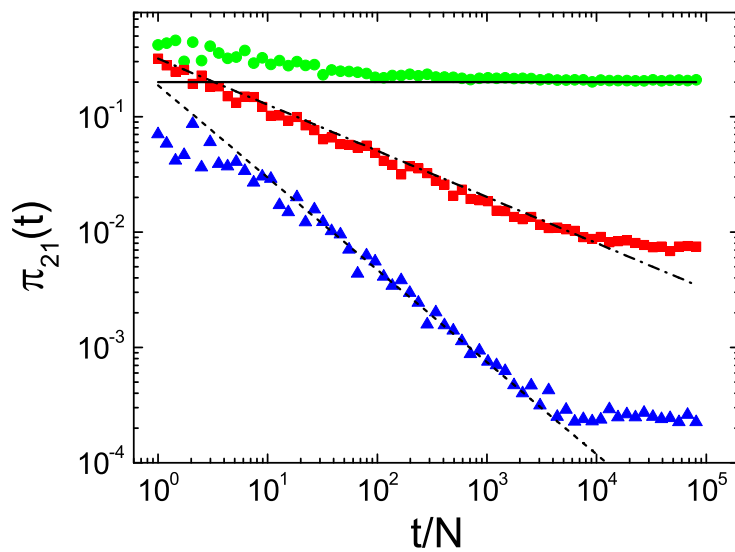


FIGURE 2.6: Evolution of the transition rate $\pi_{21}(t)$ in the different phase regions of the pairwise model of face-to-face interactions. The simulation is performed with $N = 1000$ agents for a number of time steps $T_{max} = N \times 10^5$, and averaged over 10 realizations. The simulations are performed in the stationary region with parameter values $b_1 = b_2 = 0.7$ (circles) and in the non-stationary region with parameter values $b_1 = 0.3$, $b_2 = 0.7$ (squares) and $b_1 = b_2 = 0.1$ (triangles). The lines indicate the analytical predictions Eqs. (2.7)-(2.8).

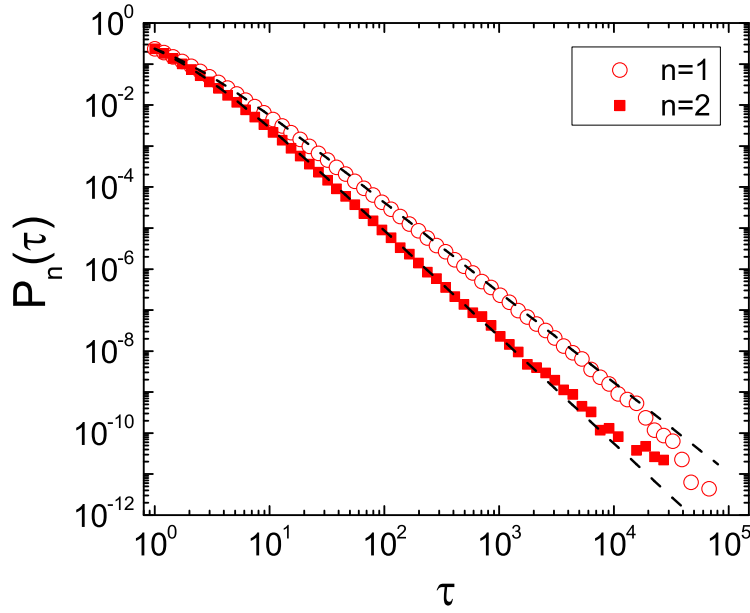


FIGURE 2.7: Probability distribution of the durations of contacts $P_2(\tau)$ and of the inter-contact durations $P_1(\tau)$ in the stationary region, for the pairwise model. The data is reported for a simulation with $N = 1000$ agents, run for $T_{max} = N \times 10^5$ elementary time steps, with parameter values $b_1 = 0.6$, $b_2 = 0.8$. The data is averaged over 10 realizations.

$\pi_{21}(t) = \tilde{\pi}_{21}$ and $\pi_{12}(t) = \tilde{\pi}_{12}$, are independent of time. On the contrary if $\alpha_1 > 0$ or $\alpha_2 > 0$, the system is non-stationary, with transition rates $\pi_{21}(t)$ and $\pi_{12}(t)$ decaying in time. The system dynamics slows down. In Appendix A, we give the details of this self-consistent calculation in the large N limit, which yields $\alpha_1 = \alpha_2 = \alpha$ and $\tilde{\pi}_{21} = \tilde{\pi}_{12} = \tilde{\pi}$, with

$$\begin{aligned} \alpha &= \max(0, 1 - 2b_2, 1 - 2b_1) \\ \tilde{\pi} &= \frac{\sin[2\pi \min(b_1, b_2)]}{\pi} [1 - \delta(\alpha, 0)] \\ &\quad + \frac{(2b_1 - 1)(2b_2 - 1)}{2(b_1 + b_2 - 1)} \delta(\alpha, 0). \end{aligned} \quad (2.8)$$

The analytically predicted dynamical behavior of the model can be summarized by the phase diagram depicted in Figure 2.5 (that we discuss now in more detail), together with the numerical simulations of the stochastic model displayed in Figure 2.6.

- *Stationary region* ($b_1 > 0.5$ and $b_2 > 0.5$) - In this region of the phase diagram, the self-consistent equation predicts $\alpha = 0$, so that a stationary state solution is expected, where $\pi_{12}(t) = \tilde{\pi}$ is given by Eq. (2.8). In this stationary state the number of isolated agents and the number of interacting agents are constant on

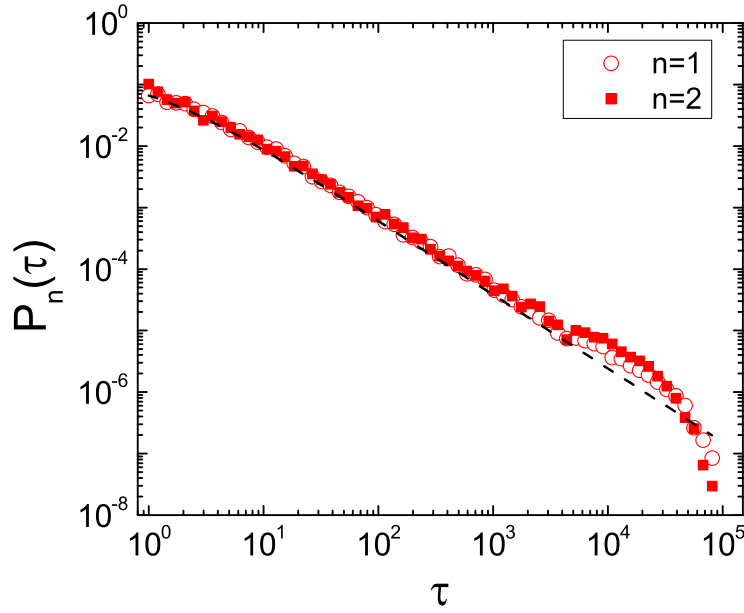


FIGURE 2.8: Probability distribution of the durations of contacts $P_2(\tau)$ and of the inter-contact durations $P_1(\tau)$ in the non-stationary region of the pairwise model, with $b_1 < 0.5$ and $b_2 < 0.5$. In this region we observe some deviations of the probabilities $P_2(\tau)$ and $P_1(\tau)$ from the power-law behavior for large durations. The data are reported for a simulation with $N = 1000$ agents run for $T_{max} = N \times 10^5$ elementary time steps, with parameter values $b_1 = b_2 = 0.1$. The data are averaged over 10 realizations.

average, but the dynamics is not frozen, since $\tilde{\pi} > 0$: agents continuously form and leave pairs. The simulations shown in Figure 2.6 for $b_1 = b_2 = 0.7$ confirm this analytical prediction.

- *Non stationary region ($b_1 < 0.5$ or $b_2 < 0.5$)* - In this region of the phase diagram, the self-consistent equation predicts a non-stationary solution with $\pi_{21}(t)$ and $\pi_{12}(t)$ decaying with t as a power-law of exponent $\alpha = \max(1 - 2b_1, 1 - 2b_2)$. Figure 2.6 shows such a decay for $b_1 = 0.3$, $b_2 = 0.7$ and for $b_1 = b_2 = 0.1$, which is however truncated by finite-size effects for t larger than $t_c(N) \propto N$. Therefore the system eventually becomes stationary with a very slow dynamics (very small transition rates $\pi_{21}(t)$ and $\pi_{12}(t)$).

Empirical studies often focus on the statistics of contact durations between individuals, and of the time intervals between two contacts of a given individual. These quantities of interest can be computed in our model, respectively, as the probabilities $P_2(\tau)$ that an agent remains in a pair during a time $\tau = (t - t')/N$, and $P_1(\tau)$ that an agent remains isolated for a time interval $\tau = (t - t')/N$. These probabilities are determined by the numbers of agents in each state and the rates at which the agents change their state. The probability distributions of the time spent in each state, integrated between the

initial time and an arbitrary time t , are given by

$$P_n(\tau) \propto \int_{t'=0}^{t-N\tau} f_n(t' + N\tau, t') N_n(t' + N\tau, t') dt' \quad (2.9)$$

for $n = 1, 2$. Inserting the expression given by Eq. (2.5) for $N_n(t, t')$ and the definition of $p_n(t, t')$ given by Eq. (2.3) in Eq. (2.9), we obtain the power-law distributions

$$P_n(\tau) \propto (1 + \tau)^{-2b_n - 1} \quad (2.10)$$

for $n = 1, 2$. These analytical predictions are compared with numerical simulations in Figure 2.7 for $b_1 = 0.6$, $b_2 = 0.8$ (stationary system) and in Figure 2.8 for $b_1 = b_2 = 0.1$ (non-stationary π_{21} and π_{12}). Interestingly, even when the system is non-stationary, the distributions $P_n(\tau)$ remain stationary.

2.4.2 Formation of groups of any size

In this subsection we extend the solution obtained for the pairwise model to the general model with arbitrary value of the parameter λ , where groups of any size can be formed. Therefore the coordination number n_i of each agent i can take any value up to $N - 1$. Extending the formalism used in the previous subsection, we denote by $N_n(t, t')$ the number of agents with coordination number $n = 1, 2, \dots, N$ at time t , who have not changed state since time t' . In the mean field approximation, the evolution equations for $N_n(t, t')$ are given by

$$\begin{aligned} \frac{\partial N_1(t, t')}{\partial t} &= -2 \frac{N_1(t, t')}{N} f_1(t, t') - (1 - \lambda) \epsilon(t) \\ &\quad \times \frac{N_1(t, t')}{N} f_1(t, t') + \sum_{i \geq 2} \pi_{i,1}(t) \delta_{tt'}, \\ \frac{\partial N_2(t, t')}{\partial t} &= -2 \frac{N_2(t, t')}{N} f_2(t, t') \\ &\quad + [\pi_{1,2}(t) + \pi_{3,2}(t)] \delta_{tt'}, \\ \frac{\partial N_n(t, t')}{\partial t} &= -n \frac{N_n(t, t')}{N} f_2(t, t') \\ &\quad + [\pi_{n-1,i}(t) + \pi_{n+1,n}(t) + \pi_{1,n}(t)] \delta_{tt'}, \quad n \geq 3. \end{aligned} \quad (2.11)$$

In these equations, the parameter $\epsilon(t)$ indicates the rate at which isolated nodes are introduced by another agent in already existing groups of interacting agents. Moreover, $\pi_{mn}(t)$ indicates the transition rate at which agents change coordination number from m to n (i.e. $m \rightarrow n$) at time t . In the mean-field approximation the value of $\epsilon(t)$ can be

expressed in terms of $N_n(t, t')$ as

$$\epsilon(t) = \frac{\sum_{n \geq 2} \sum_{t'=1}^t N_n(t, t') f_2(t, t')}{\sum_{t'=1}^t N_2(t, t') f_2(t, t')}. \quad (2.12)$$

In the case of reinforcement dynamics described by the probabilities $f_n(t, t')$ given by Eq. (2.3), and assuming that asymptotically in time $\epsilon(t)$ converges to a time-independent variable, that is, $\lim_{t \rightarrow \infty} \epsilon(t) = \hat{\epsilon}$, the solution to the rate equations (2.11) in the large time limit is given by

$$\begin{aligned} N_1(t, t') &= N_1(t', t') \left(1 + \frac{t - t'}{N}\right)^{-b_1[2+(1-\lambda)\hat{\epsilon}]}, \\ N_2(t, t') &= N_2(t', t') \left(1 + \frac{t - t'}{N}\right)^{-2b_2}, \\ N_n(t, t') &= N_n(t', t') \left(1 + \frac{t - t'}{N}\right)^{-nb_1} \quad \text{for } n \geq 2, \end{aligned} \quad (2.13)$$

with

$$\begin{aligned} N_1(t', t') &= \sum_{n \geq 2} \pi_{n,1}(t'), \\ N_2(t', t') &= \pi_{1,2}(t') + \pi_{3,2}(t'), \\ N_n(t', t') &= \pi_{n-1,n}(t') + \pi_{n+1,n}(t') + \pi_{1,n}(t') \quad \text{for } n \geq 3. \end{aligned} \quad (2.14)$$

The transition rates $\pi_{m,n}(t)$ can be determined in terms of $N_n(t, t')$ as shown in the Appendix A. In order to solve the equations we make the further assumption that the transition rates $\pi_{mn}(t)$ are either constant or decaying with time according to a power law, that is.

$$\pi_{m,n}(t) = \tilde{\pi}_{m,n} \left(\frac{t}{N}\right)^{-\alpha_{m,n}}. \quad (2.15)$$

Self-consistent calculations (see Appendix A) determine the value of the quantities $\hat{\epsilon}$, α_{mn} , and $\tilde{\pi}_{mn}$. For $\lambda > 0.5$ the self-consistent assumption Eq. (2.15) is valid and we find, as in the case of pairwise interactions, that $\alpha_{m,n} = \alpha \forall (m, n)$, with

$$\alpha = \max \left(0, 1 - b_1 \frac{3\lambda - 1}{2\lambda - 1}, 1 - 2b_2 \right). \quad (2.16)$$

This solution generalizes the case of the pairwise model, which is recovered by setting $\lambda = 1$. For $\lambda \leq 0.5$ the self-consistent assumption breaks down and we will resort to numerical simulations.

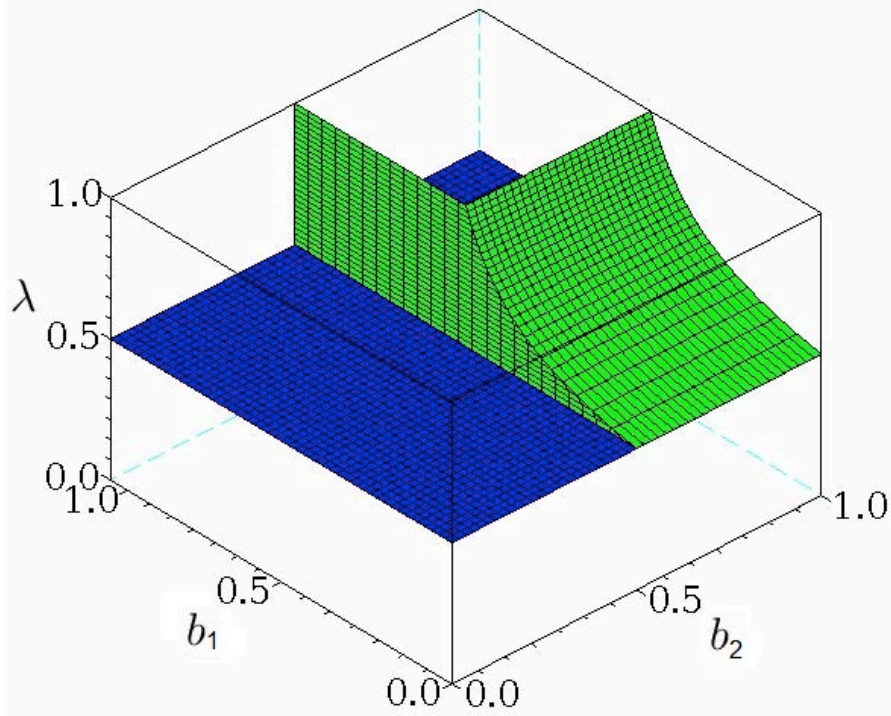


FIGURE 2.9: Phase diagram of the general model of face-to-face interactions with formation of groups of arbitrary size. The region behind the green surface corresponds to the stationary phase [i.e., Region (I), with $\lambda > 0.5$, $b_2 > 0.5$ and $b_1 > \frac{2\lambda-1}{3\lambda-1}$]. The region in front of the green surface and above the blue one [Region (II)] corresponds to a non-stationary system with decaying transition rates. Strong finite size effects with a temporary formation of a large cluster are observed in the region below the blue surface [i.e., Region (III) with $\lambda < 0.5$].

The probability distributions of the time spent in each state, integrated between the initial time and an arbitrary time t , are given by

$$P_n(\tau) \propto \int_{t'=0}^{t-N\tau} p_n(t' + N\tau, t') N_n(t' + N\tau, t') dt'. \quad (2.17)$$

Inserting the expression given by Eq. (2.13) for $N_n(t, t')$ and the definition of $p_n(t, t')$ given by Eq. (2.3) in Eq. (2.17), we obtain the power-law distributions

$$\begin{aligned} P_1(\tau) &\propto (1 + \tau)^{-b_1[2+(1-\lambda\hat{\epsilon})]-1} \\ P_n(\tau) &\propto (1 + \tau)^{-nb_2-1} \text{ for } n \geq 2. \end{aligned} \quad (2.18)$$

The phase diagram of the model is summarized in Figure 2.9. We can distinguish between three phases.

- *Region (I) -The stationary region:* $b_2 > 0.5$, $b_1 > (2\lambda - 1)/(3\lambda - 1)$ and $\lambda > 0.5$ - In this region, the self-consistent solution yields $\alpha = 0$: the transition rates $\pi_{mn}(t)$ converge rapidly to a constant value (see Figure 2.10 for a comparison between numerics

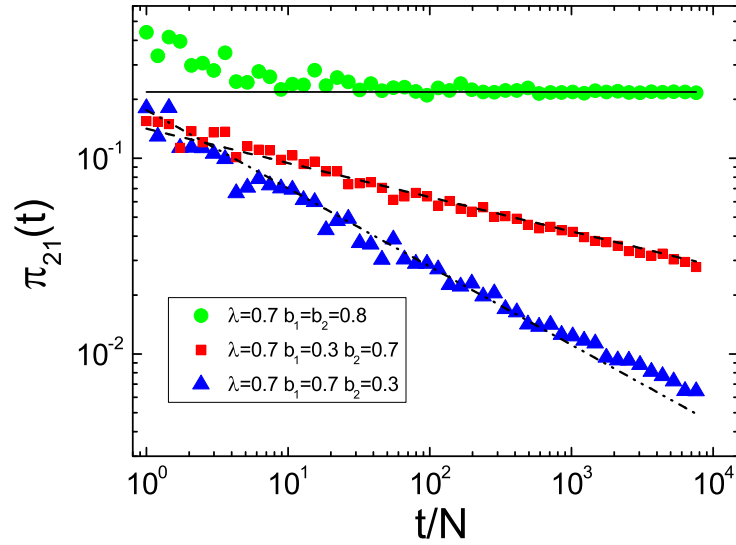


FIGURE 2.10: Transition rate $\pi_{21}(t)$ for the model of face-to-face interactions in the presence of groups of any size, for different parameters λ , b_1 , b_2 corresponding to the different regions of the phase diagram. The straight lines correspond to the analytical predictions. The simulation is performed with $N = 1000$ agents for a number of time steps $T_{max} = N \times 10^4$. The data are averaged over 10 realizations.

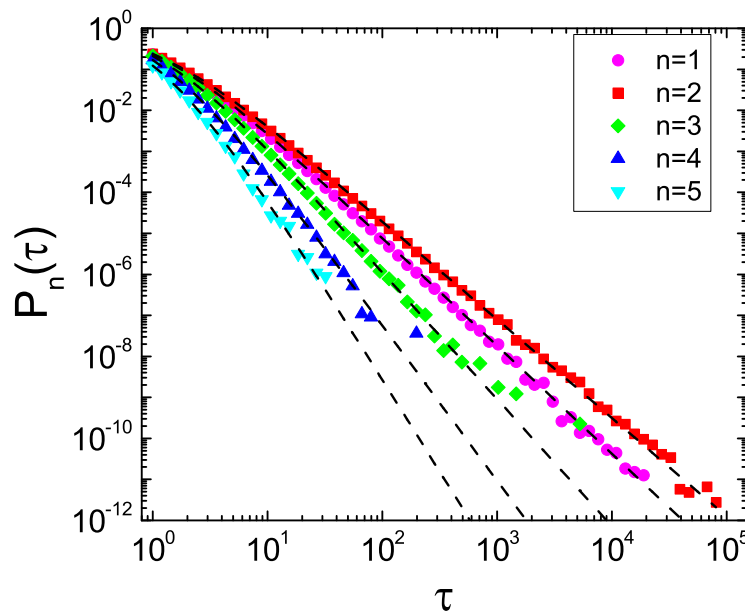


FIGURE 2.11: Distribution $P_n(\tau)$ of durations of groups of size n in the stationary region for the model of face-to-face interactions. The simulation is performed with $N = 1000$ agents for a number of time steps $T_{max} = N \times 10^5$. The parameter used are $b_1 = b_2 = 0.7$, $\lambda = 0.8$. The data are averaged over 10 realizations. The dashed lines correspond to the analytical predictions Eqs. (2.18).

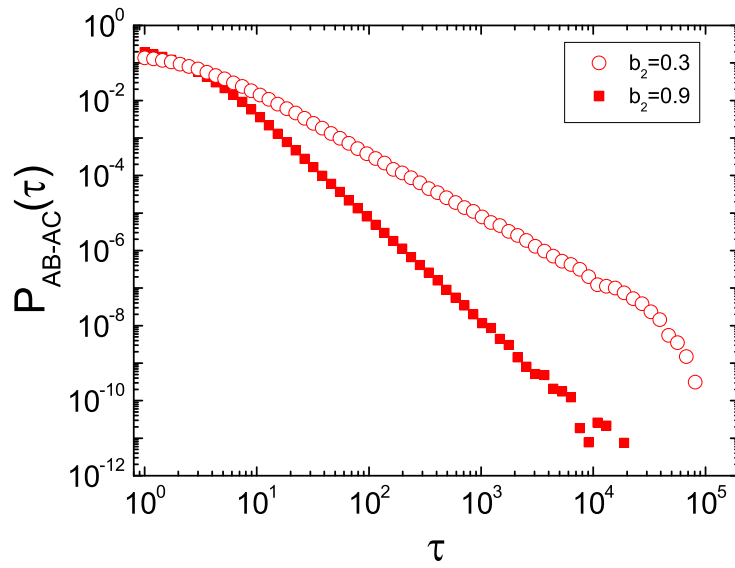


FIGURE 2.12: Distribution of time intervals between successive contacts of an individual for the model of face-to-face interactions with $\lambda = 0.8$, $b_1 = 0.7$ and $b_2 = 0.3$ and 0.9 . The simulation is performed with $N = 10^4$ for a number of time steps $T_{max} = N \times 10^5$. The data are averaged over 10 realizations.

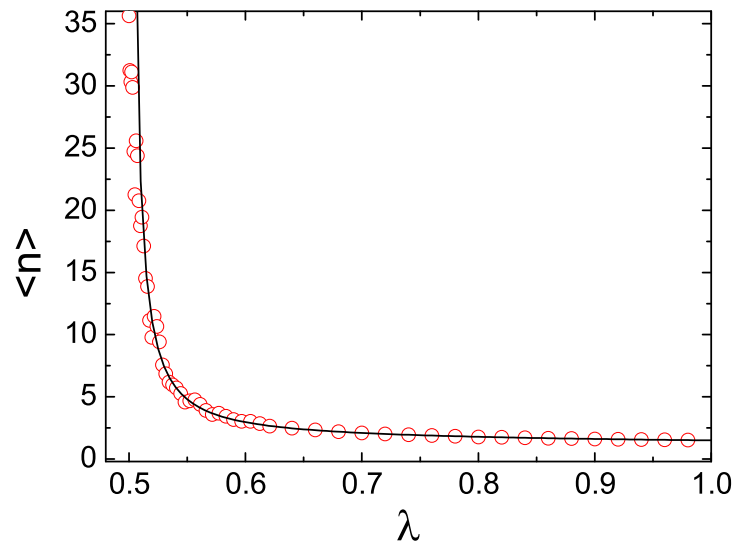


FIGURE 2.13: Average coordination number $\langle n \rangle$ vs λ for the model of face-to-face interactions with $b_1 = b_2 = 0.7$. The simulation is performed with $N = 2000$ agents for a number of time steps $T_{max} = N \times 10^3$. $\langle n \rangle$ is computed in the final state over 30 realizations. The solid line indicates the theoretical prediction given by Eq. (2.19).

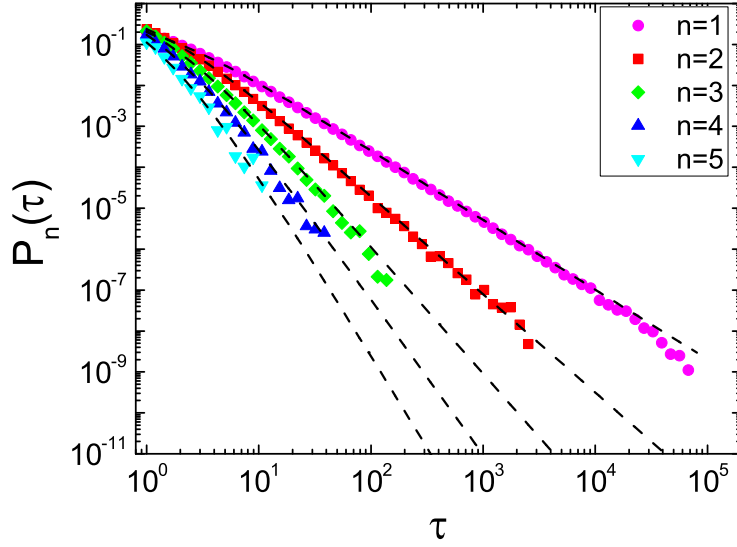


FIGURE 2.14: Distribution $P_n(\tau)$ of durations of groups of size 1 for the model of face-to-face interactions in the non-stationary region, i.e. Region (II). The simulation is performed with $N = 1000$ agents for a number of time steps $T_{max} = N \times 10^5$. The parameter used are $b_1 = 0.3$ and $b_2 = 0.7$, $\lambda = 0.8$. The data are averaged over 10 realizations. The dashed lines correspond to the analytical predictions Eqs. (2.18).

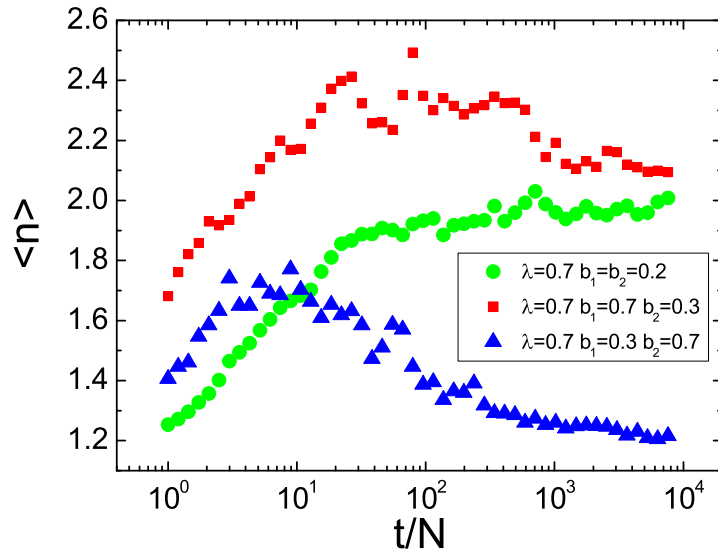


FIGURE 2.15: Average coordination number $\langle n \rangle$ for the model of face-to-face interactions as a function of time in Region (II) of the phase diagram for different values of the parameters λ , b_1 and b_2 . The data is in very good agreement with the theoretical expectations given by Eqs. (2.20) – (2.21). The simulations are performed with $N = 1000$ agents for a number of time steps $T_{max} = N \times 10^4$. The data are averaged over 10 realizations.

and analytics for $\pi_{21}(t)$ and the system reaches a stationary state. In Figure 2.11 we compare the analytical solution given by Eqs. (2.18) with the numerical simulations in the stability region, finding perfect agreement. As predicted by Eqs. (2.18), $P_n(\tau)$ decays faster as n increases: larger groups are less stable than smaller ones, as found in the empirical data sets. Figure 2.12 displays the distribution $P_{AB-AC}(\tau)$ of time intervals between the start of two consecutive contacts of a given individual, which is as well stationary and displays a power-law behavior.

The average coordination number $\langle n \rangle$ is given by

$$\langle n \rangle = \frac{\pi_{21}}{2\lambda} \sum_{n \geq 2} \frac{n(n-1)}{nb_2 - 1} \left(\frac{1-\lambda}{\lambda} \right)^{n-2}, \quad (2.19)$$

where the detailed calculation and the value of $\pi_{21}(t)$ are given in Appendix A. This expression diverges as $\lambda \rightarrow 0.5$. In Figure 2.13 we show the perfect agreement between the result of numerical simulations of $\langle n \rangle$ and the theoretical prediction.

- *Region (II) -Non-stationary region:* $b_2 < 0.5$ or $b_1 < (2\lambda - 1)/(3\lambda - 1)$, and $\lambda > 0.5$ - The dynamics in this region is non-stationary and the transition rate is decaying with time as a power-law, as shown in Figure 2.10 where we report $\pi_{21}(t)$ as a function of t . Nevertheless, the distributions of lifetimes of groups of various sizes $P_n(\tau)$, and of inter-contact times $P_{AB-AC}(\tau)$, remain stationary. These distributions are shown in Figure 2.14 and Figure 2.12. In this region, the average coordination number in the limit $t/N \gg 1$ remains small, even as $\lambda \rightarrow 0.5$. In particular from the mean-field solution of the dynamics (see appendix A) the theoretical solution of the model predicts that, for $\lambda > 0.5$ and $t \rightarrow \infty$

$$\langle n \rangle = 2 \quad \text{for } \alpha = 1 - 2b_2, \quad (2.20)$$

and

$$\langle n \rangle = 1 \quad \text{for } \alpha = 1 - b_1 \frac{3\lambda - 1}{2\lambda - 1}. \quad (2.21)$$

Figure 2.15 shows the agreement of this predicted behavior with simulation results for several values of b_1 and b_2 and $\lambda = 0.7$. In this region, as $\lambda \rightarrow 0.5$ with fixed b_1 and b_2 , we have $\alpha = 1 - 2b_2$ and $\langle n \rangle \rightarrow 2$. Therefore no diverging behavior is observed.

- *Region (III) Strong dependence on the number of agents N and non-stationary dynamics:* $\lambda < 0.5$ - In this region the self-consistent assumption given by Eq. (2.15) breaks down, and we find numerically that the average coordination number $\langle n \rangle$ strongly depends on the number of agents N and on time. In order to give a typical example of the corresponding dynamical behavior, Figure 2.16 displays $\langle n \rangle$ as a function of time

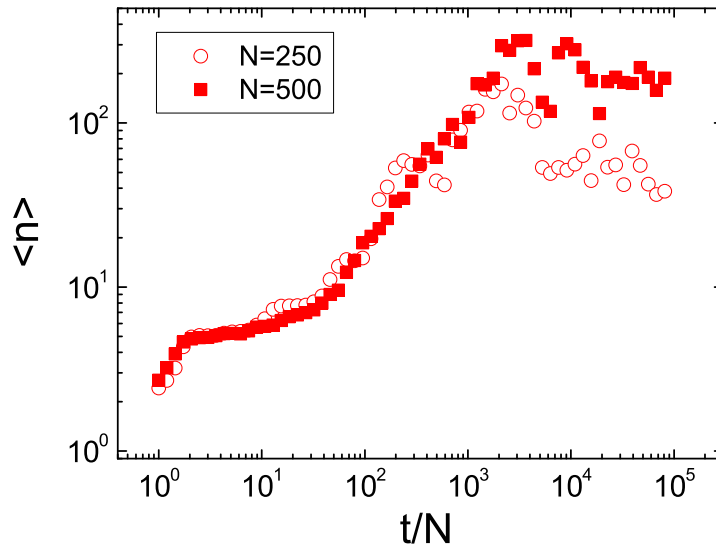


FIGURE 2.16: Average coordination number $\langle n \rangle$ for the model of face-to-face interactions with $\lambda = 0.2$, $b_1 = b_2 = 0.7$. The simulations of a single realization are performed with $N = 250$ and $N = 500$ agents, respectively, for a number of time steps $T_{max} = N \times 10^5$.

for two single realizations of the model corresponding to two different values of N . Interestingly, the distributions of lifetimes of groups of various sizes $P_n(\tau)$ remain stationary even in this parameter region (not shown).

2.4.3 Heterogeneous model

In the previous section, we have assumed that all the agents have the same tendency to form a group or to leave a group, that is, the probabilities p_n do not depend on the agent who performs a status update. Real social systems display however additional complexity since the social behavior of individuals may vary significantly across the population. A natural extension of the model presented above consists therefore of making the probabilities p_n dependent on the agent who is updating his/her state. To this aim, we assign to each agent i a parameter η_i that characterizes his/her propensity to form social interactions. In real networks this propensity will depend on the features of the agents [90]. In the model we assume that this propensity, that we call "sociability", is a quenched random variable, which is assigned to each agent at the start of the dynamical evolution and remains constant, and we assume for simplicity that it is uniformly distributed in $[0, 1]$. In this modified model, the probability $p_n^i(t, t')$ that an agent i with coordination number n since time t' changes his/her coordination number at time t is

given by

$$\begin{aligned} f_1^i(t, t') &= \frac{\eta_i}{1 + (t - t')/N}, \\ f_n^i(t, t') &= \frac{1 - \eta_i}{1 + (t - t')/N}, \text{ for } n \geq 2. \end{aligned} \quad (2.22)$$

In this setup, the parameters (b_1, b_2) , which did not depend on i in Eq. (2.3), are replaced for each agent i by the values $(\eta_i, 1 - \eta_i)$: a large η_i corresponds to an agent who prefers not to be isolated.

The agents' heterogeneity adds a significant amount of complexity to the problem, and we have reached an analytical solution of the evolution equations only in the case of pairwise interactions ($\lambda = 1$). The general case can be studied through numerical simulations as we discuss at the end of this section.

Let us denote by $N_1(t, t', \eta)$ the number of isolated agents with parameter $\eta_i \in [\eta, \eta + \Delta\eta]$ who have not changed their state since time t' . Similarly, we indicate by $N_2(t, t', \eta, \eta')$ the number of agents in a pair joining two agents i and j with $\eta_i \in [\eta, \eta + \Delta\eta]$, $\eta_j \in [\eta', \eta' + \Delta\eta]$, who have been interacting since time t' . The mean-field equations for the model are then given by

$$\begin{aligned} \frac{\partial N_1(t, t', \eta)}{\partial t} &= -2 \frac{N_1(t, t', \eta)}{N} f_1(t, t', \eta) \\ &\quad + \pi_{21}^\eta(t) \delta_{tt'}, \\ \frac{\partial N_2(t, t', \eta, \eta')}{\partial t} &= - \frac{N_2(t, t', \eta, \eta')}{N} [f_2(t, t', \eta) + f_2(t, t', \eta')] \\ &\quad + \pi_{12}^{\eta\eta'}(t) \delta_{tt'}. \end{aligned} \quad (2.23)$$

With the expression for $p_n(t, t', \eta)$ given by Eqs.(2.22) we find

$$\begin{aligned} N_1(t, t', \eta) &= \pi_{21}^\eta(t') \left(1 + \frac{t - t'}{N}\right)^{-2\eta}, \\ N_2(t, t', \eta, \eta') &= \pi_{12}^{\eta\eta'}(t') \left(1 + \frac{t - t'}{N}\right)^{-2+\eta+\eta'}. \end{aligned} \quad (2.24)$$

The transition rate π_{21}^η gives the rate at which agents with $\eta_i \in [\eta, \eta + \Delta\eta]$ become isolated, and $\pi_{12}^{\eta\eta'}$ is the rate at which pairs ij with $\eta_i \in [\eta, \eta + \Delta\eta]$, $\eta_j \in [\eta', \eta' + \Delta\eta]$ are formed. These rates can be expressed as a function of $N_1(t, t', \eta)$ and $N_2(t, t', \eta, \eta')$ according to

$$\begin{aligned} \pi_{21}^\eta(t) &= \sum_{t', \eta'} \frac{N_2(t, t', \eta, \eta')}{N} [f_2(t, t', \eta) + f_2(t, t', \eta')], \\ \pi_{12}^{\eta\eta'}(t) &= 2 \sum_{t', t''} \frac{N_1(t, t', \eta) N_1(t, t'', \eta')}{C(t)N} f_1(t, t', \eta) f_1(t, t'', \eta'), \end{aligned} \quad (2.25)$$

where $C(t)$ is a normalization factor given by

$$C(t) = \sum_{t'=1}^t \sum_{\eta} N_1(t, t', \eta) f_1(t, t', \eta). \quad (2.26)$$

To solve this problem with the same strategy used for the model without heterogeneity we make the self-consistent assumption that the transition rates are either constant or decaying as a power law with time:

$$\pi_{21}^{\eta}(t) = \Delta\eta \tilde{\pi}_{21}^{\eta} \left(\frac{t}{N}\right)^{-\alpha(\eta)}, \quad (2.27)$$

$$\pi_{12}^{\eta\eta'}(t) = \Delta\eta \Delta\eta' \tilde{\pi}_{12}^{\eta\eta'} \left(\frac{t}{N}\right)^{-\alpha(\eta, \eta')}. \quad (2.28)$$

In appendix A we give the details of the self-consistent calculation, which leads to the analytical prediction

$$\begin{aligned} \alpha(\eta) &= \max\left(1 - 2\eta, \eta - \frac{1}{2}\right), \\ \alpha(\eta, \eta') &= \alpha(\eta) + \alpha(\eta') \end{aligned} \quad (2.29)$$

and the value of $\tilde{\pi}_{21}^{\eta}$ is given by

$$\tilde{\pi}_{21}^{\eta} = \begin{cases} \frac{\rho(\eta)}{B(1-2\eta, 2\eta)} & \eta \leq \frac{1}{2} \\ \frac{\rho(\eta)}{B(\eta-\frac{1}{2}, 1)} & \eta \geq \frac{1}{2} \end{cases}. \quad (2.30)$$

In order to check the validity of our mean-field calculation, we study the probability distribution $P_1(\tau)$ of the durations of inter-contact periods and the distribution $P_2(\tau)$ of the durations of pairwise contacts, which are given, when averaged for a total simulation time T_{max} , by

$$\begin{aligned} P_1(\tau) &\propto \int_0^{T_{max}-N\tau} dt \int_0^1 d\eta \pi_{21}^{\eta}(t) \eta (1+\tau)^{-2\eta-1}, \\ P_2(\tau) &\propto \int_0^{T_{max}-N\tau} dt \int_0^1 d\eta \int_0^1 d\eta' \pi_{12}^{\eta\eta'} \\ &\times (2 - \eta - \eta')(1 + \tau)^{\eta+\eta'-3}, \end{aligned} \quad (2.31)$$

where $\rho(\eta)$ is the probability distribution of η . In Figure 2.17 we compare the probabilities of intercontact time $P_1(\tau)$ and contact time $P_2(\tau)$ averaged over the full population together with the numerical solution of the stochastic model, showing a perfect agreement. In Figure 2.18 moreover, we show the distributions $P_1^{\eta}(\tau)$ of the contact durations of agents with $\eta_i \in (\eta, \eta + \Delta\eta)$. Power-law behaviors are obtained even at fixed sociability, and the broadness of the contact duration distribution of an agent increases with

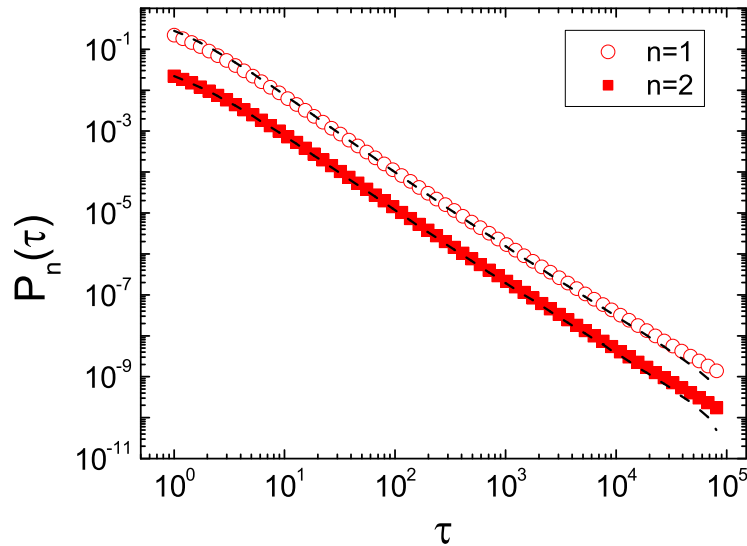


FIGURE 2.17: Distributions of times spent in state 0 and 1 for the heterogeneous model. The simulation is performed with $N = 10^4$ for a number of time steps $T_{max} = N \times 10^5$. The data are averaged over 10 realizations. The symbols represent the simulation results (circles for $n = 1$ and squares for $n = 2$). The dashed lines represent our analytical prediction. In order to improve the readability of the figure we have multiplied $P_2(\tau)$ by a factor of 10^{-1} .

the “sociability” of the agent under consideration.

As previously mentioned, the model can be extended by allowing the formation of large groups, by setting $\lambda < 1$. The results of numerical simulations performed for a particular value of λ are shown in Figure 2.19. Power law distributions of the lifetime of groups are again found and, as in the basic model without heterogeneity of the agents, larger groups are more unstable than smaller groups, as $P_n(\tau)$ decays faster if the coordination number n is larger. As the parameter $\lambda \rightarrow 0.5$ there is a phase transition and the average coordination number diverges. In Figure 2.20 we show that $\langle n \rangle - 1 \propto (\lambda - 0.5)^{-\delta}$ with $\delta = 1$ within the statistical fitting error, similarly to what happens in the homogeneous case. Overall, the main features of the model are therefore robust with respect to the introduction of heterogeneity in the agents’ individual behavior.

2.5 Model of phone-call communication

To model cell-phone communication, we consider once again a system of N agents representing the mobile phone users. Moreover, we introduce a static weighted network G , of which the nodes are the agents in the system, the edges represent the social ties between the agents, such as friendships, collaborations or acquaintances, and the weights

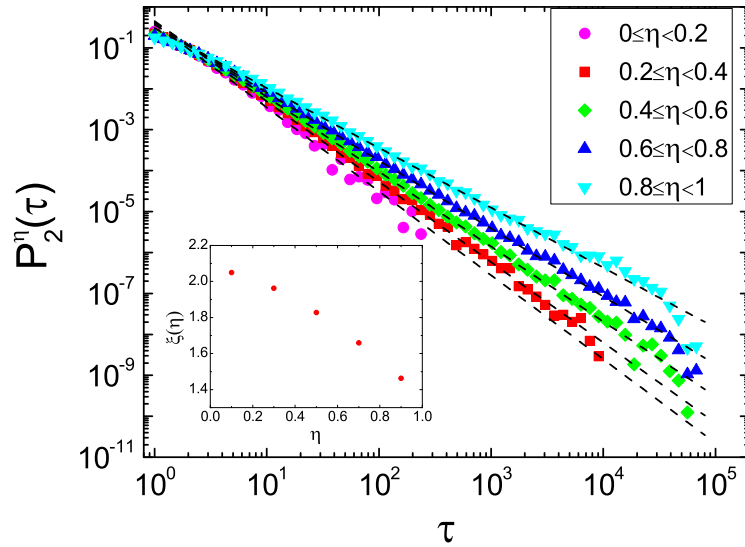


FIGURE 2.18: Distribution $P_2^\eta(\tau)$ of contact durations of individuals with sociability η in the pairwise heterogeneous model. The simulations are performed with $N = 1000$ agents and $T_{max} = N \times 10^5$ time steps. The data are averaged over 10 realizations. The data decays as a power-law $P_2^\eta(\tau) \propto \tau^{-\xi(\eta)}$, and we report the exponents $\xi(\eta)$ as a function of η in the inset.

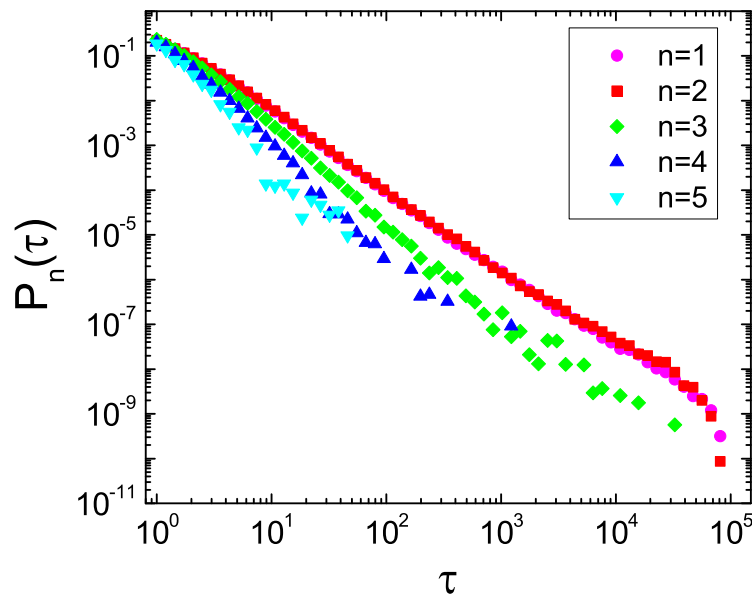


FIGURE 2.19: Distribution $P_n(\tau)$ of the durations of groups of size n in the heterogeneous model with formation of groups of any size. The data are shown for simulations of $N = 1000$ agents performed over $T_{max} = N \times 10^5$ time steps and $\lambda = 0.8$, averaged over 10 realizations.

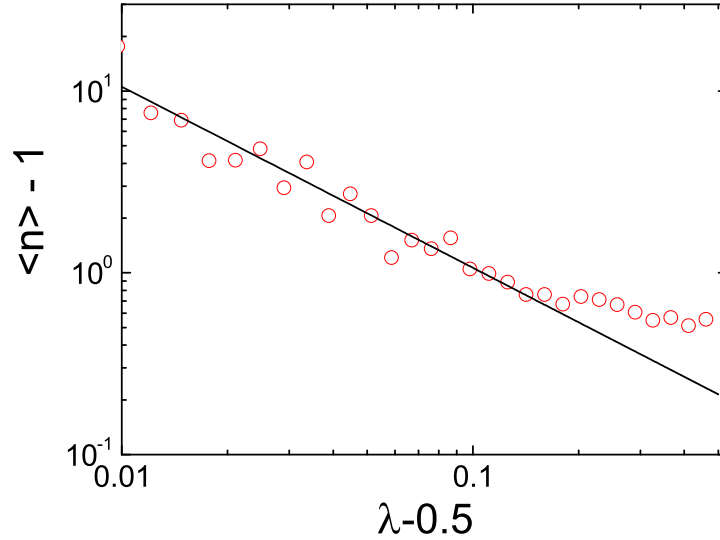


FIGURE 2.20: $\langle n \rangle - 1$ as a function of λ for the heterogeneous case where $\langle n \rangle$ is the average coordination number. The solid line indicates the best fit with $\langle n \rangle \propto (\lambda - 0.5)^{-\delta}$ with $\delta = 0.996$ in agreement with the exponent -1 within the statistical uncertainty. The data correspond to simulations of $N = 500$ agents performed over $T_{max} = N \times 10^3$ time steps. The data are averaged over 10 realizations.

of the edges indicate the strengths of the social ties. Therefore the interactions between agents can only take place along the network G (an agent can only interact with his/her neighbors on the network G). Here we propose a model for mobile-phone communication constructed with the use of the reinforcement dynamic mechanism. This model shares significant similarities with the previously discussed model for face-to-face interactions, but has two major differences. Firstly, only pairwise interactions are allowed in the case of cell-phone communication. Therefore, the state n of an agent only takes the values of either 1 (non-interacting) or 2 (interacting). Secondly, the probability that an agent ends his/her interaction depends on the weight of network G . The stochastic dynamics of phone-call communication at each time step t is then implemented as the following algorithm.

- (1) An agent i is chosen randomly at time t .
- (2) The subsequent action of agent i depends on his/her current state (i.e. n_i):
 - (i) If $n_i = 1$, he/she starts an interaction with one of his/her non-interacting neighbors j of G with probability $f_1(t_i, t)$ where t_i denotes the last time at which agent i has changed his/her state. If the interaction is started, agent j is chosen randomly with probability proportional to $f_1(t_j, t)$ and the coordination numbers of agent i and j are then updated ($n_i \rightarrow 2$ and $n_j \rightarrow 2$).

- (ii) If $n_i = 2$, he/she ends his/her current interaction with probability $f_2(t_i, t|w_{ij})$ where w_{ij} is the weight of the edge between i and the neighbor j that is interacting with i . If the interaction is ended, the coordination numbers of agent i and j are then updated ($n_i \rightarrow 1$ and $n_j \rightarrow 1$).
- (3) Time t is updated as $t \rightarrow t + 1/N$ (initially $t = 0$). The algorithm is repeated from (1) until $t = T_{max}$.

Here we take the probabilities $f_1(t, t')$, $f_2(t, t'|w)$ according to the following functional dependence

$$\begin{aligned} f_1(t, t') &= f_1(\tau) = \frac{b_1}{(1 + \tau)^\beta} \\ f_2(t, t'|w) &= f_2(\tau|w) = \frac{b_2 g(w)}{(1 + \tau)^\beta} \end{aligned} \quad (2.32)$$

where the parameters are chosen in the range $b_1 > 0$, $b_2 > 0$, $0 \leq \beta \leq 1$, $g(w)$ is a positive decreasing function of its argument, and τ is given by $\tau = (t - t')/N$.

In order to solve the model analytically, we assume the quenched network G to be annealed and uncorrelated. Here we outline the main result of this approach and the details of the calculations are given in Appendix B. Therefore we assume that the network is rewired while the degree distribution $p(k)$ and the weight distribution $p(w)$ remain constant. We denote by $N_1^k(t, t')$ the number of non-interacting agents with degree k at time t who have not changed their state since time t' . Similarly we denote by $N_2^{k, k', w}(t, t')$ the number of interacting agent pairs (with degree respectively k and k' and weight of the edge w) at time t who have not changed their states since time t' . In the annealed approximation the probability that an agent with degree k is called by another agent is proportional to its degree. Therefore the evolution equations of the model are given by

$$\begin{aligned} \frac{\partial N_1^k(t, t')}{\partial t} &= -\frac{N_1^k(t, t')}{N} f_1(t - t') - ck \frac{N_1^k(t, t')}{N} f_1(t - t') + \pi_{21}^k(t) \delta_{tt'} \\ \frac{\partial N_2^{k, k', w}(t, t')}{\partial t} &= -2 \frac{N_2^{k, k', w}(t, t')}{N} f_2(t - t'|w) + \pi_{12}^{k, k', w}(t) \delta_{tt'} \end{aligned} \quad (2.33)$$

where the constant c is given by

$$c = \frac{\sum_{k'} \int_0^t dt' N_1^{k'}(t, t') f_1(t - t')}{\sum_{k'} k' \int_0^t dt' N_1^{k'}(t, t') f_1(t - t')}. \quad (2.34)$$

In Eqs. (2.33) the rates $\pi_{pq}(t)$ indicate the average number of agents changing from state $p = 1, 2$ to state $q = 1, 2$ at time t . The solution of the dynamics must of course

satisfy the conservation equation

$$\int dt' [N_1^k(t, t') + \sum_{k', w} N_2^{k, k', w}(t, t')] = Np(k). \quad (2.35)$$

In the following we will denote by $P_1^k(t, t')$ the probability distribution that an agent with degree k is non-interacting in the period between time t' and time t and we will denote by $P_2^w(t, t')$ the probability that an interaction of weight w is lasting from time t' to time t which satisfy

$$\begin{aligned} P_1^k(t, t') &= (1 + ck)f_1(t, t')N_1^k(t, t') \\ P_2^w(t, t') &= 2f_2(t, t'|w) \sum_{k, k'} N_2^{k, k', w}(t, t'). \end{aligned} \quad (2.36)$$

As a function of the value of the parameter of the model we found different distribution of duration of contacts and non-interaction times.

- *Case* $0 < \beta < 1$. The system allows always for a stationary solution with $N_1^k(t, t') = N_1^k(\tau)$ and $N_2^{k, k', w}(t, t') = N_2^{k, k', w}(\tau)$. The distribution of duration of non-interaction times $P_1^k(\tau)$ for agents of degree k in the network and the distribution of interaction times $P_2^w(\tau)$ for links of weight w is given by

$$\begin{aligned} P_1^k(\tau) &\propto \frac{b_1(1 + ck)}{(1 + \tau)^\beta} e^{-\frac{b_1(1+ck)}{1-\beta}(1+\tau)^{1-\beta}} \\ P_2^w(\tau) &\propto \frac{2b_2g(w)}{(1 + \tau)^\beta} e^{-\frac{2b_2g(w)}{1-\beta}(1+\tau)^{1-\beta}}. \end{aligned} \quad (2.37)$$

Rescaling Eqs.(2.37), we obtain the Weibull distribution which is in good agreement with the results observed in mobile-phone datasets.

- *Case* $\beta = 1$. Another interesting limiting case of the mobile-phone communication model is the case $\beta = 1$ for which we have $f_1^k(\tau) \propto (1 + \tau)^{-1}$ and $f_2^w(\tau|w) \propto (1 + \tau)^{-1}$. In this case the model is much similar to the model used to mimic face-to-face interactions described in the previous subsection [85, 96], but the interactions are binary and they occur on a weighted network. In this case we get the solution

$$\begin{aligned} N_1^k(\tau) &= N\pi_{21}^k (1 + \tau)^{-b_1(1+ck)} \\ N_2^{k, k', w}(\tau) &= N\pi_{12}^{k, k', w} (1 + \tau)^{-2b_2g(w)}. \end{aligned} \quad (2.38)$$

and consequently the distributions of duration of given states Eqs. (2.36) are given by

$$\begin{aligned} P_1^k(\tau) &\propto \pi_{21}^k (1 + \tau)^{-b_1(1+ck)-1} \\ P_2^w(\tau) &\propto \pi_{12}^{k,k',w} (1 + \tau)^{-2b_2g(w)-1}. \end{aligned} \quad (2.39)$$

The probability distributions are power-laws. This result remains valid for every value of the parameters $b_1, b_2, g(w)$ nevertheless the stationary condition is only valid for

$$\begin{aligned} b_1(1 + ck) &> 1 \\ 2b_2g(w) &> 1. \end{aligned} \quad (2.40)$$

Indeed this condition ensures that the self-consistent constraints Eqs. (2.34), and the conservation law Eq. (2.35) have a stationary solution.

- *Case $\beta = 0$* This is the case in which the process described by the model is a Poisson process and there is no reinforcement dynamics in the system. Therefore we find that the distribution of durations are exponentially distributed. In fact for $\beta = 0$ the functions $f_1(\tau)$ and $f_2(\tau|w)$ given by Eqs.(2.32) reduce to constants, therefore the process of creation of an interaction is a Poisson process. In this case the social interactions do not follow the reinforcement dynamics. The solution that we get for the number of non interacting agents of degree k , $N_1^k(\tau)$ and the number of interacting pairs $N_2^{k,k',w}(\tau)$ is given by

$$\begin{aligned} N_1^k(\tau) &= N\pi_{21}^k e^{-b_1(1+ck)\tau} \\ N_2^{k,k',w}(\tau) &= N\pi_{12}^{k,k',w} e^{-2b_2g(w)\tau}. \end{aligned} \quad (2.41)$$

Consequently the distributions of duration of given states Eqs. (2.36) are given by

$$\begin{aligned} P_1^k(\tau) &\propto e^{-b_1(1+ck)\tau} \\ P_2^w(\tau) &\propto e^{-2b_2g(w)\tau}. \end{aligned} \quad (2.42)$$

Therefore the probability distributions $P_1^k(\tau)$ and $P_2^w(\tau)$ are exponentials as expected in a Poisson process.

2.6 Conclusion

The goal of network science is to model, characterize, and predict the behavior of complex networks. In this chapter, we have focused on modelling phenomenologically social interactions on the fast time scale, such as face-to-face interactions and mobile phone communication activity. We have found that human social interactions are bursty and adaptive. Indeed, the duration of social contacts can be modulated by the adaptive behavior of humans: while in face-to-face interactions dataset a power-law distribution of duration of contacts has been observed, we have found, from the analysis of a large dataset of mobile-phone communication, that mobile-phone calls are distributed according to a Weibull distribution. Moreover, we have modeled this adaptive behavior by assuming that the dynamics underlying the formation of social contacts implements a reinforcement dynamics. Finally, we have concluded that the duration of social contacts in humans has a distribution that strongly deviates from an exponential.

Chapter 3

Entropy of Temporal Networks and Growing Networks

New entropy measures have been recently introduced for the quantification of the complexity of networks. Nevertheless, most of these entropy measures apply to static networks or to dynamical processes defined on static networks. In this chapter, we investigate entropy of temporal networks and growing networks in which nodes and links are not static. In temporal networks, nodes and links are created and annihilated over time. In growing networks, nodes and links are continuously added to the system. In particular, as a solid example of temporal networks, we investigate the entropy of temporal social networks formed by human contacts such as face-to-face interactions and phone calls. Moreover, we investigate the entropy rate of growing network models, which quantifies how many labeled networks are typically generated by the growing network models. This chapter is based on the author's work [85, 86, 100].

3.1 Background

One of the outstanding problems in statistical mechanics of complex networks is to quantify the complexity of networks. Recently, new entropy measures have been introduced to tackle this problem [69–73, 90, 106–117]. Methods for quantifying complexity are not only valuable from the theoretical point of view, but may also lead to important operational interpretations. In fact, it opens the way for a new information theory of complex network topologies which will provide an evaluation of the information encoded in complex networks.

3.1.1 Entropy measures of social networks and human social behaviors

Networks encode information in their topological structures. In social networks [93, 94] this information is essential to build strong collaborations [118] that enhance the performance of a society, to build reputation trust and to navigate [119] efficiently the networks. Therefore to understand how social network evolve, adapt and respond to external stimuli, we need to develop a new information theory of complex social networks.

Recently, attention has been addressed to entropy measures of email correspondence [52] and mobility patterns [43]. It has been shown that mutual information for the data of email correspondence can characterize the community structure of the networks and the entropy of human mobility is able to set the limit of predictability of human movements [43]. Still we lack methods to assess the information encoded in the dynamical social interaction networks.

Social networks are characterized by complex organizational structures revealed by network community and degree correlations [88]. These structures are sometimes correlated with annotated features of the nodes or of the links such as age, gender, and other annotated features of the links such as shared interests, family ties or common work locations [28, 89]. It has been shown by studying social, technological and biological networks that the network entropy measures can assess how significant are the annotated features for the network structure [90].

Moreover social networks evolve on many different time-scales and relevant information is encoded in their dynamics. Indeed social ties can appear or disappear depending on the dynamical process occurring on the networks such as epidemic spreading or opinion dynamics. Several models for adaptive social evolution have been proposed showing phase transitions in different universality classes [29–32]. Social ties have in addition to that a microscopic structure constituted by fast social interactions of the duration of a phone call or of a face-to-face interaction. In fact, as discussed in the previous chapter, most human social interactions in short-time scale can be modelled in the framework of temporal social networks. Therefore, to develop a better way of assessing the information encoded in human social behaviors, new tools of information theory such as entropy measures for temporal social networks are needed.

3.1.2 Entropy measures of complex networks

Recently, various entropy measures of complex networks based on network ensembles have been proposed. The entropy of network ensembles quantifies the number of graphs

with given structural features such as degree distribution, degree correlations, community structure or spatial embedding [69–72, 107–109, 120]. This quantity is very useful for inference problems defined on networks and it has been successfully applied to the problem of assessing the significance of features for network structure [90]. Other entropy measures of quantum mechanical nature have been derived by mapping the network either to a density matrix or to a quantum state [73, 112–114]. These entropies, defined on single networks, set a path for the application of tools of quantum information theory to describe the complexity of single networks and to introduce new kind of network parameters (for example, by considering the notion of correlations and subsystems). Entropy rate of random walks on networks [115–117] are extensively studied as well. Such entropy rate can predict how evenly the random walk spreads in the network and help construct maximally entropic random walks for many applications.

3.1.3 Motivation

One should note that most of these studies on entropy measures of complex networks in the last decade have been focusing on static networks or dynamical processes defined on static networks, with little emphasis on networks in which nodes and links are not static but time-varying, e.g. temporal networks or growing networks. In other words we still lack a general framework for entropy measures of time-varying networks. In this chapter, to fill the gap, we propose a new framework for entropy measures of temporal social networks, which can be applied to most circumstances of human social interactions in short-time scale. Moreover, we define and measure the entropy rate of growing network models.

3.2 Entropy of temporal social networks

In this section we characterize the entropy of temporal social networks as a proxy to characterize the predictability of the dynamical nature of social interaction networks. This entropy quantifies how many typical distribution of configuration we expect at any given time, given the history of the network dynamical process. We evaluate this entropy on a typical day of mobile-phone communication directly from data showing modulation of the dynamical entropy during the circadian rhythm. Moreover we show that when the distribution of duration of contacts changes from a power-law distribution to a Weibull distribution the level of information and the value of the dynamical entropy significantly change indicating that human adaptability to new technology is a further way to modulate the information content of dynamical social networks.

3.2.1 Definition

In this subsection we will define the entropy of temporal social networks as a measure of information encoded in their dynamics. We assume that the following stochastic dynamics takes place in the network: according to this dynamics at each time step t , different interacting groups can appear and disappear giving rise to the temporal social network. The agents are embedded in a social network G such that interaction can occur only by acquaintances between first neighbors of the network G . This is a good approximation if we want to model social interactions on the fast time scale. In the case of a small conference, where each participant is likely to discuss with any other participant we can consider a fully connected network as the underlying network G of social interactions. In the network G each set of interacting agents can be seen as a connected subgraph of \mathcal{G} , as shown in Figure 3.1. We use an indicator function $g_{i_1, i_2, \dots, i_n}(t)$ to denote, at time t , the maximal set i_1, i_2, \dots, i_n of interacting agents in a group. If (i_1, i_2, \dots, i_n) is the maximal set of interacting agents in a group, we let $g_{i_1, i_2, \dots, i_n}(t) = 1$ otherwise we put $g_{i_1, i_2, \dots, i_n}(t) = 0$. Therefore at any given time the following relation is satisfied,

$$\sum_{\mathcal{G}=(i_1, i_2, \dots, i_n) | i \in \mathcal{G}} g_{i_1, i_2, \dots, i_n}(t) = 1. \quad (3.1)$$

where \mathcal{G} is an arbitrary connected subgraph of G . Then we denote by

$$\mathcal{S}_t = \{g_{i_1, i_2, \dots, i_n}(t') \forall t' < t\}$$

the history of the dynamical social networks, and $p(g_{i_1, i_2, \dots, i_n}(t) = 1 | \mathcal{S}_t)$ the probability that $g_{i_1, i_2, \dots, i_n}(t) = 1$ given the history \mathcal{S}_t . Therefore the likelihood that at time t the dynamical social networks has a group configuration $g_{i_1, i_2, \dots, i_n}(t)$ is given by

$$\mathcal{L} = \prod_{\mathcal{G}} p(g_{i_1, i_2, \dots, i_n}(t) = 1 | \mathcal{S}_t)^{g_{i_1, i_2, \dots, i_n}(t)}. \quad (3.2)$$

We denote the entropy of the dynamical networks as $S = -\langle \log \mathcal{L} \rangle_{\mathcal{S}_t}$ indicating the logarithm of the typical number of all possible group configurations at time t which can be explicitly written as

$$S = -\sum_{\mathcal{G}} p(g_{i_1, i_2, \dots, i_n}(t) = 1 | \mathcal{S}_t) \log p(g_{i_1, i_2, \dots, i_n}(t) = 1 | \mathcal{S}_t). \quad (3.3)$$

The value of the entropy can be interpreted as following: if the entropy is larger, the dynamical network is less predictable, and several possible dynamic configurations of

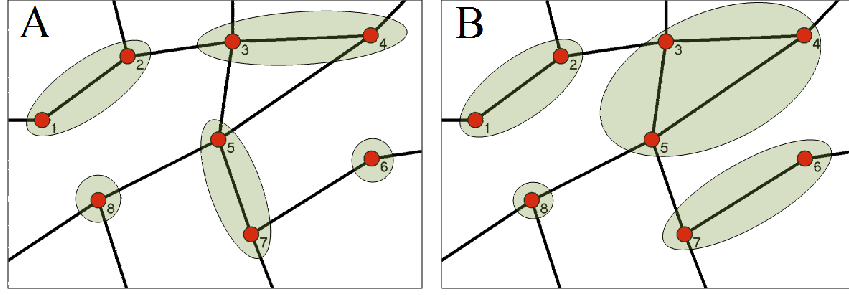


FIGURE 3.1: The dynamical social networks are composed by different dynamically changing groups of interacting agents. In panel (A) we allow only for groups of size one or two as it typically happens in mobile phone communication. In panel (B) we allow for groups of any size as in face-to-face interactions.

groups are expected in the system at time t . On the other hand, a smaller entropy indicates a smaller number of possible future configuration and a temporal network state which is more predictable.

3.2.2 Entropy of phone-call communication

In this subsection we simplify the general expansion for the entropy S of temporal networks given by Eq. (3.3) for the case of phone-call communication, we only allow pairwise interaction in the system such that the product in Eq.(3.2) is only taken over all single nodes and edges of the quenched network G which yields

$$\mathcal{L} = \prod_i p(g_i(t) = 1 | \mathcal{S}_t)^{g_i(t)} \prod_{ij|a_{ij}=1} p(g_{ij}(t) = 1 | \mathcal{S}_t)^{g_{ij}(t)} \quad (3.4)$$

with

$$g_i(t) + \sum_j a_{ij} g_{ij}(t) = 1. \quad (3.5)$$

where a_{ij} is the adjacency matrix of G . The entropy then takes a simple form

$$\begin{aligned} S &= - \sum_i p(g_i(t) = 1 | \mathcal{S}_t) \log p(g_i(t) = 1 | \mathcal{S}_t) \\ &\quad - \sum_{ij} a_{ij} p(g_{ij}(t) = 1 | \mathcal{S}_t) \log p(g_{ij}(t) = 1 | \mathcal{S}_t). \end{aligned} \quad (3.6)$$

3.2.3 Analysis of the entropy of a large dataset of mobile phone communication

In this subsection we use the entropy of temporal social networks to analyze the information encoded in a major European mobile service provider, making use of the same

dataset that we have used to measure the distribution of call duration in Section 2. Here we evaluate the entropy of the temporal networks formed by the phone-call communication in a typical week-day in order to study how the entropy of temporal social networks is affected by circadian rhythms of human behavior.

For the evaluation of the entropy of temporal social networks we consider a subset of the large dataset of mobile-phone communication. We selected 562,337 users who executed at least one call a day during a weeklong period. We denote by $f_n(t, t')$ the transition probability that an agent in state n ($n = 1, 2$) changes its state at time t given that he/she has been in his/her current state for a duration $\tau = t - t'$. The probability $f_n(t, t')$ can be estimated directly from the data. Therefore, we evaluate the entropy in a typical weekday of the dataset by using the transition probabilities $f_n(t, t')$ and the definition of entropy of temporal social networks. In Figure 3.2 we show the resulting evaluation of entropy in a typical day of our phone-call communication dataset. The entropy of the temporal social network is plotted as a function of time during one typical day. The mentioned figure shows evidence that the entropy of temporal social networks changes significantly during the day reflecting the circadian rhythms of human behavior.

More details of calculations in this subsection are given in Appendix C.

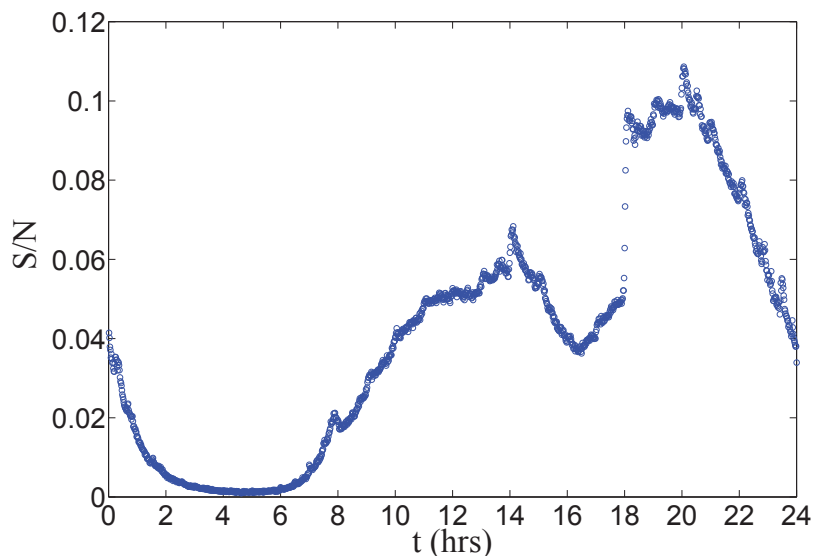


FIGURE 3.2: Mean-field evaluation of the entropy of the dynamical social networks of phone calls communication in a typical week-day. In the nights the social dynamical network is more predictable.

3.2.4 Entropy modulated by the adaptability of human behavior

The adaptability of human behavior is evident when comparing the distribution of the duration of phone-calls with the duration of face-to-face interactions, as it has been discussed in Chapter 2. In the framework of the model for mobile-phone interactions described in Chapter 2, this adaptability, can be understood, as a possibility to change the exponent β in Eqs. (2.32) regulating the duration of social interactions.

Changes in the parameter β correspond to different values entropy of the dynamical social networks. Therefore, by modulating the exponent β , the human behavior is able to modulate the information encoded in temporal social networks. In order to show the effect on entropy of a variation of the exponent β in the dynamics of social interaction networks, we considered the entropy corresponding to the model of temporal social networks described in chapter 2 as a function of the parameters β and b_1 modulating the probabilities $f_1(t, t')$, $f_2(t, t'|w)$ Eqs.(2.32). In Figure 3.3 we report the entropy S of the proposed model a function of β and b_1 . The entropy S , given by Eq.(3.6), is calculated using the annealed approximation for the solution of the model and assuming the large network limit. In the calculation of the entropy S we have taken a network of size $N = 2000$ with exponential degree distribution of average degree $\langle k \rangle = 6$, weight distribution $P(w) = Cw^{-2}$ and function $g(w) = 1/w$ and $b_2 = 0.05$. Our aim in Figure 3.3 is to show only the effects on the entropy due to the different distributions of duration of contacts and non-interaction periods. Therefore we have normalized the entropy S with the entropy S_R of a null model of social interactions in which the duration of groups are Poisson distributed but the average time of interaction and non-interaction time are the same as in the model of cell-phone communication. From Figure 3.3 we observe that if we keep b_1 constant, the ratio S/S_R is a decreasing function of the parameter β . This indicates that the broader is the distribution of probability of duration of contacts, the higher is the information encoded in the dynamics of the network. Therefore the heterogeneity in the distribution of duration of contacts and no-interaction periods implies higher level of information in the social network. The human adaptive behavior by changing the exponent β in face-to-face interactions and mobile phone communication effectively changes the entropy of the dynamical network.

More details of calculations in this subsection are given in Appendix C.

3.2.5 Remarks

In the last ten years it has been recognized that the vast majority of complex systems can be described by networks of interacting units. Network theory has made tremendous

progresses in this period and we have gained important insight into the microscopic properties of complex networks. Key statistical properties have been found to occur universally in the networks, such as the small world properties and broad degree distributions. Moreover the local structure of networks has been characterized by degree correlations, clustering coefficient, loop structure, cliques, motifs and communities. The level of information present in these characteristic of the network can be now studied with the tools of information theory. An additional fundamental aspect of social networks is their dynamics. This dynamics encode for information and can be modulated by adaptive human behavior. In this section we have introduced the entropy of social dynamical networks and we have evaluated the information present in dynamical data of phone-call communication. By analysing the phone-call interaction networks we have shown that the entropy of the network depends on the circadian rhythms. Finally we have evaluated how the information encoded in social dynamical networks change if we allow a parametrization of the duration of contacts mimicking the adaptability of human behavior. Therefore the entropy of social dynamical networks is able to quantify how the social networks dynamically change during the day and how they dynamically adapt to different technologies.

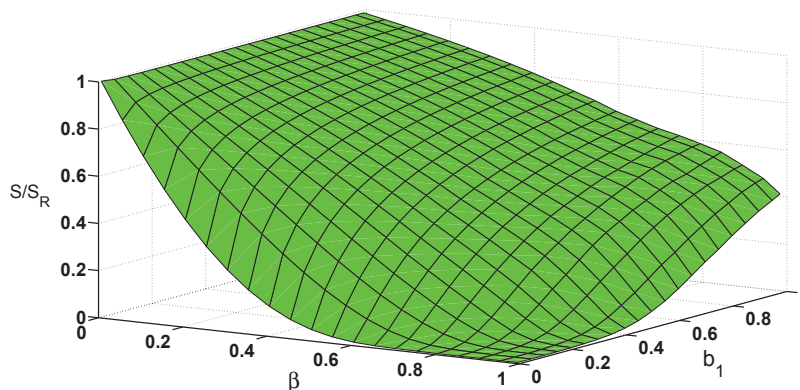


FIGURE 3.3: Entropy S of the phone-call communication model defined in Chapter 2 normalized with the entropy S_R of a null model in which the expected average duration of phone-calls is the same but the distribution of duration of phone-calls and non-interaction time are Poisson distributed. The network size is $N = 2000$ the degree distribution of the network is exponential with average $\langle k \rangle = 6$, the weight distribution is $p(w) = Cw^{-2}$ and $g(w)$ is taken to be $g(w) = b_2/w$ with $b_2 = 0.05$. The value of S/S_R is depending on the two parameters β, b_1 . For every value of b_1 the normalized entropy is smaller for $\beta \rightarrow 1$.

3.3 Entropy of growing networks

In this section we define and evaluate the entropy rate of growing network models. The literature in the field of growing network models generating scale-free networks is very large [7, 8, 11, 13, 121]. By studying the entropy rate of these models we aim at quantifying the number of typical networks that are generated by these models. Finally this entropy rate is the number of networks that is possible to construct with the same degree distribution. In order to allow for an analytic treatment of the problem, only tree networks are considered in this section. Trees are networks in which no cycle is allowed. The maximal number of possible tree networks generated by a growing network model scales like $N!$ where N is the number of nodes (and links) in the network. The minimal number of tree networks generated by a growing network model is one, corresponding to the formation of a star or of a linear chain. The entropy rate of growing scale-free networks lies in between these two limiting values. Understanding the value of the entropy of graphs is informative because it describes the complexity of growing network models. In fact the value of the entropy will quantify with a unique number the size of the space of typical networks generated by the growing network model. The smaller is the entropy rate of the networks the more complex the network structural properties implied by the growing model. In particular it is essential to determine the scaling with N of the entropy rate, and in the case in which the entropy rate is not constant but depends on N it is important to evaluate the subleading terms that encode for the topology of the networks also for other entropy measures [69, 70, 114].

The main model of growing scale-free networks is the Barabási-Albert (BA) model [22] that generates scale-free networks with power-law exponent $\gamma = 3$. The BA networks are known to have weak degree correlations due to their causal structure, while the growing network model with initial attractiveness of the nodes [2] and the fitness model [23] have more significant correlations. To quantify these correlations different measures have been introduced such as the average degree of the neighbor of the nodes or the degree correlation matrix. Still we lack a way to quantify how much information is encoded in growing network models with respect to the networks constructed by the configuration model with the same degree distribution.

Here we propose to quantify the number of typical tree graphs generated by the non-equilibrium growing network models [2–6, 22, 23] as a proxy of their complexity. This quantity can be used to measure the fraction of networks of given degree sequence that is generated by growing network models and to quantify in this way the complexity of growing network models. Moreover growing network models as the Bianconi and Barabási fitness model [5, 23] and the non-linear preferential attachment model of Krapivsky and Redner [3, 4] or the growing network model with aging of the nodes [6] are known to

undergo structural phase transitions as a function of their parameters. Interestingly these phase transitions are characterized by a sharp drop of the entropy rate and strong finite size effects indicating that the network is reduced to a more ordered state below the structural phase transition.

The remainder of this section is structured as follows. In Section 3.3.1, we define the Gibbs entropy of networks with a given degree distribution. In Section 3.3.2, we introduce the necessary material for studying the entropy rate of growing trees. Firstly, we recall the main growing network models. Then, we obtain min/max bounds to the entropy. In Section 3.3.3, we study growing trees with stationary degree distribution. In particular, we consider the BA model, initial attractiveness, the Bianconi-Barabási fitness model, and networks with structural phase transitions. We draw some concluding remarks in Section 3.3.4.

3.3.1 Gibbs entropy of networks with a given degree distribution

The Gibbs entropy $\Sigma[\{k_i\}]$ [69–72, 107] of a network ensemble with given (graphical) degree sequence $\{k_i\}$ [122, 123] is given by

$$\Sigma[\{k_i\}] = \frac{1}{N} \log \mathcal{N}[\{k_i\}] \quad (3.7)$$

where $\mathcal{N}[\{k_i\}]$ is the number of networks with the specified degree sequence and N is the number of labeled nodes $i = 1, 2, \dots, N$. The Gibbs entropy depends on the number of links but also on the specific details of the degree sequence. In Table 3.1 we give two illustrative examples for two degree sequence compatible with 5 links but defining ensembles of networks with different entropy.

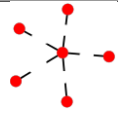

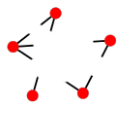
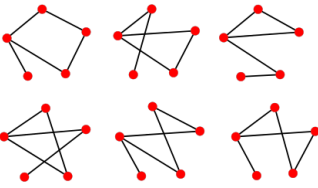
Degree Sequence	Networks	Entropy
		$\Sigma[\{k_i\}] = 0$
		$\Sigma[\{k_i\}] \neq 0$

TABLE 3.1: The configuration of networks with degree sequence $\{1,1,1,1,5\}$ (on top, $\mathcal{N}[\{k_i\}] = 1$) and $\{1,2,2,2,3\}$ (on bottom, $\mathcal{N}[\{k_i\}] = 6$).

It turns out that the ensemble of networks having a given degree distribution is a type of *microcanonical network ensemble* satisfying a large number of hard constraints (the degree of each node is fixed). It is also possible to construct *canonical network ensembles* similar to what happens in classical statistical mechanics when one distinguishes the microcanonical and canonical ensembles according to the fact that the energy is perfectly conserved or conserved in average. A canonical network ensemble with given expected degree sequence is an ensemble of graphs in which the degree of each node is distributed as a Poisson variable with given expected degree $\{\bar{k}_i\}$. The entropy of the canonical network ensemble is the logarithm of the typical number of networks in the ensemble. This entropy $S[\{\bar{k}_i\}]$ is given by

$$S[\{\bar{k}_i\}] = -\frac{1}{N} \left[\sum_{ij} p_{ij} \log p_{ij} + \sum_{ij} (1 - p_{ij}) \log(1 - p_{ij}) \right] \quad (3.8)$$

where p_{ij} indicates the probability that a node i is linked to a node j . We can evaluate the entropy of a maximally random network ensemble with given expected degree distribution $\{\bar{k}_i\}$ by maximizing the entropy $S[\{\bar{k}_i\}]$ with respect to p_{ij} under the conditions

$$\bar{k}_i = \sum_j p_{ij}. \quad (3.9)$$

In this way we get for the marginal probabilities p_{ij} [71]

$$p_{ij} = \frac{\theta_i \theta_j}{1 + \theta_i \theta_j}, \quad (3.10)$$

where θ_i are related to the lagrangian multipliers, or “hidden variables” fixed by the constraints given by Eqs. (3.9). In particular, for the uncorrelated network model in which $\bar{k}_i < \sqrt{\langle k \rangle N}$ and $p_{ij} = \frac{\bar{k}_i \bar{k}_j}{\langle k \rangle N}$, the Shannon entropy network ensemble takes a direct form [70]

$$S[\{\bar{k}_i\}] = \frac{1}{2} \langle k \rangle [\log(\langle k \rangle N) - 1] - \frac{1}{N} \sum_i (\ln \bar{k}_i - 1) \bar{k}_i. \quad (3.11)$$

The Gibbs entropy Σ of a microcanonical ensemble of networks with degree sequence $\{k_i\}$ with $k_i = \bar{k}_i$ is given by [72]

$$\Sigma[\{k_i\}] = S[\{k_i\}] - \Omega[\{k_i\}] \quad (3.12)$$

where $\Omega[\{k_i\}]$ is the entropy of large deviations of the canonical ensemble

$$\Omega[\{k_i\}] = -\frac{1}{N} \log \left[\sum_{a_{ij}} p_{ij}^{a_{ij}} (1 - p_{ij})^{1 - a_{ij}} \prod_i \delta \left(\sum_j a_{ij}, k_i \right) \right]. \quad (3.13)$$

where $\{a_{ij}\}$ is the adjacency matrix of the network. In particular the matrix element a_{ij} of the adjacency matrix is given by $a_{ij} = 1$ if a link is present between node i and node j while $a_{ij} = 0$ otherwise. By replica methods and the cavity method [72, 107] it is possible to derive the given expression for $\Omega[\{k_i\}]$,

$$\Omega[\{k_i\}] = -\frac{1}{N} \sum_i \log \pi_{k_i}(k_i), \quad (3.14)$$

where $\pi_r(n)$ is the Poisson distribution with $\langle n \rangle = r$. In particular, for the uncorrelated network model in which $k_i < \sqrt{\langle k \rangle N}$ and $p_{ij} = \frac{k_i k_j}{\langle k \rangle N}$, the Gibbs entropy network ensemble takes a direct form [70]

$$\begin{aligned} \Sigma[\{k_i\}] &= \frac{1}{2} \langle k \rangle [\log(\langle k \rangle N) - 1] - \frac{1}{N} \sum_i (\ln k_i - 1) k_i + \\ &\quad - \frac{1}{2N} \sum_i \log(2\pi k_i). \end{aligned} \quad (3.15)$$

We might as well define the Gibbs entropy $\Sigma[\{N_k\}]$ of networks with given degree distribution $\{N_k\}$. Since the number of graphs with given degree distribution $\mathcal{N}[\{N_k\}]$ is just given by

$$\mathcal{N}[\{N_k\}] = \mathcal{N}[\{k_i\}] \frac{N!}{\prod_k N_k!} \quad (3.16)$$

it follows that

$$\Sigma[\{N_k\}] = \Sigma[\{k_i\}] - \sum_k \frac{N_k}{N} \log \left(\frac{N_k}{N} \right). \quad (3.17)$$

3.3.2 Entropy rate of growing trees

Many networks are non static but they are growing by the addition of new nodes and links. A major class of growing networks are growing trees in which at each time a new node and a new link is added to the network. In the last ten years, many growing network models have been proposed. Special attention has been addressed to growing network models generating scale-free networks. In fact these stylized models explain the basic mechanism according to which many growing natural networks develop the universally found scale free degree distribution. The fundamental model for scale-free growing network is the BA model [22] which generates networks with degree distribution $P(k) \sim k^{-\gamma}$ and $\gamma = 3$. This model is based of two ingredients: growth of the network and preferential attachment meaning that nodes with large degree are more likely to acquire new links. Here we consider this model and other different significant variations to this model including different additional mechanisms as initial attractiveness of the nodes [2], fitness of the nodes [5, 23], non-linear preferential attachment [3, 4] and aging

of the nodes [6]. Some of these models as explained below undergo structural phase transitions to be studied by statistical mechanics methods.

3.3.2.1 Growing network models

In the growing scale-free network model we start from two nodes linked together, at each time $t = 1, 2, \dots$

- we add a new node $i = t + 2$;
- we link the new node to a node i_t of the network chosen with probability

$$\Pi(i_t) = \frac{A_{i_t}}{\mathcal{N}}, \quad (3.18)$$

where $\mathcal{N} = \sum_{i=1}^{t+1} A_i$;

- the number of nodes in the network is $N = t + 2$.

As a function of the choice of A_j different networks model are defined. In particular we consider the following growing network models:

- If we take $A_i = \delta_{i,1}$, we get a star graph;
- If we take $A_i = \delta_{i,t+1}$, we get the linear chain;
- If we take $A_i = 1$, we get a maximally random connected and growing tree;
- If we take $A_i = k_i$, where k_i is the degree of the node i , we get the BA model [22];
- If we take $A_i = k_i - 1 + a$, with $a < 1$, we get a generalized BA model with initial attractiveness of the nodes [2];
- If we assign to each node a fitness value η_i from a distribution $\rho(\eta) = 1$ and $\eta \in (0, 1)$ and we take $A_i = \eta_i k_i$, we get the Bianconi-Barabási fitness model [23].
- If we take $A_i = k_i^{\gamma'}$, we get the non-linear preferential attachment model of Krapivsky-Redner [3, 4]. This network model undergoes a gelation phenomenon for $\gamma' > 1$. Namely, there is an emergence of a single dominant node linked to almost every other node. For $\gamma' > 2$, there is a finite probability that the dominating node is the first node of the network.
- If we assign to each node a fitness value $\eta_i = e^{-\beta \epsilon_i}$, with ϵ_i drawn from a distribution $g(\epsilon) \propto \epsilon^\kappa$ and $\kappa > 0$, and we take $A_i = \eta_i k_i$, we get as a function of β the so

called "Bose-Einstein condensation in complex networks" of Bianconi and Barabási [5]. When this happens, for $\beta > \beta_c$ one node with high fitness is connected to a finite fraction of other nodes in the network.

- If we take $A_i = (t - t_i)^{-\alpha} k_i$ where t_i indicates the time at which the node i has joined the network, we get the preferential attachment model with aging of the sites of Dorogovtsev-Mendes [6]. In this growing network the power-law exponent γ of the degree distribution is diverging as $\gamma \simeq \frac{1}{c_1} \frac{1}{1-\alpha}$ when $\alpha \rightarrow 1^-$. For $\alpha > 1$ the network is exponential and becomes more and more similar to a linear chain.

3.3.2.2 Entropy rate

The growing connected trees are fully determined by the sequence of symbol $\mathcal{X} = (i_1, i_2, \dots, i_N)$ where i_t is the node linked at time t to the node $i = t + 2$. In order to evaluate the entropy rate of growing networks it is sufficient to determine the entropy rate of the sequence (i_1, i_2, \dots, i_t) :

$$h(t, \mathcal{X}) = - \sum_{i_t} P(i_t | i_1, i_2, \dots, i_{t-1}) \log P(i_t | i_1, i_2, \dots, i_{t-1}), \quad (3.19)$$

where $P(i_t | i_1, i_2, \dots, i_{t-1})$ is the conditional probability that the node i_t is chosen at time t given the history of the process. The entropy of the process evaluating how many networks are typically constructed by the growing network process is $S(\{\mathcal{X}\})$

$$S(\{\mathcal{X}\}) = - \sum_{\{i_1, i_2, \dots, i_t\}} P(i_1, i_2, \dots, i_t) \log P(i_1, i_2, \dots, i_t). \quad (3.20)$$

3.3.2.3 Maximal and minimal bound to the entropy rate of growing network trees

It is instructive to study the limits of the entropy rate of connected growing trees. The minimal entropy rate is given by the entropy rate of the star or of the linear chain. Indeed by taking $A_i = \delta_{1,i}$ we have that the entropy rate is zero. Indeed the growing network model becomes deterministic and it gives rise to a unique star network with the center on the node $i = 1$. The entropy rate of a linear chain $A_i = \delta_{i,t+1}$ is also zero by a similar argument and the model generates a unique linear chain network structure. On the other hand the maximal entropy rate is given by the maximally random growing connected trees that is generated by taking $A_i = 1$ and $\Pi_i = 1/(t+1)$. For this process the entropy rate is given by

$$h(t, \mathcal{X}) = \log(t+1) \quad (3.21)$$

Therefore this entropy rate increases logarithmically with time and the probability of each tree with $N = t + 2$ nodes is given by

$$P(N) = \frac{1}{(N-1)!} \quad (3.22)$$

Therefore $S(\{\mathcal{X}\}) = \log[(N-1)!]$. This is the maximal entropy of a growing connected tree.

3.3.3 Growing trees with stationary degree distribution

For growing network models with stationary degree distributions there are simple relations between $h(t, \mathcal{X})$ and $S(\{\mathcal{X}\})$. Indeed let us define the entropy rate

$$H(\mathcal{X}) = \lim_{N \rightarrow \infty} \frac{1}{N} [S(\{\mathcal{X}\}) - \log[(N-1)!]. \quad (3.23)$$

For a growing tree network with stationary degree distribution, by the recursive application of chain rule $P(i_1, i_2, \dots, i_t) = P(i_t | i_1, i_2, \dots, i_{t-1}) P(i_1, i_2, \dots, i_{t-1})$ we can easily get

$$H(\mathcal{X}) = \lim_{N \rightarrow \infty} \frac{1}{N} \left[\sum_{n=1}^{N-2} h(n, \mathcal{X}) - \log((N-1)!) \right]. \quad (3.24)$$

If the entropy rate of growing networks H is a constant, it means that the number of graphs generated by the growing network model has a dominating term which goes like $N!$ and a subleading term that is exponential with the number of nodes N . On the contrary if $H = -\infty$ it means that the number of networks generated by the growing network model increases with the number of nodes in the network N at most exponentially. Usually the typical number of labeled networks generated by growing network models with convergent degree distribution is less than the number of networks with the same degree distribution. In order to evaluate the ratio between these two cardinalities, we introduce here the difference Δ between the Gibbs entropy $\Sigma[\{N_k\}]$ of the network with the same degree distribution and the entropy of the networks generated by the growing network model. Therefore Δ is

$$\Delta = \lim_{N \rightarrow \infty} \left\{ \Sigma[\{N_k\}] - \frac{1}{N} \log[(N-1)!] - H(\mathcal{X}) \right\}. \quad (3.25)$$

The larger the value of Δ is, the smaller the fraction of networks generated by the growing model compared with the networks generated by the configuration model. This implies that the larger is Δ the more complex the networks generated by the growing models are. In fact these networks need the dynamics of the networks implicitly force

the networks to satisfy more stringent set of structural conditions beyond the degree distribution.

3.3.3.1 The entropy rate of the BA model

We consider the BA model, we take $A_i = k_i$ and $\Pi_i = \frac{k_i}{2(N-1)}$ therefore

$$P(i_t|i_1, i_2, \dots, i_{t-1}) = \frac{k_t}{2(N-1)}. \quad (3.26)$$

The BA model, asymptotically in time has a degree distribution that converges to the value N_k given by

$$N_k = \frac{4N}{k(k+1)(k+2)}, \quad (3.27)$$

Therefore, asymptotically in time the entropy rate of the BA model is

$$h(t = N - 2, \mathcal{X}) \rightarrow - \sum_{k=1}^{\infty} N_k \frac{k}{2(N-1)} \log \left(\frac{k}{2(N-1)} \right). \quad (3.28)$$

Hence, the entropy rate $h(\mathcal{X})$ increases in time as the logarithm of the number of nodes in the network, but it has a subleading term which is constant in time and depends on the degree sequence, *i.e.*

$$\begin{aligned} h(t = N - 2, \mathcal{X}) &\rightarrow \log(N-1) + \log(2) \\ &\quad - \sum_{k=1}^{N-1} \log(k) \frac{2}{(k+1)(k+2)} \\ &\rightarrow \log(N-1) - 0.51(0) \end{aligned} \quad (3.29)$$

The entropy rate $H(\mathcal{X})$ in the limit $N \rightarrow \infty$ is therefore given by

$$H(\mathcal{X}) \simeq -0.51 \dots \quad (3.30)$$

We note here that the degree distribution N_k is known to have interesting finite size effects[8, 124], in addition to the asymptotic scaling Eq. (3.27). Here we checked that the value of the entropy rate is not modified by these corrections up to the significant digit we have considered. Finally, in order to compare the number of networks generated by the BA model with the network that we can construct with the same degree sequence,

we evaluate the value of Δ in the thermodynamic limit. This can be written as

$$\begin{aligned} \Delta &= \lim_{N \rightarrow \infty} \left\{ \frac{1}{N} \sum_{t=1}^{N-1} \log(N/t) \right. \\ &\quad - \frac{1}{2N} \sum_k N_k [k \log(k) + \log(2\pi k)] \\ &\quad \left. - \sum_k \frac{N_k}{N} \log \left(\frac{N_k}{N} \right) + 1 \right\} \\ &\simeq 0.9(1) \end{aligned} \quad (3.31)$$

3.3.3.2 The entropy rate of the growing network model with initial attractiveness

If we take $A_i = k_i - 1 + a$, the network generated is scale free with power-law exponent $\gamma = 2 + a$ [2]. The probability to choose the node i_t given the history of the process is therefore given by

$$P(i_t | i_1, i_2, \dots, i_{t-1}) = \frac{A_{i_t}}{\mathcal{N}} = \frac{k_{i_t} - 1 + a}{(a+1)(N-1)}. \quad (3.32)$$

Asymptotically in time the degree distribution for trees converges to the value [2, 8]

$$N_k = N(1+a) \frac{\Gamma(1+2a)\Gamma(k+a-1)}{\Gamma(a)\Gamma(k+1+2a)}. \quad (3.33)$$

From this, the entropy rate $h(t, \mathcal{X})$ is asymptotically

$$\begin{aligned} h(t = N - 2, \mathcal{X}) &\rightarrow \\ &- \sum_{k=1}^{\infty} N_k \frac{k-1+a}{(a+1)(N-1)} \log \left[\frac{k-1+a}{(a+1)(N-1)} \right], \end{aligned} \quad (3.34)$$

which can be simplified as

$$\begin{aligned} h(t = N - 2, \mathcal{X}) &\rightarrow \log(N-1) + \log(a+1) \\ &\quad - \sum_{k=1}^{N-1} \log \left[(k-1+a) \frac{\Gamma(1+2a)\Gamma(k+a)}{\Gamma(a)\Gamma(k+1+2a)} \right]. \end{aligned} \quad (3.35)$$

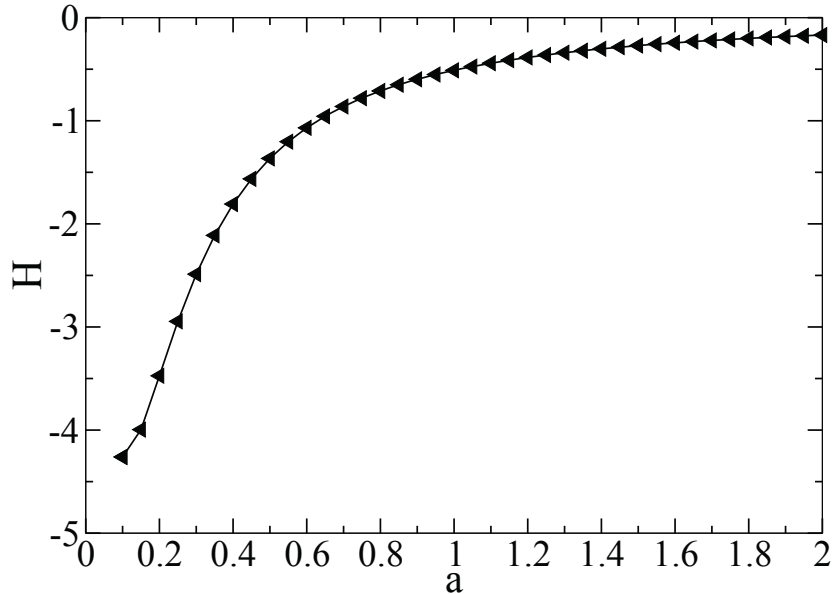


FIGURE 3.4: The entropy rate H calculated for the growing network model with initial attractiveness [2] as a function of a and evaluated by Eq. (3.36) using a maximal degree equal to $K = 10^7$.

In the limit $N \rightarrow \infty$, the entropy rate $H(\mathcal{X})$ is

$$H(\mathcal{X}) = \log(a + 1) - \sum_{k=1}^{N-1} \log \left[(k - 1 + a) \frac{\Gamma(1 + 2a)\Gamma(k + a)}{\Gamma(a)\Gamma(k + 1 + 2a)} \right]. \quad (3.36)$$

When $a \rightarrow 1$, the solution reduces to the solution of the BA model. In Figure 3.4 we plot the value of $H = H(\mathcal{X})$ versus a calculated by Eq. (3.36) using an upper cutoff for the degree $k_i < K \forall i = 1, \dots, N$. As the parameter $a \rightarrow 0$ the entropy rate decreases indicating that the network model generates an exponentially smaller number of networks. Also the Gibbs entropy of scale free networks decreases as long as the power-law exponent converges toward 2, *i.e.* in the limit $\gamma \rightarrow 2$. In order to evaluate the change in the ratio of networks generated by the growing network model to the number of possible networks with the same degree distribution, in Figure 3.5 we plotted Δ as a function of a . As $a \rightarrow 0$ and $\gamma \rightarrow 2$ the number of networks generated by the growing network models are a smaller function of the total number of networks that is possible to build with the same degree distribution. This is an indication and quantification of the importance of correlations generated by the growing network model with given initial attractiveness a .

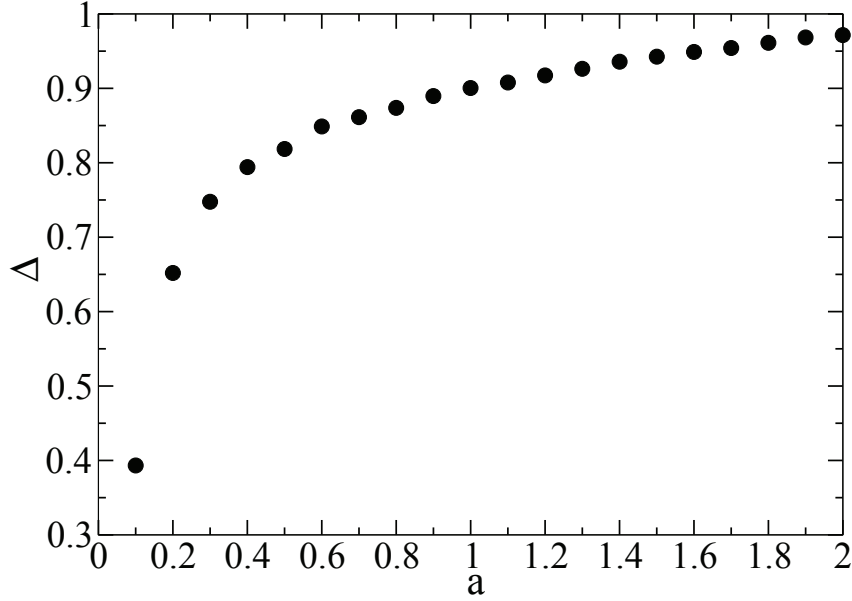


FIGURE 3.5: The value of Δ calculated for the growing network model with initial attractiveness [2] as a function of a evaluated for networks of $N = 50000$ nodes and over 20 realizations of the process.

3.3.3.3 The entropy rate of the Bianconi-Barabási fitness model

If the kernel A_i is heterogeneous and specifically given by $A_i = \eta_i k_i$, the model is called Bianconi-Barabási fitness model [23]. The probability to choose the node i_t given the history of the process is therefore given by

$$P(i_t | i_1, i_2, \dots, i_{t-1}) = \frac{A_i}{\mathcal{N}} = \frac{\eta_i k_i}{\mu(N-1)}, \quad (3.37)$$

where $\mu(N-1) = \sum_{i=1}^{N-1} \eta_i k_i$. The degree distribution $N_k(\eta)$ for nodes of fitness η , asymptotically in time converges to [13]

$$N_k(\eta) = \frac{N\mu\rho(\eta)}{\eta} \frac{\Gamma(k)\Gamma(1+\mu/\eta)}{\Gamma(k+1+\mu/\eta)}, \quad (3.38)$$

where $\rho(\eta)$ is the distribution of η . Given the analytic solution of the model [13, 23], μ is determined by the self-consistent relation

$$\int_0^{\eta_0} \rho(\eta)(\mu/\eta - 1)^{-1} d\eta = 1 \quad (3.39)$$

We consider here the case of uniform distribution of the fitness, *i.e.* $\rho(\eta) = 1$ with $\eta \in (0, 1)$. Therefore the entropy rate is given by

$$h(t = N - 2, \mathcal{X}) \rightarrow - \sum_{k=1}^{N-1} \int_0^1 N_k(\eta) \frac{\eta k}{\mu(N-1)} \log \left[\frac{\eta k}{\mu(N-1)} \right], \quad (3.40)$$

which gives

$$H(\mathcal{X}) = -1.59 \dots \quad (3.41)$$

3.3.3.4 Entropy rate for growing network models with structural phase transitions

We have measured the entropy rate for three growing network models showing a phase transition:

- The Krapivsky-Redner model [3, 4] with

$$h(t, \mathcal{X}) = - \sum_{i=1}^t \frac{k_i^{\gamma'}}{\mathcal{N}} \log \left(\frac{k_i^{\gamma'}}{\mathcal{N}} \right) \quad (3.42)$$

and $\mathcal{N} = \sum_{i=1}^t k_i^{\gamma'}$

- The Bianconi-Barabási model showing a Bose-Einstein condensation in complex networks [5] with

$$h(t, \mathcal{X}) = - \sum_{i_t} \frac{e^{-\beta \epsilon_i k_i}}{\mathcal{N}} \log \left(\frac{e^{-\beta \epsilon_i k_i}}{\mathcal{N}} \right) \quad (3.43)$$

and $\mathcal{N} = \sum_{i=1}^t e^{-\beta \epsilon_i k_i}$.

- The Dorogovtsev-Mendes model with aging of the nodes [6] with

$$h(t, \mathcal{X}) = - \sum_{i_t} \frac{\tau_i^{-\alpha} k_i}{\mathcal{N}} \log \left(\frac{\tau_i^{-\alpha} k_i}{\mathcal{N}} \right) \quad (3.44)$$

where $\tau_i = t - t_i$ is the age of node i and $\mathcal{N} = \sum_{i=1}^t \tau_i^{-\alpha} k_i$.

In Figure 3.6 the entropy rate $H(\mathcal{X})$ is calculated by numerical simulations using

$$H(\mathcal{X}) = \frac{1}{N} \left[\sum_{n=1}^{N-2} h(n, \mathcal{X}) - \log((N-1)!) \right]. \quad (3.45)$$

for a network of sufficiently large size N for the three models as a function of the parameters γ , β and α respectively. We show that at the transition point the scaling

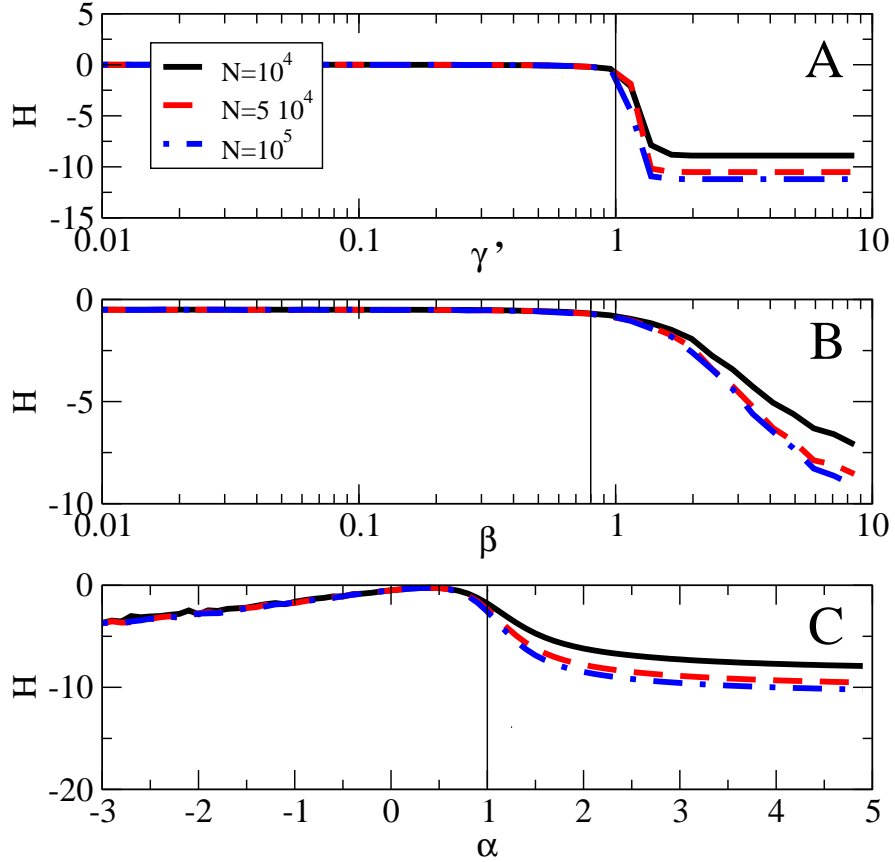


FIGURE 3.6: The entropy rate H is evaluated for the Krapivsky-Redner model [3, 4] (panel A), for the "Bose-Einstein condensation in complex networks" of Bianconi-Barabási with $g(\epsilon) = 2\epsilon$, and $\epsilon \in (0, 1)$, ($\kappa = 1$) [5] (panel B) and for the aging model [6] of Dorogovtsev-Mendes (panel C). The data are averaged over N_{run} different realizations of the network. We took $N_{run} = 100$ for simulations with $N = 10^4$ and $N_{run} = 30$ otherwise. Above the structural phase transition indicated with the solid line, the entropy rate H strongly depends on N .

of H evaluated for a network of size N changes from constant to an N dependent behavior. In particular we checked that in the three cases $H \propto \log(N)$ indicating that as the network grows the typical number of networks that are generated scales only exponentially with N (and not like $N!$).

This behavior signifies a disordered-ordered phase-transition in the topology of the network. In the Bose-Einstein condensation network model and in the Krapivsky-Redner model, below the phase transition, the network is dominated by a hub node that grabs a finite fraction of the nodes. In the aging model, below the phase transition, the network develops a structure more similar to a linear chain.

3.3.4 Remarks

In conclusion, we have studied growing network models and their entropy rate. We have seen that the entropy rate of growing simple trees have maximal and minimal bound and we have studied the entropy rate of scale-free tree networks. This entropy rate allows us to calculate the number of typical graphs generated by growing scale-free network models and to quantify their complexity by comparing this number to the total number of graphs with the same degree distribution. Although we have focused on trees the definition of entropy rate can be easily extended to growing network models with cycles. However the probabilities of adding two or more links at a given time should explicitly account for the fact that the new links must be distinct, fact which induces a small correction to the simple preferential attachment. We have analyzed a variety of growing network models and we have studied non-equilibrium growing network models showing structural phase transitions. By numerical investigations, we have shown that when a growing network model has a phase transition, the entropy rate changes its scaling with the system size indicating the disorder-to-order transition. In the future, we believe that an integrated view of information theory of complex networks will provide a framework to extend quantitative measures of complexity to a large variety of network structures, models and dynamics. The present work is a step in this direction.

Chapter 4

Percolation on Interacting Networks

In the last decade, large attention has been addressed to the dynamical processes defined on single networks. Recently, it has been shown that dynamical processes on interacting networks can lead to new critical phenomena. For instance, new results on percolation of interdependent networks have shown that the percolation transition can be first-order. In this chapter, we introduce and investigate antagonistic interactions between interacting networks. The percolation process on antagonistic networks may present not only first-order transition but also a bistability of the equilibrium solution. Moreover, as a practical application of antagonistic networks, we investigate a model of political election. This chapter is based on the author's work [125–127].

4.1 Background

Percolation [75, 76, 128] is one of the most relevant critical phenomena [12, 14, 91, 92, 120, 129–142] that can be defined on a complex network. Investigating the properties of percolation on single network reveals the essential role of the topology of the network in determining its robustness. Indeed scale-free networks are found to be more robust to random attacks than networks with a finite second moment of the degree distribution $\langle k^2 \rangle$ [75, 76]. Recently, large attention has been paid to the study of the percolation transition on complex networks and surprising new phenomena have been observed. On one side, new results have shown that the percolation can be retarded and sharpened by the Ochlioptas process [82, 143–145]. On the other side, it has been shown that when considering interacting networks, the percolation transition can be first-order [77, 146, 147]. This last result is extremely interesting because a large variety of networks are

not isolated but are strongly interacting [17, 18, 77, 146–149, 149–151]. In these systems one network function depends on the operational level of other networks. Examples of investigated interacting networks go from infrastructure networks as the power-grid [17] and the Internet to interacting biological networks in physiology [151]. Nodes in interacting networks can be interdependent, and therefore the function or activity of a node depends on the function or activity of the linked nodes in the others networks. Recent results have shown that interdependent networks are more fragile than single networks [17, 18] with serious implications that these results have on an increasingly interconnected world.

The chapter is organized as follows. In Section 4.2 we review the theory of percolation on single random networks and interdependent networks. In Section 4.3 we characterize the percolation phase diagram of two Poisson networks with purely antagonistic interactions. In section 4.4 we characterize the percolation phase diagram in networks with a fraction q of antagonistic nodes and a fraction $1 - q$ of interdependent nodes. In Section 4.5 we discuss a model of political election based on antagonistic networks. Finally in Section 4.6 we give the conclusion of the chapter.

4.2 Review of percolation on single networks and interdependent networks

In this section we review the theory of percolation on single networks and interdependent networks, based on the framework presented by Son et al. [77].

4.2.1 Percolation on single network

In the last decade percolation on single networks has been studied extensively. In this section we will review the theory of percolation on single networks. In percolation theory, one essential problem is to determine the existence and the size of the percolating cluster. The percolating cluster in a single Poisson network emerges at a second order phase transition when the average degree of the network is $\langle k \rangle = 1$. Nevertheless, this result can change significantly for networks with different degree distributions.

To solve the percolation problem in a random network with degree distribution p_k , it is useful to define the following generating functions $G_0(x), G_1(x)$:

$$\begin{aligned} G_1(x) &= \sum_k \frac{k p_k}{\langle k \rangle} x^{k-1} \\ G_0(x) &= \sum_k p_k x^k. \end{aligned} \quad (4.1)$$

We denote by S the probability that a random node belongs to the percolating cluster, and by S' the probability that following a link we reach a node that belongs to the percolating cluster. A node of degree k belongs to the percolating cluster if and only if at least one of its neighbors belongs to the percolating cluster. Therefore the probability S_k that a node of degree k belongs to the giant percolating cluster is given by

$$S_k = 1 - (1 - S')^k \quad (4.2)$$

where k is the degree of the node. Averaging over all the nodes, we obtain the relation

$$S = [1 - G_0(1 - S')]. \quad (4.3)$$

Similarly, assuming the network is locally tree-like, the probability S' can be found by the following recursive equation

$$S' = [1 - G_1(1 - S')]. \quad (4.4)$$

These equations are the well known equations for the percolation transition on single network [75, 76] with given degree distribution. A non trivial solution $S' > 0$ emerges continuously at a second order phase transition when

$$\frac{\langle k(k-1) \rangle}{\langle k \rangle} = 1. \quad (4.5)$$

The percolating cluster will be present in the network as long as

$$\frac{\langle k(k-1) \rangle}{\langle k \rangle} > 1, \quad (4.6)$$

which is also called the Molloy-Reed criteria. For Poisson networks, the percolation condition Eq. (4.6) is equivalent to $z = \langle k \rangle = \langle k(k-1) \rangle > 1$, which means to have a Poisson network percolating the average connectivity must be greater than one. For scale-free networks with power-law degree distribution $p(k) \propto k^{-\gamma}$, the percolation condition Eq. (4.6) implies that the network, as long as the power-law exponent $\gamma \leq 3$, is always percolating in the thermodynamic limit $N \rightarrow \infty$. Indeed in this case the second moment

of the degree distribution is diverging with the network size, i.e. $\langle k^2 \rangle \rightarrow \infty$ for $N \rightarrow \infty$. This is a crucial result in complex networks theory and implies that scale-free networks with exponent $\gamma \leq 3$ are more robust than any other network with finite second moment of the degree distribution, i.e. with $\langle k^2 \rangle < \infty$.

4.2.2 Percolation on two interdependent networks

The percolation on interdependent networks was first studied in [17, 146] and then further characterized in [77]. In this section we will review the theory of percolation on two interdependent networks following the approach developed by Son et al [77]. We denote the two networks by network A and network B. For simplicity, we assume both networks have the same number of nodes N . Every node is represented in both networks. A node belonging to the percolating cluster of the interdependent networks must satisfy the two following conditions:

- (i) at least one of the nodes reached by following the links in network A belongs to the percolating cluster of the interdependent networks;
- (ii) at least one of the nodes reached by following the links in network B belongs to the percolating cluster of the interdependent networks.

If we denote by S the probability that a node belongs to the percolating cluster of two interdependent networks and by S'_A (S'_B) the probability that following a link of network A (network B) we reach a node in the percolating cluster of the interdependent network we have

$$S = [1 - G_0^A(1 - S')][1 - G_0^B(1 - S')] \quad (4.7)$$

On locally tree-like random networks S'_A (S'_B) can be found by the recursive equation

$$\begin{aligned} S'_A &= [1 - G_1^A(1 - S'_A)][1 - G_0^B(1 - S'_B)] \\ S'_B &= [1 - G_1^B(1 - S'_B)][1 - G_0^A(1 - S'_A)] \end{aligned} \quad (4.8)$$

The percolation transition can now be also first-order [17, 77, 146, 147]. In the following subsections we will show some simple cases.

4.2.2.1 Two Poisson networks with equal average degree

We start with the simplest example of two interdependent Poisson networks with the same average degree $z = \langle k \rangle_A = \langle k \rangle_B$. For Poisson networks the generating functions

are given by $G_0^A(x) = G_1^A(x) = G_0^B(x) = G_1^B(x) = e^{z(x-1)}$. Therefore Eqs. (4.7)-(4.8) reduce to a single equation

$$S = [1 - e^{-zS}]^2. \quad (4.9)$$

We define $g(S) = S - [1 - e^{-zS}]^2$ such that Eq. (4.9) is equivalent to $g(S) = 0$. This equation has always the solution $S = 0$ but as a function for $z = z_c$ the curve $g(S)$ is tangential to the x axis and another non trivial solution emerge.

The point $z = z_c$ can be found by imposing the condition

$$\begin{aligned} g(S) &= 0, \\ \frac{dg(S)}{dS} &= 0, \end{aligned} \quad (4.10)$$

identifying the point when the function $g(S)$ is tangential to the x axis. Solving this system of equations we get $z = z_c = 2.455407\dots$ and $S_c = 0.511699\dots$. In Figure 4.1 we show a plot of the function $g(S)$ for different values of the average connectivity of the network z below and above the first-order phase transition $z = z_c$. For $z < z_c$ the only solution to Eq. (4.9) is $S = 0$ for $z = z_c$ a new non trivial solution emerge with $S = S_c$. Therefore at $z = z_c$ we observe a phase transition of the first-order in the percolation problem.

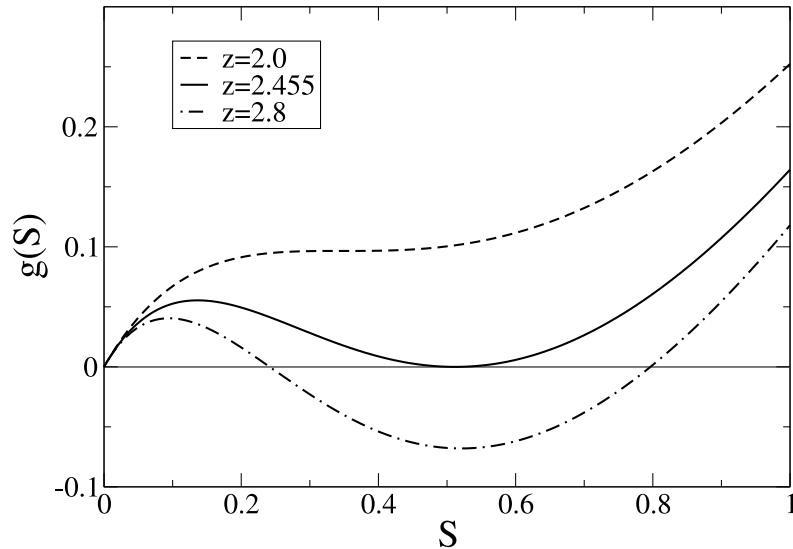


FIGURE 4.1: Plot of the function $g(S)$ for different values of average connectivity z . At $z = z_c = 2.455\dots$ a new non-trivial solution of the function $g(S) = 0$ indicates the onset of a first-order phase transition.

4.2.2.2 Two Poisson networks with different average degree

Another important example is the the case of two Poisson networks with different average degrees $\langle k \rangle_A = z_A$ and $\langle k \rangle_B = z_B$ investigated in [77]. For Poisson networks the generating functions are given by $G_0(x) = G_1(x) = e^{z(x-1)}$. Therefore Eqs. (4.7)-(4.8) reduce to a single equation since $S = S'$,

$$\Psi(S) = S - (1 - e^{z_A S})(1 - e^{z_B S}) = 0 \quad (4.11)$$

The critical line of discontinuous phase transition can be found by imposing the following conditions

$$\begin{aligned} \Psi(S) &= 0, \\ \frac{d\Psi(S)}{dS} &= 0. \end{aligned} \quad (4.12)$$

In Figure 4.2 we plot the phase diagram of the percolation on these two interdependent networks. In this phase diagram we have a large region (Region II) in which both networks are percolating ($S > 0$) and we observe a first-order percolation phase transition on the critical line of the phase diagram.

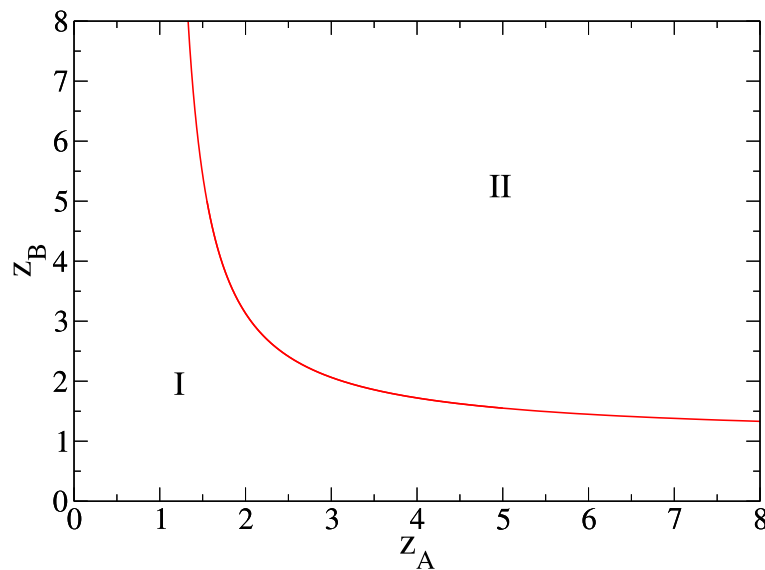


FIGURE 4.2: Phase diagram of two interdependent Poisson networks with average degree z_A and z_B respectively. In region I we have $S = 0$, in region II we have $S > 0$ and the critical line indicates the points where the first-order transition occurs.

4.2.3 Antagonistic interactions and antagonistic networks

In interacting networks, we might not only observe besides interdependent interactions but also antagonistic interactions. If two nodes have an antagonistic interaction, the functionality, or activity, of a node in a network is incompatible with the functionality, of the other node in the interacting network. This new possibility [126], opens the way to introduce in the interaction networks antagonistic interactions that generate a bistability of the solutions.

4.3 Percolation on two antagonistic networks

In this section, we introduce antagonistic interactions in the percolation of two interacting networks [126]. As in the case of interdependent networks we still consider two networks of N nodes, denoted by network A and network B respectively. Every node i is represented in both networks. In the case of two antagonistic networks, different from the case of interdependent networks, if a node i belongs to the percolating cluster of one network it cannot belong to the percolating cluster of the other one. A node i belonging to the percolating cluster of antagonistic network A (or B) must satisfy the following two conditions:

- (i) at least one node reached by following the links in network A (or B) belongs to the percolating cluster in network A (or B);
- (ii) none of the nodes reached by following the links in network B (or A) belongs to the percolating cluster in network B (or A).

We denote by S_A, S_B the probability that a node in network A (network B) belongs to the percolating cluster in network A (network B), and denote by $S'_A (S'_B)$ the probability that following a link in network A (network B) we reach a node in the percolating cluster of network A (network B), we have

$$\begin{aligned} S_A &= [1 - G_0^A(1 - S'_A)]G_0^B(1 - S'_B) \\ S_B &= [1 - G_0^B(1 - S'_B)]G_0^A(1 - S'_A) \end{aligned} \quad (4.13)$$

In the same time, on locally-tree like random networks the probabilities S'_A and S'_B can be found by the following recursive equations

$$\begin{aligned} S'_A &= [1 - G_1^A(1 - S'_A)]G_0^B(1 - S'_B) \\ S'_B &= [1 - G_1^B(1 - S'_B)]G_0^A(1 - S'_A). \end{aligned} \quad (4.14)$$

4.3.1 The stability of solution

The solutions to the recursive Eqs. (4.14) can be classified into three categories:

(i) The trivial solution in which neither of the network is percolating $S'_A = S'_B = 0$.

(ii) The solutions in which just one network is percolating. In this case we have either $S'_A > 0, S'_B = 0$ or $S'_B > 0, S'_A = 0$. From Eqs. (4.14) we find that the solution $S'_A > 0, S'_B = 0$ emerges at a critical line of second order phase transition, characterized by the condition

$$\left. \frac{dG_1^A(z)}{dz} \right|_{z=1} \equiv \frac{\langle k(k-1) \rangle_A}{\langle k \rangle_A} = 1. \quad (4.15)$$

Similarly the solution $S'_B > 0, S'_A = 0$ emerges at a second order phase transition when we have $\frac{\langle k(k-1) \rangle_B}{\langle k \rangle_B} = 1$. This condition is equivalent to the critical condition for percolation in single networks, as it should, because one of the two networks is not percolating.

(iii) The solutions for which both networks are percolating. In this case we have $S'_A > 0, S'_B > 0$. This solution can either emerge (a) at a critical line indicating a continuous phase transition or (b) at a critical line indicating discontinuous phase transition. For situation (a) the critical line can be determined by imposing, for example, $S'_A \rightarrow 0$ in Eqs. (4.14), which yields

$$\begin{aligned} S'_B &= 1 - G_1^B(1 - S'_B), \\ 1 &= \frac{\langle k(k-1) \rangle_A}{\langle k \rangle_A} G_0^B(1 - S'_B). \end{aligned} \quad (4.16)$$

A similar system of equation can be found by using Eqs. (4.14) and imposing $S'_B \rightarrow 0$. For situation (b) the critical line can be determined imposing that the curves $S'_A = f_A(S'_A, S'_B)$ and $S'_B = f_B(S'_A, S'_B)$, are tangent to each other at the point where they intercept. This condition can be written as

$$\left(\frac{\partial f_A}{\partial S'_A} - 1 \right) \left(\frac{\partial f_B}{\partial S'_B} - 1 \right) - \frac{\partial f_A}{\partial S'_B} \frac{\partial f_B}{\partial S'_A} = 0, \quad (4.17)$$

where S'_A, S'_B must satisfy the Eqs. (4.14).

Not every solution of the recursive Eqs. (4.14) is stable. Therefore, we check the stability of the fixed points solutions of Eqs. (4.14) by linearizing the equations around each solution. A solution is stable only if the eigenvalues of the Jacobian of Eqs. (4.14) are less than one. Moreover, the eigenvalues $\lambda_{1,2}$ of the Jacobian can be found by solving

the characteristic equation $|J - \lambda I| = 0$, which reads for our specific problem,

$$\left(\frac{\partial f_A}{\partial S'_A} - \lambda \right) \left(\frac{\partial f_B}{\partial S'_B} - \lambda \right) - \frac{\partial f_A}{\partial S'_B} \frac{\partial f_B}{\partial S'_A} = 0. \quad (4.18)$$

Assuming that the eigenvalues of the Jacobian corresponding to each solution of the Eqs. (4.14) change continuously when we smoothly change the parameters determining the topology of the networks, the change of stability of each solution will occur when $\max(\lambda_1, \lambda_2) = 1$. In the following we will discuss the stability of the solutions of type (i)-(iii).

(i) *Stability of the trivial solution* $S'_A = S'_B = 0$. The solution is stable as long as the following two conditions are satisfied: $\lambda_{1,2} = \frac{\langle k(k-1) \rangle_{A/B}}{\langle k \rangle_{A/B}} < 1$. Therefore the stability of this solution change on the critical lines $\frac{\langle k(k-1) \rangle_A}{\langle k \rangle_A} = 1$ and $\frac{\langle k(k-1) \rangle_B}{\langle k \rangle_B} = 1$.

(ii) *Stability of the solutions in which only one network is percolating*. For the case of $S'_A = 0$, $S'_B > 0$ the stability condition reads $\lambda_1 = \left. \frac{G_1^B(z)}{dz} \right|_{z=1-S'_B} < 1$ and $\lambda_2 = \frac{\langle k(k-1) \rangle_A}{\langle k \rangle_A} G_0^B(1 - S'_B) < 1$. We note here that if $\lambda_2 > \lambda_1$ we expect to observe a change in the stability of the solution on the critical line given by Eqs. (4.16). A similar condition holds for the stability of the solution $S'_A > 0$, $S'_B = 0$.

(iii) *Stability of the solution in which both networks are percolating* $S'_A > 0$, $S'_B > 0$. For characterizing the stability of the solutions of type (iii) we have to solve Eq. (4.18) and impose that the eigenvalues $\lambda_{1,2}$ are less than 1, i.e. $\lambda_{1,2} < 1$. We observe here that for $\lambda = 1$ Eq. (4.18) reduces to Eq. (4.17). Therefore we expect to have a stability change of these solutions on the critical line given by Eq. (4.17). In the following particular cases that we have studied, we have always found that the critical lines determining the stability of the phases are the same as the critical lines determining the emergence of new solutions to the Eqs. (4.14).

4.3.2 Two Poisson networks

We consider the case of two Poisson networks with average connectivity $\langle k \rangle_A = z_A$ and $\langle k \rangle_B = z_B$.

For Poisson networks, the generating functions are given by $G_1^A(x) = G_0^A(x) = e^{-z_A(1-x)}$ and $G_1^B(x) = G_0^B(x) = e^{-z_B(1-x)}$. Therefore, taking into consideration Eqs.(4.13) and Eqs. (4.14) we have $S'_A = S_A$ and $S'_B = S_B$. Moreover the Eqs.(4.14) take the following

form:

$$\begin{aligned} S_A &= (1 - e^{-z_A S_A})e^{-z_B S_B} \\ S_B &= (1 - e^{-z_B S_B})e^{-z_A S_A}. \end{aligned} \quad (4.19)$$

The system of equations (4.20) can be rearranged as

$$\begin{aligned} S_B(S_A) &= -\frac{1}{z_B} \log\left(\frac{S_A}{1 - e^{-z_A S_A}}\right), S_A \neq 0; \forall S_B, S_A = 0 \\ S_A(S_B) &= -\frac{1}{z_A} \log\left(\frac{S_B}{1 - e^{-z_B S_B}}\right), S_B \neq 0; \forall S_A, S_B = 0. \end{aligned} \quad (4.20)$$

Now we discuss different scenarios of solution by plotting $S_B(S_A)$ and $S_A(S_B)$ on a same coordination plane, as shown in Figure 4.3. These equations have always the trivial solution $S_A = 0, S_B = 0$ but depending on the value of the average connectivity in the two networks, z_A, z_B , other non trivial solutions might emerge. In the following we characterize the phase diagram described by the solution to the Eqs. (4.20) keeping in mind that in order to draw the phase diagram of the percolation problem we should consider only the stable solutions of Eqs. (4.20). Here we summarize the phase diagram in Figure 4.4

- Region I $z_A < 1, z_B < 1$. In this region there is only the solution $S_A = 0, S_B = 0$ to the Eqs. (4.20).
- Region II-A $z_A > 1, z_B < \ln(z_A)/(1 - 1/z_A)$. In this regions there is only one stable solution to the percolation problem $S_A > 0, S_B = 0$
- Region II-B $z_B > 1, z_A < \ln(z_B)/(1 - 1/z_B)$. In this regions there is only one stable solution to the percolation problem $S_A = 0, S_B > 0$
- Region III $z_A > \ln(z_B)/(1 - 1/z_B)$ and $z_B > \ln(z_A)/(1 - 1/z_A)$ In this region we observe two stable solutions of the percolation problem with $S_A > 0, S_B = 0$ and $S_A = 0, S_B > 0$. Therefore in this region we observe a bistability of the percolation configurations.

We observe that in this case for each steady state configurations, only one of the two networks can be percolating also in the region in which we observe a bistability of the solutions.

In order to demonstrate the bistability of the percolation solution in region III of the phase diagram we solved recursively the Eqs. (4.14) for $z_B = 1.5$ and variable values

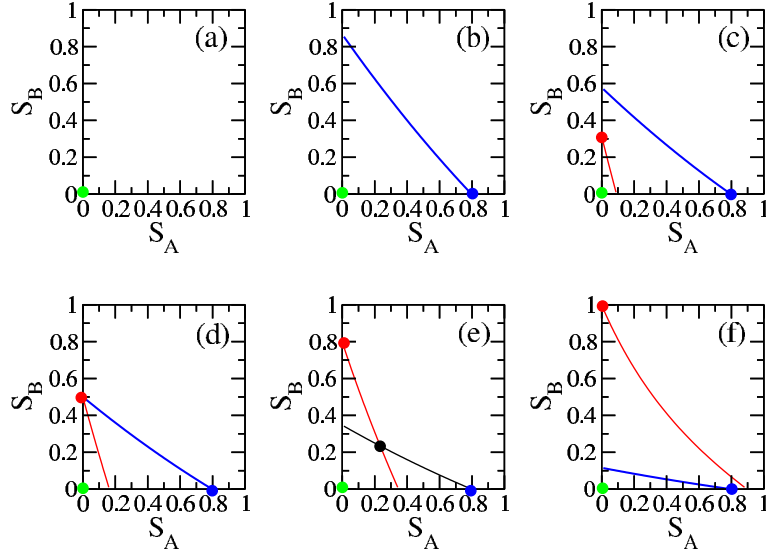


FIGURE 4.3: Solution scenarios by plotting $S_B(S_A)$ (blue line) and $S_A(S_B)$ (red line) in Eqs. (4.20) with different Z_A and Z_B . (a) $Z_A \leq 1$, $Z_B \leq 1$. (b) $Z_A = 2$, $Z_B = 0.8$. (c) $Z_A = 2$, $Z_B = 1.2$. (d) $Z_A = 2$, $Z_B = 1.3863$. (e) $Z_A = Z_B = 2$. (f) $Z_A = 2$, $Z_B = 6$. The color dots in the figure represent the valid solutions for Eqs. (4.20).

of z_A (see Figure 4.5). We start from values of $z_A = 4$, and we solve recursively the Eqs. (4.14). We find the solutions $S'_A = S'_A(z_A = 4) > 0$, $S'_B = S'_B(z_A = 4) = 0$. Then we lower slightly z_A and we solve again the Eqs. (4.14) recursively, starting from the initial condition $S'^o_A = S'_A(z_A = 4) + \epsilon$, $S'^o_B = S'_B(z_A = 4) + \epsilon$, and plot the result. (The small perturbation $\epsilon > 0$ is necessary in order not to end up with the trivial solution $S'_A = 0, S'_B = 0$.) Using this procedure we show that if we first lower the value of z_A and then again we raise it, spanning the region III of the phase diagram as shown in Figure 4.5, the solution present an hysteresis loop. This means that in the region III either network A or network B might end up to be percolating depending on the details of the percolation dynamics.

4.3.3 Two scale-free networks

Here, we characterize the phase diagram of two antagonistic scale-free networks with power-law exponents γ_A, γ_B , as shown in Figure 4.6. The two networks have minimal connectivity $m = 1$ and varying value of the maximal degree K .

The critical lines of the phase diagram depend on the value of the maximal degree K of the networks. Therefore, the plot in Figure 4.6 has to be considered as the effective phase diagrams of the percolation problem on antagonistic networks with a finite cutoff

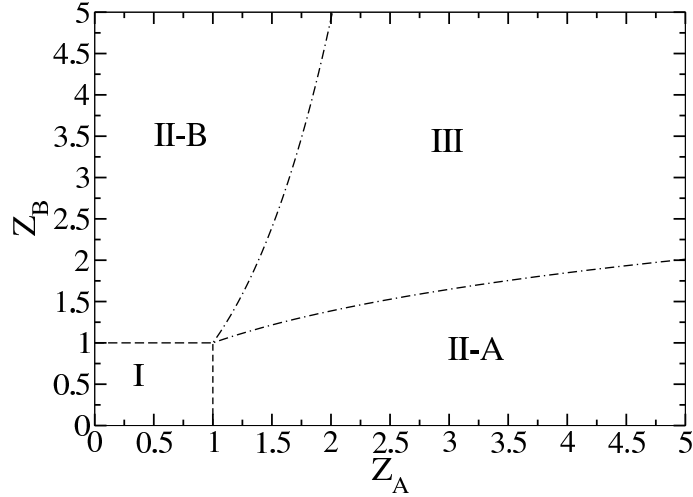


FIGURE 4.4: Phase diagram of two antagonistic Poisson networks with average degree z_A and z_B respectively. In region I the only stable solution is the trivial solution $S_A = S_B = 0$. In region II-A we have only one stable solution $S_A > 0, S_B = 0$, Symmetrically in region II-B we have only one stable solution $S_A = 0, S_B > 0$. On the contrary in region III we have two stable solutions $S_A > 0, S_B = 0$ and $S_A = 0, S_B > 0$ and we observe a bistability of the percolation steady state solution.

Region I	$S'_A = S'_B = 0$
Region II-A	$S'_A > 0, S'_B = 0$
Region II-B	$S'_B > 0, S'_A = 0$
Region III	either $S'_A > 0, S'_B = 0$ or $S'_B > 0, S'_A = 0$

TABLE 4.1: Stable phases in the different regions of the phase diagram of the percolation problem on two antagonistic Poisson networks (Figure 4.4).

K . The phase diagram is rich, showing a region (Region III) in the figure where both networks are percolating demonstrating an interesting interplay between the percolation dynamics and the topology of the network.

A description of the stable phases in the different regions of the phase diagram is provided by Table 4.2.

4.3.4 A Poisson network and a scale-free network

Finally we consider the case of a Poisson network (network A) with average connectivity $\langle k \rangle_A = z_A$, and a network B with scale-free degree distribution and power-law exponent of the degree distribution γ_B . The scale-free network has minimal connectivity $m = 1$ and maximal degree given by K . In Figure 4.7 we show the phase diagram of the model in the plane (γ_B, z_A) . The critical lines of the phase diagram are dependent on the value of the cutoff K of the scale-degree distribution and therefore for finite value of

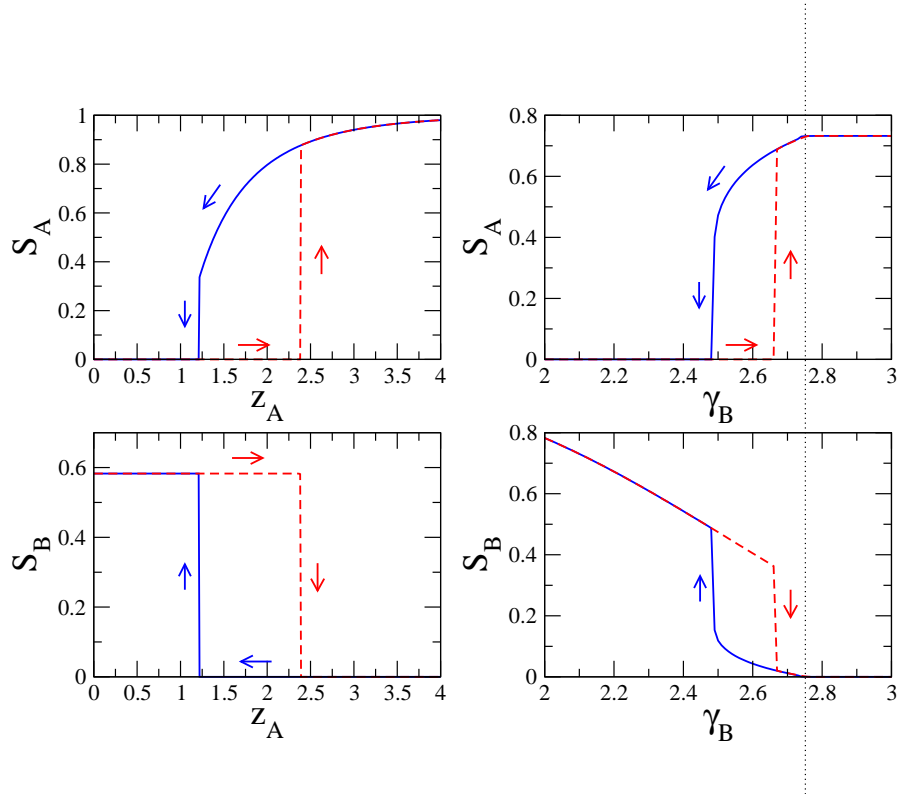


FIGURE 4.5: Panels (a) and (b) show the hysteresis loop for the percolation problem on two antagonistic Poisson networks with $z_B = 1.5$. Panels (c) and (d) show the hysteresis loop for the percolation problem on two antagonistic networks of different topology: a Poisson network of average degree $z_A = 1.8$ and a scale-free networks with power-law exponent γ_B , minimal degree $m = 1$ and maximal degree $K = 100$. The hysteresis loop is performed using the method explained in the main text. The value of the parameter ϵ used in this figure is $\epsilon = 10^{-3}$.

K we observe an effective phase diagram converging in the $K \rightarrow \infty$ limit to the phase diagram of an infinite network. For these reasons we have to consider the phase diagrams in Figure 4.7 as effective phase diagrams of the percolation problem on networks with maximal degree K . The phase diagram includes two regions, (region III and region V) with bistability of the solutions and two regions (region IV and region V) in which the solution in which both networks are percolating is stable. In Table 4.3 we describe the percolation stable solutions in the different regions of the phase diagram shown in Figure 4.7.

In order to demonstrate the bistability of the percolation problem we solved recursively the Eqs. (4.14) for $z_B = 1.8$ (see Figure 4.13). We start from values of $\gamma_B = 3$, and we solve the Eqs. (4.14) using the same method explained for the two antagonistic Poisson networks. Using this procedure we show in Figure 4.13 that the solution present a second order phase transition to a phase in which both networks are percolating and also an hysteresis loop in correspondence of region V. This demonstrates the bistability of the

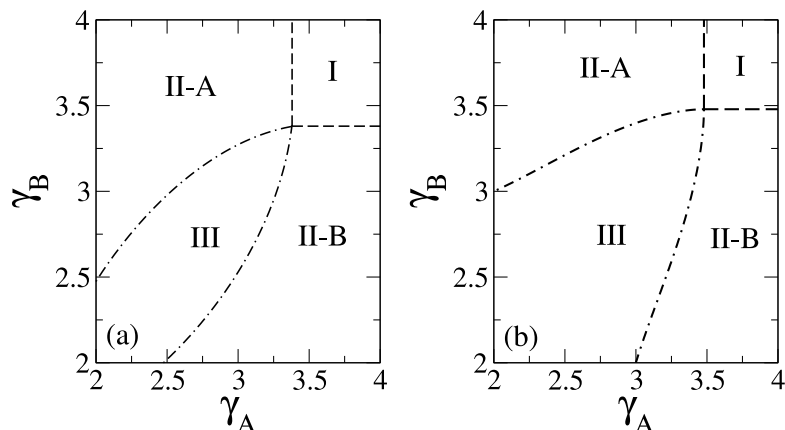


FIGURE 4.6: The phase diagram of the percolation process in two antagonistic scale-free networks with power-law exponents γ_A, γ_B . The minimal degree of the two networks is $m = 1$ and the maximal degree K . Panel (a) show the effective phase diagram with $K = 100$, the panel (b) show the phase diagram in the limit of an infinite network $K = \infty$.

Region I	$S'_A = S'_B = 0$
Region II-A	$S'_A > 0, S'_B = 0$
Region II-B	$S'_B > 0, S'_A = 0$
Region III	$S'_A > 0, S'_B > 0$

TABLE 4.2: Stable phases in the different regions of the phase diagram of the percolation on two antagonistic scale-free networks (Figure 4.6).

solutions in region V and the existence of a phase in which both network percolate in region IV and region V.

In order to demonstrate the bistability of the percolation problem we solved recursively the Eqs. (4.14) for $z_B = 1.8$ (see Figure 4.5). We start from values of $\gamma_B = 3$, and we solve the Eqs. (4.14) using the same method explained for the two antagonistic Poisson networks. Using this procedure we show in Figure 4.5 that the solution present a second order phase transition to a phase in which both networks are percolating and also an hysteresis loop in correspondence of region V. This demonstrates the bistability of the solutions in region V and the existence of a phase in which both network percolate in region IV and region V.

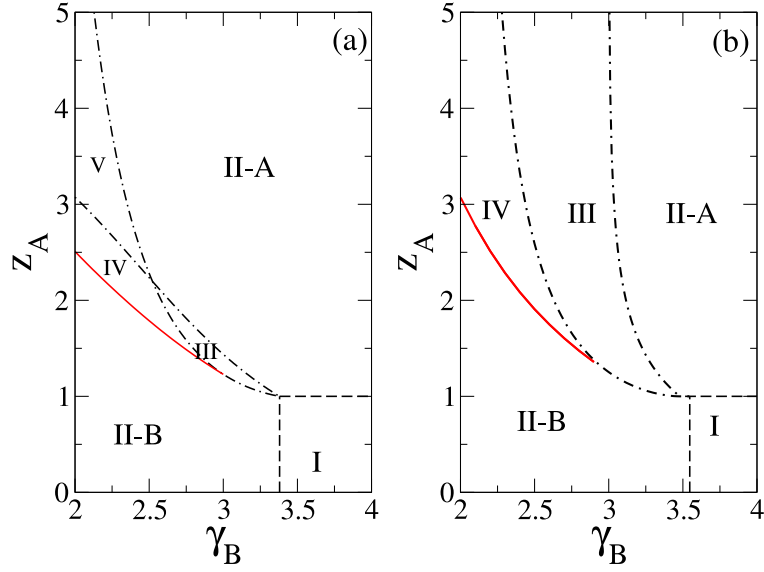


FIGURE 4.7: Phase diagram of the percolation process on a Poisson network with average degree $\langle k \rangle_A = z_A$ interacting with a scale-free network of power-law exponent γ_B , minimal degree $m = 1$ and maximal degree K . The panel on the left show the effective phase diagram for $K = 100$ and the panel on the right show the effective phase diagram for $K = \infty$.

Region I	$S'_A = S'_B = 0$
Region II-A	$S'_A > 0, S'_B = 0$
Region II-B	$S'_B > 0, S'_A = 0$
Region III	$S'_A > 0, S'_B > 0$
Region IV	either $S'_B > 0, S'_A = 0$ or $S'_A > 0, S'_B > 0$
Region V	either $S'_A > 0, S'_B = 0$ or $S'_B > 0, S'_A = 0$

TABLE 4.3: Stable phases in the phase diagram for the percolation on two antagonistic networks: a Poisson network (network A) and a scale-free network (network B). (Figure 4.7)

4.4 Percolation on interdependent networks with a fraction q of antagonistic nodes

In this section the percolation phase diagram when we allow for a combination of antagonistic and interdependent nodes is explored. In particular the interplay between interdependencies and antagonistic interactions is investigated. For simplicity, we consider this problem in the settings of two interacting Poisson networks. For two Poisson networks with exclusively interdependent interactions, the steady state of the percolation dynamics has a large region of the phase diagram in which both networks are percolating. In interdependent networks, a fraction $q > q_c = 2/3$ of antagonistic interactions is necessary in order to significantly reduce the phase in which both networks are

percolating. This show that interdependent networks display a significant robustness in presence of antagonistic interactions, and that also a minority of interdependent nodes is enough to sustain two percolating networks.

As in the previous case we consider two networks of N nodes. We call the networks, network A and network B respectively and every node i is represented in both networks.

If we indicate by $S_A(S_B)$ the probability that a random node in network A (network B) belongs to the percolating cluster in network A(network B), and if we indicate by $S'_A(S'_B)$ the probability that following a link in network A (network B) we reach a node in the percolating cluster of network A (network B), we have

$$\begin{aligned} S_A &= q[1 - G_0^A(1 - S'_A)]G_0^B(1 - S'_B) + \\ &\quad + (1 - q)[1 - G_0^A(1 - S'_A)][1 - G_0^B(1 - S'_B)], \\ S_B &= q[1 - G_0^B(1 - S'_B)]G_0^A(1 - S'_A) + \\ &\quad + (1 - q)[1 - G_0^B(1 - S'_B)][1 - G_0^A(1 - S'_A)]. \end{aligned} \quad (4.21)$$

In the same time, in a random networks with local tree structure the probabilities S'_A and S'_B satisfy the following recursive equations

$$\begin{aligned} S'_A &= q[1 - G_1^A(1 - S'_A)]G_0^B(1 - S'_B) + \\ &\quad + (1 - q)[1 - G_1^A(1 - S'_A)][1 - G_0^B(1 - S'_B)], \\ S'_B &= q[1 - G_1^B(1 - S'_B)]G_0^A(1 - S'_A) + \\ &\quad + (1 - q)[1 - G_1^B(1 - S'_B)][1 - G_0^A(1 - S'_A)]. \end{aligned} \quad (4.22)$$

Region I	$S_A = S_B = 0$
Region II-A	$S_A > 0, S_B = 0$
Region II-B	$S_A = 0, S_B > 0$
Region III	$S_A > 0, S_B > 0$
Region IV	$S_A = S_B = 0$ and $S_A > 0, S_B > 0$
Region V-A	$S_A > 0, S_B = 0$ and $S_A > 0, S_B > 0$
Region V-B	$S_A = 0, S_B > 0$ and $S_A > 0, S_B > 0$

TABLE 4.4: Stable phases in the different regions of the phase diagram of the percolation on two antagonistic Poisson networks with a fraction $q = 0.3$ of antagonistic nodes (Figure 4.8)

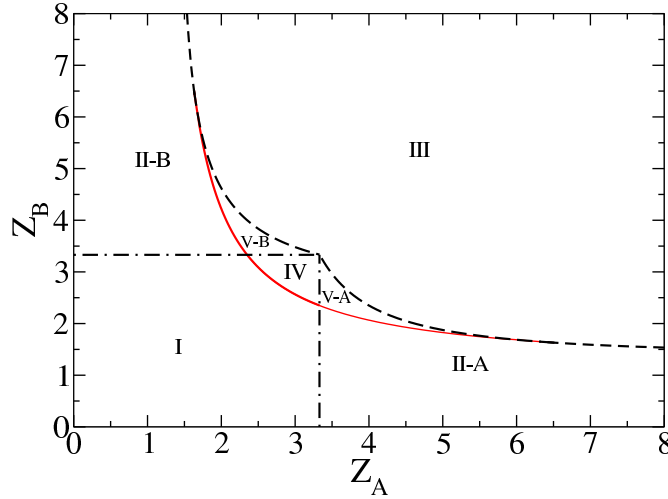


FIGURE 4.8: Phase diagram two Poisson interdependent networks with a fraction $q = 0.3$ of antagonistic interactions.

4.4.1 Two Poisson networks

We consider the case of two interacting Poisson networks with average connectivities $z_A = \langle k \rangle_A$ and $z_B = \langle k \rangle_B$. We have seen that for the case of two fully antagonistic Poisson networks the stable percolation configurations correspond to states in which either one of the two networks is percolating. Therefore with purely antagonistic interactions the system is not able to sustain the coexistence of two percolating clusters present in both networks. Here we want to generalize the above case to two interacting networks with only a fraction q of antagonistic interactions. For two Poisson networks we have $G_0^A(x) = G_1^A(x) = e^{z_A(x-1)}$ and $G_0^B(x) = G_1^B(x) = e^{z_B(x-1)}$ and therefore $S_A = S'_A$ and $S_B = S'_B$. The Eqs. (4.22), (4.21) can be explicitly written in terms of the average connectivities of the two networks z_A, z_B as

$$\begin{aligned}
 S_A &= f_A(S_A, S_B) = \\
 &= (1 - e^{-z_A S_A})[(2q - 1)e^{-z_B S_B} + 1 - q] \\
 S_B &= f_B(S_A, S_B) = \\
 &= (1 - e^{-z_B S_B})[(2q - 1)e^{-z_A S_A} + 1 - q]
 \end{aligned} \tag{4.23}$$

The solutions to the recursive Eqs. (4.23) can be classified into three categories:

- (i) The trivial solution in which neither of the network is percolating $S_A = S_B = 0$.

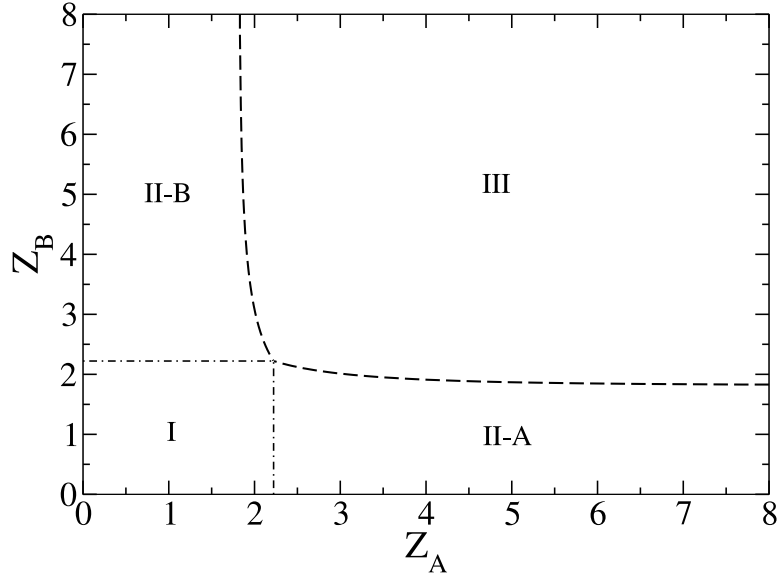


FIGURE 4.9: Phase diagram two Poisson interdependent networks with a fraction $q = 0.45$ of antagonistic interactions.

Region I	$S_A = S_B = 0$
Region II-A	$S_A > 0, S_B = 0$
Region II-B	$S_A = 0, S_B > 0$
Region III	$S_A > 0, S_B > 0$

TABLE 4.5: Stable phases in the different regions of the phase diagram of the percolation on two antagonistic Poisson networks with a fraction $q = 0.45$ of antagonistic nodes (Figure 4.9).

Region I	$S_A = S_B = 0$
Region II-A	$S_A > 0, S_B = 0$
Region II-B	$S_A = 0, S_B > 0$
Region III	$S_A > 0, S_B > 0$

TABLE 4.6: Stable phases in the different regions of the phase diagram of the percolation on two antagonistic Poisson networks with a fraction $q = 0.6$ of antagonistic nodes (Figure 4.10)

- (ii) The solutions in which just one network is percolating. In this case we have either $S_A > 0, S_B = 0$ or $S_A = 0, S_B > 0$. From Eqs. (4.23) we find that the solution $S_A > 0, S_B = 0$ emerges at a critical line of second order phase transition, characterized by the condition

$$z_A = \frac{1}{q} \quad (4.24)$$

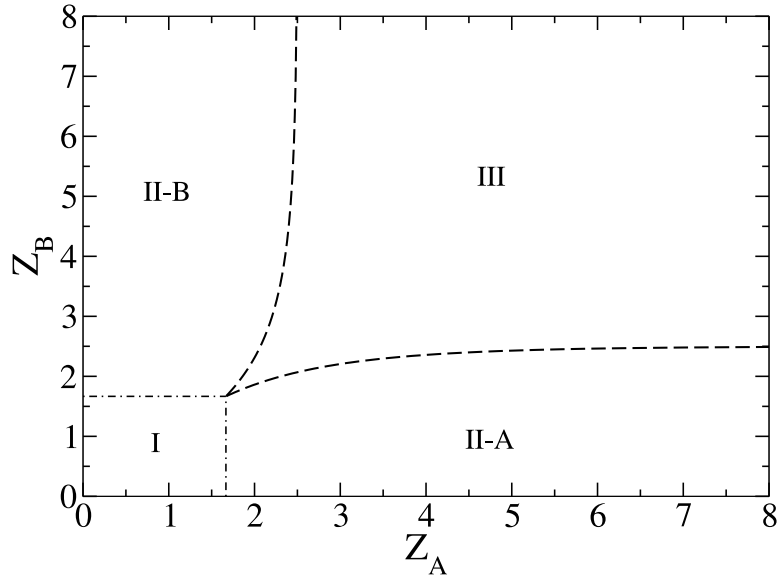


FIGURE 4.10: Phase diagram two Poisson interdependent networks with a fraction $q = 0.6$ of antagonistic interactions.

Similarly the solution $S_B > 0, S_A = 0$ emerges at a second order phase transition when we have

$$z_B = \frac{1}{q}.$$

Therefore we observe the phases where just one network percolates, as long as $q > 0$. This is a major difference with respect to the phase diagram (Figure 4.2) of two purely interdependent networks.

- (iii) The solutions for which both networks are percolating. In this case we have $S_A > 0, S_B > 0$. This solution can either emerge (a) at a critical line indicating a continuous phase transition or (b) at a critical line indicating discontinuous phase transition. For situation (a) the critical line can be determined by imposing, for example, $S_A \rightarrow 0$ in Eqs. (4.14), which yields

$$\begin{aligned} z_B &= \psi(z_A, q) \\ &= -\frac{\ln\left(\left[\frac{1}{z_A} - (1-q)\right]/(2q-1)\right)}{q\left(1 - \left[\frac{1}{z_A} - (1-q)\right]/(2q-1)\right)}. \end{aligned} \quad (4.25)$$

The function $\psi(z_A, q)$ for $q < 0.5$ is a decreasing function of z_A defined for $z_A > 1/(1-q)$, for $q > 0.5$ is an increasing function of z_A defined for $z_A < 1/(1-q)$. For $q = 0.5$ the function $\psi(z_A, q)$ is not defined but has limit $\psi(z_A, q) \rightarrow 0$. A condition similar to Eq. (4.25) can be found for z_A, z_B by using Eqs. (4.23) and

imposing $S_B \rightarrow 0$. In particular we obtain the other critical line

$$z_A = \psi(z_B, q). \quad (4.26)$$

For situation (b) the critical line can be determined imposing that the curves $S_A = f_A(S_A, S_B)$ and $S_B = f_B(S_A, S_B)$, are tangent to each other at the point where they intercept. This condition can be written as

$$\left(\frac{\partial f_A}{\partial S_A} - 1\right) \left(\frac{\partial f_B}{\partial S_B} - 1\right) - \frac{\partial f_A}{\partial S_B} \frac{\partial f_B}{\partial S_A} = 0, \quad (4.27)$$

where S_A, S_B must satisfy the Eqs. (4.23). This is the equation determines the critical line of first-order phase transition points. We indicate this line in red in the phase digrams of the percolation transition.

The condition for having a tricritical point is that Eq.(4.25) and Eq. (4.26) are satisfied together with Eq. (4.27). If we impose that both Eq. (4.25) and Eq. (4.27) are satisfied at the same point, the average connectivities z_A and z_B must satisfy the following conditions

$$\begin{aligned} z_B &= \psi(z_A, q) \\ z_B &= \phi(z_A, q) = \\ &= \frac{z_A(2q-1)}{[1-z_A(1-q)][2qz_A(2q-1)+2-3q]} \end{aligned} \quad (4.28)$$

If we impose that both Eq. (4.26) and Eq. (4.27) are satisfied at the same point, the average connectivities z_A and z_B must satisfy the following conditions

$$\begin{aligned} z_A &= \psi(z_B, q) \\ z_A &= \phi(z_B, q) = \\ &= \frac{z_A(2q-1)}{[1-z_A(1-q)][2qz_A(2q-1)+2-3q]} \end{aligned} \quad (4.29)$$

In general the systems of Eqs. (4.28) and Eqs. (4.29) have at most two solutions each. One trivial solution to Eqs. (4.28) and Eqs. (4.29) is $z_A = z_B = \frac{1}{q}$ corresponding to $S_A = S_B = 0$. In the following we will characterize the solutions to Eqs. (4.28) as a function of the fraction of the antagonist interactions q . Similar results can be drawn by studying the system of Eqs. (4.29).

- *Case $q < 0.4$.* The system of Eqs. (4.28) has two solutions, the trivial solution $z_A = z_B = \frac{1}{q}$ and another non-trivial solution with $z_A < \frac{1}{q}$.

- *Case $q = 0.4$.* The system of Eqs. (4.28) has only one trivial solution with $z_A = z_B = \frac{1}{q}$. Therefore the non-trivial tricritical point disappears.
- *Case $0.5 < q < 0.4$.* The system of Eqs. (4.28) has two solutions, the trivial solution $z_A = z_B = \frac{1}{q}$ and another non-trivial solution with $z_A > \frac{1}{q}$. It turns out that this point is not physical because it is in the region in which the coexistence phase $S_A > 0$ and $S_B > 0$ cannot be sustained by the system. Therefore in this region we do not have a non-trivial tricritical point.
- *Case $0.5 < q \leq \frac{2}{3}$.* The system of Eqs. (4.28) has only the trivial solution $z_A = z_B = \frac{1}{q}$. Therefore the non-trivial tricritical point disappears.
- *Case $q > \frac{2}{3}$.* The system of Eqs. (4.28) has two solutions, the trivial solutions $z_A = z_B = \frac{1}{q}$ and another non-trivial solution with $z_A > \frac{1}{q}$.

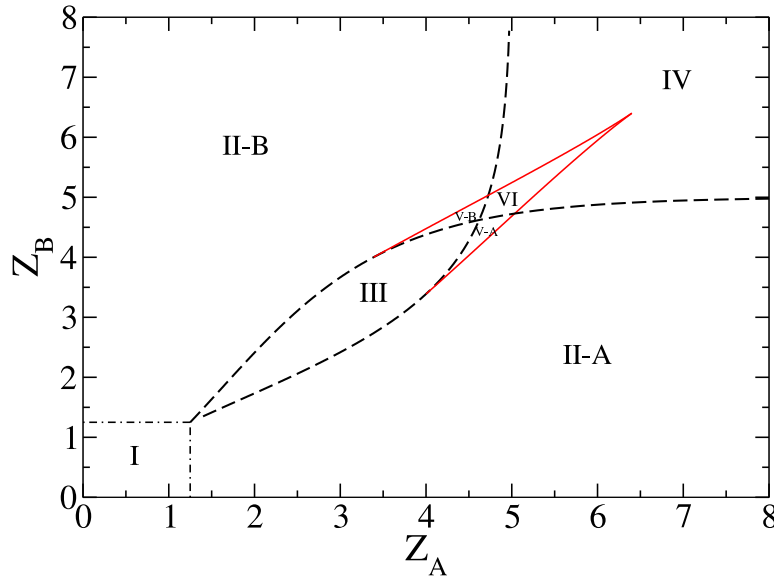


FIGURE 4.11: Phase diagram two Poisson interdependent networks with a fraction $q = 0.8$ of antagonistic interactions.

4.4.2 The phase diagram as a function of q

As a function of the number of antagonistic interactions q the phase diagram of the percolation problem change significantly.

- *Case $q < 0.4$.*

In Figure 4.8 we show the phase diagram for $q = 0.3$ which is a typical phase diagram in the region $0 < q < 0.4$. The stable phases in the different regions of

Region I	$S_A = S_B = 0$
Region II-A	$S_A > 0, S_B = 0$
Region II-B	$S_A = 0, S_B > 0$
Region III	$S_A > 0, S_B = 0$ and $S_A = 0, S_B > 0$
Region IV	$S_A > 0, S_B > 0$
Region V-A	$S_A > 0, S_B = 0$ and $S_A > 0, S_B > 0$
Region V-B	$S_A = 0, S_B > 0$ and $S_A > 0, S_B > 0$
Region VI	$S_A > S_B > 0$ and $S_B > S_A > 0$

TABLE 4.7: Stable phases in the different regions of the phase diagram of the percolation on two antagonistic Poisson networks with a fraction $q = 0.8$ of antagonistic nodes (Figure 4.11).

the phase space are characterized in Table 4.4. From this table it is evident that in regions IV, V-A and V-B we observe a bistability of the solutions.

In order to demonstrate the bistability of the percolation solution in region IV and V-A, V-B of the phase diagram we solved recursively the Eqs. (4.23) for $z_B = 4.0$ (or $z_B = 2.8$) and variable values of z_A (see Figure 4.12). We start from values of $z_A = 3$, and we solve recursively the Eqs. (4.23). We find the solutions $S_A = S_A(z_A = 3) > 0$, $S_B = S_B(z_A = 3) = 0$. Then we lower slightly z_A and we solve again the Eqs. (4.23) recursively, starting from the initial condition $S_A^o = S_A(z_A = 3) + \epsilon$, $S_B^o = S_B(z_A = 3) + \epsilon$, and plot the result. (The small perturbation $\epsilon > 0$ is necessary in order not to end up with the trivial solution $S_A = 0, S_B = 0$.) Using this procedure we show that if we first lower the value of z_A and then again we raise it, as shown in Figure 4.12, the solution present an hysteresis loop. This means that in the region IV and V-A, V-B there is a bistability of the solution.

- *Case* $0.4 < q < 0.5$.

In Figure 4.9 we show the phase diagram for $q = 0.45$ which is a typical phase diagram in the range $0.4 < q < 0.5$. The stable phases in the different regions of the phase space are characterized in Table 4.5. For this range of parameters we do not observe a bistability of the solutions.

- *Case* $0.5 < q < \frac{2}{3}$.

In Figure 4.10 we show the phase diagram for $q = 0.6$ which is a typical phase diagram in the range $0.5 < q < \frac{2}{3}$. The stable phases in the different regions of phase space are characterized in Table 4.6. From this table it is evident that in this case we do not observe bistability of the solutions. Moreover from the phase diagram Figure 4.10 it is clear that also if the majority of the nodes are antagonistic the interdependent nodes are enough to sustain a phase in which both networks are percolating at the same time (Region III).

- Case $q > \frac{2}{3}$.

In Figure 4.11 we show the phase diagram for $q = 0.8$ which is a typical phase diagram in the range $q > \frac{2}{3}$. In Table 4.7 we characterize the stable phases in the different regions of the phase diagram. Region III, V-A, V-B and VI show a bistability of the solutions. In Figure 4.13 we show evidence that in these regions we can observe an hysteresis loop if we proceed by calculating S_A , and S_B recursively from Eqs. (4.23) using the same technique used to produce Figure 4.12. For $q > \frac{2}{3}$ the regions in phase space where we observe the coexistence of two percolating phases (Region IV, V-A, V-B and VI) are reduced and disappear as $q \rightarrow 1$.

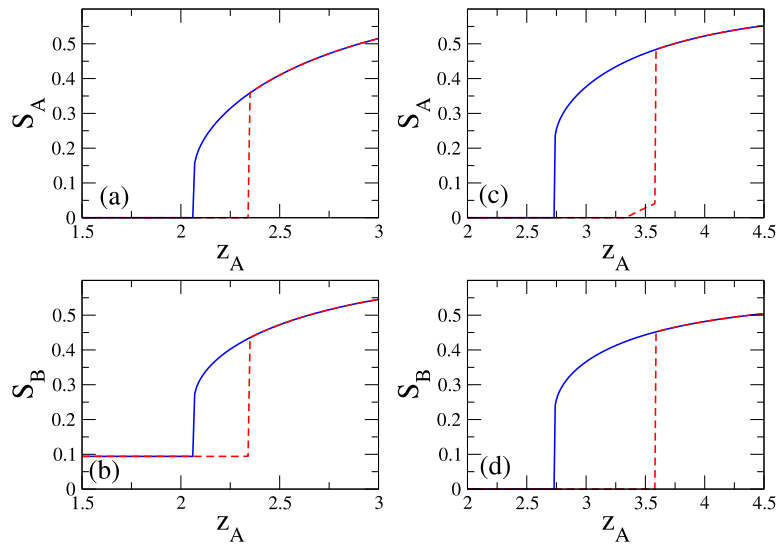


FIGURE 4.12: Hysteresis loop for $q = 0.3$. The hysteresis loop is performed using the method explained in the main text. The value of the parameter ϵ used in this figure is $\epsilon = 10^{-3}$. In panel (a) and (b) $z_B = 4.0$. In panel (c) and (d) $z_B = 2.8$.

4.5 A model of political election

So far we have discussed various cases of percolation on antagonistic networks from the theoretical point of view. In this section, as a practical example of percolation on antagonistic networks, we propose a simple model of opinion dynamics that describes two parties competing for votes during a political campaign. Every opinion, i.e., party, is modeled as a social network through which a contagion dynamics can take place. Individuals, on the other hand, are represented by a node on each network, and can be active only in one of the two networks (vote for one party) at the moment of the election. Each agent has also a third option [152–155], namely not to vote, and in that case she

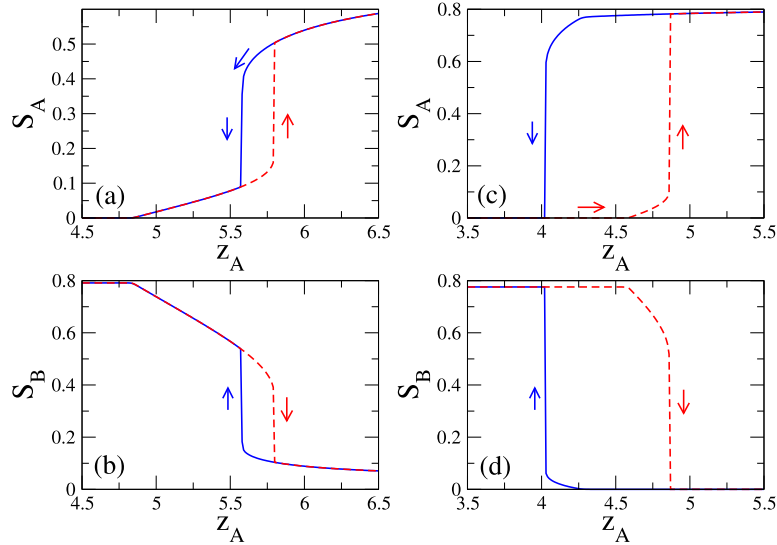


FIGURE 4.13: Hysteresis loop for $q = 0.8$. The hysteresis loop is performed using the method explained in the main text. The value of the parameter ϵ used in this figure is $\epsilon = 10^{-3}$. In panel (a) and (b) $z_B = 5.7$. In panel (c) and (d) $z_B = 4.5$.

will be inactive in both networks. Crucially, agents are affected by the opinion of their neighbors, and the nodes tend to be active in the networks where their neighbors are also active. Moreover, the chance of changing opinion decreases as the decision moment approaches, in line with the observation that vote preferences stabilize as the election day comes closer [156].

The aim of the model is to provide insights in the role of multiple social networks in the voting problem through a simple and clear mathematical model, in the spirit, for example, of recent work concerning the issue of ideological conflict [154]. We describe the dynamics of social influence in the two networks, and we model the uncertainty reduction preceding the vote through a simulated annealing process. Long before the election the agents change opinions and can sustain a small fraction of antagonistic relations, but as the election approaches their dynamics slows down, until they reach the state in which the dynamics is frozen, at the election day. At that moment, the party winning the elections is the one with more active nodes. Finally, we focus on the case in which the networks sustaining each party are represented by two Poisson graphs, and address the role of different average connectivities. This choice is consistent for example with the data on social networks of mobile phone communication, which are characterized by a typical scale in the degree (being fitted with a power-law distribution of exponent $\gamma = 8.4$) [63].

4.5.1 Parties as antagonistic social networks

We consider two antagonistic networks A, B representing the social networks of two competing political parties. Each agent i is represented in each network and can choose to be active in one of the networks. In particular $\sigma_i^A = 0$ if agent i is inactive in network A and $\sigma_i^A = 1$ if agent i is active in network A . Similarly $\sigma_i^B = 0, 1$ indicates if a node is active or inactive in network B . Since ultimately the activity of an individual in a network corresponds to the agent voting for the corresponding party, each agent can be active only on one network on the election day (i.e. if $\sigma_i^A = 1$ then $\sigma_i^B = 0$ and if $\sigma_i^B = 1$ then $\sigma_i^A = 0$). Nevertheless we leave to the agent the freedom not to vote, in that case $\sigma_i^A = \sigma_i^B = 0$. Moreover agents are influenced by their neighbors. Therefore, we assume that, on the election day, if at least one neighbor of agent i is active in network A , the agent will be active in the same network (network A) provided that it is not already active in network B . We assume that a symmetrical process is occurring for the opinion dynamics in network B. Hence, the mathematical constraints that our agent opinions need to satisfy at the election day are:

$$\begin{aligned}\sigma_i^A &= \left[1 - \prod_{j \in N_A(i)} (1 - \sigma_j^A) \right] (1 - \sigma_i^B) \\ \sigma_i^B &= \left[1 - \prod_{j \in N_B(i)} (1 - \sigma_j^B) \right] (1 - \sigma_i^A),\end{aligned}\tag{4.30}$$

where $N_A(i)$ ($N_B(i)$) are the set of neighbors of node i in network A (network B). Therefore at the election day people cannot anymore change their opinion. On the contrary before the election we allow for some conflicts in the system, and in general the constraints provided by Eqs. (4.30) will not be satisfied.

4.5.2 Dynamics of the model

To model how agents decide on their vote during the pre-election period we consider the following algorithm. We consider a Hamiltonian that counts the number of the constraints in Eq. (4.30) that are violated. Therefore we take a Hamiltonian H of the following form

$$\begin{aligned}H &= \sum_i \left\{ \sigma_i^A - \left[1 - \prod_{j \in N_A(i)} (1 - \sigma_j^A) \right] (1 - \sigma_i^B) \right\}^2 + \\ &\quad \sum_i \left\{ \sigma_i^B - \left[1 - \prod_{j \in N_B(i)} (1 - \sigma_j^B) \right] (1 - \sigma_i^A) \right\}^2.\end{aligned}\tag{4.31}$$

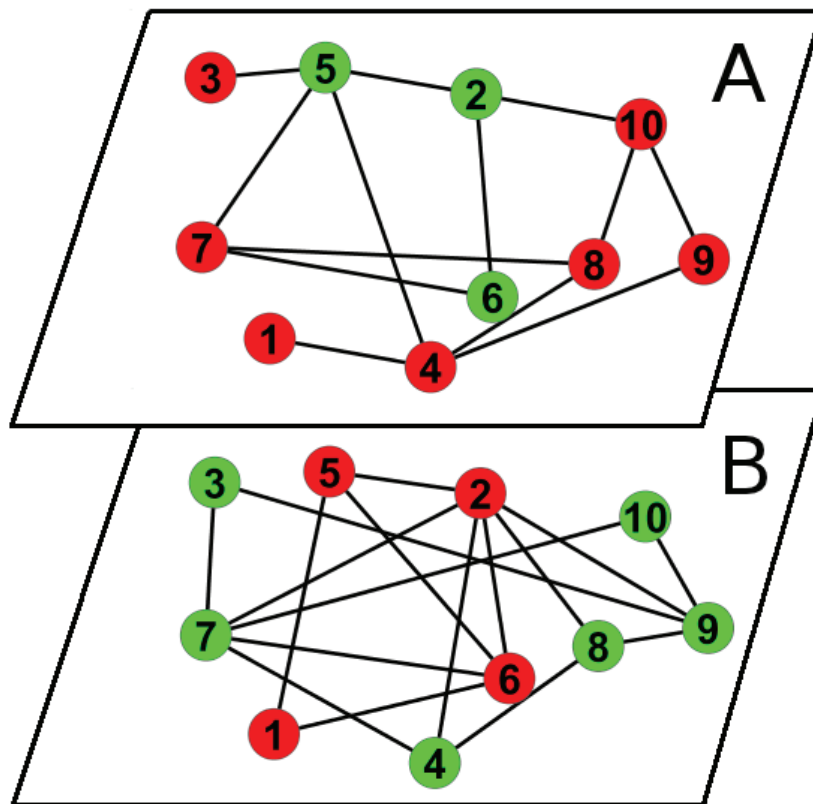


FIGURE 4.14: The two competing political parties are represented by two networks. Each agent is represented in both networks but can either be active (green node) in only one of the two or inactive (red node) in both networks. Moreover the activity of neighbor nodes influence the opinion of any given node.

The terms in the brackets can take on the values $\pm 1, 0$, therefore a natural choice of Hamiltonian to count the number of constraint violations involves squares of these terms.

We start from given initial conditions, and we consider the fact that long before the election the agents are free to change opinion. Therefore we model their dynamics as a Monte Carlo dynamics which equilibrates following the Hamiltonian H with a relatively high initial temperature, i.e. some conflicts are allowed in the system. As the election day approaches, the effective temperature of the opinion dynamics decreases and the agents tend to reduce to zero the number of conflicts with their neighbors. The opinion dynamics described in this way is implemented with a simulated annealing algorithm. The model just described is depicted in Figure 4.14. We start at a high temperature $T = 1$ and we allow the system to equilibrate by $N_A + N_B$ Monte Carlo steps where a node is picked randomly in either of the networks with equal probability and its opinion changed, then we slowly reduce the temperature by a multiplicative factor of 0.95 until we reach the temperature state $T = 0.01$ where the Hamiltonian is $H = 0$, there are no more conflicts in the network, and the probability of one spin flip is about $e^{-1/0.01} \simeq 10^{-44}$.

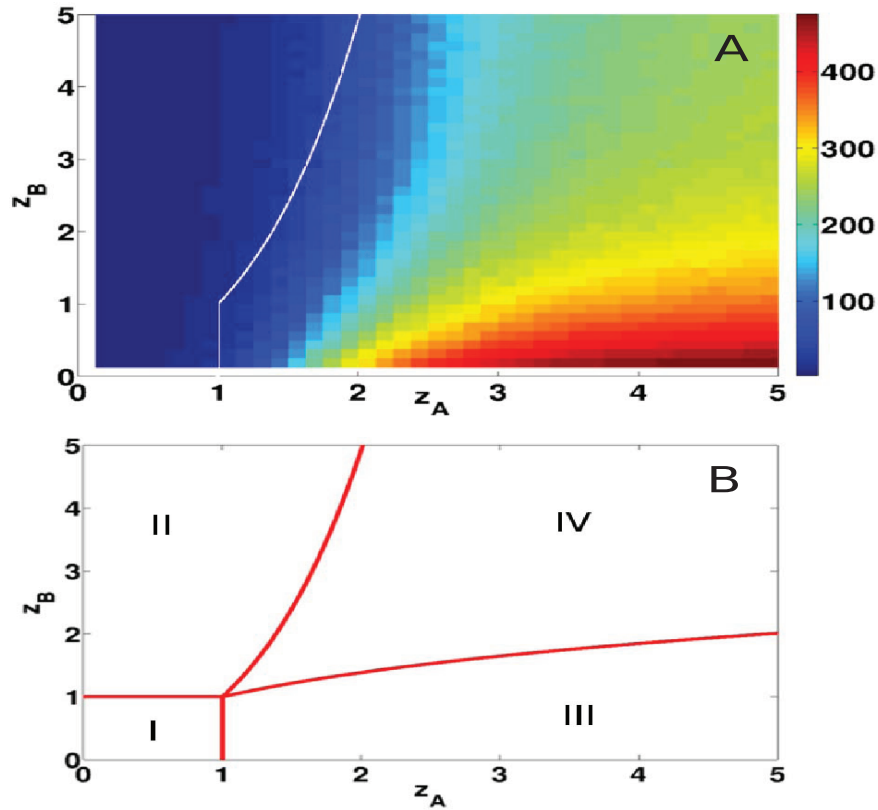


FIGURE 4.15: (Panel A) The size of the largest connected component S_A in network A at the end of the simulated annealing calculation as a function of the average connectivity of the two networks: z_A and z_B respectively. The data is simulated for two networks for $N = 500$ nodes and averaged 60 times. The simulated annealing algorithm is independent of initial conditions. The white line represent the boundary between the region in which network A is percolating and the region in which network A is not percolating. (Panel B) The schematic representation of the different phases of the proposed model. In region I none of the networks is percolating, in region II network B is percolating in region III network A is percolating in region IV both networks are percolating.

It turns out that the Hamiltonian H has in general multiple fundamental states and the simulated annealing algorithm always find one of these states. The final configuration for the model just described is depicted in Figure 4.14.

4.5.3 Phase diagram

In Figure 4.15 we report the result of this opinion dynamics for two antagonistic networks A, B with Poisson degree distributions and different average connectivities z_A , z_B , respectively. In particular we plot the size S_A of the giant component of the percolating cluster in network A. Additionally we have characterized the finite size effects (see Figure 4.16) and concluded that the phase diagram of the model is consistent with the following scenario valid in the limit of large network sizes:

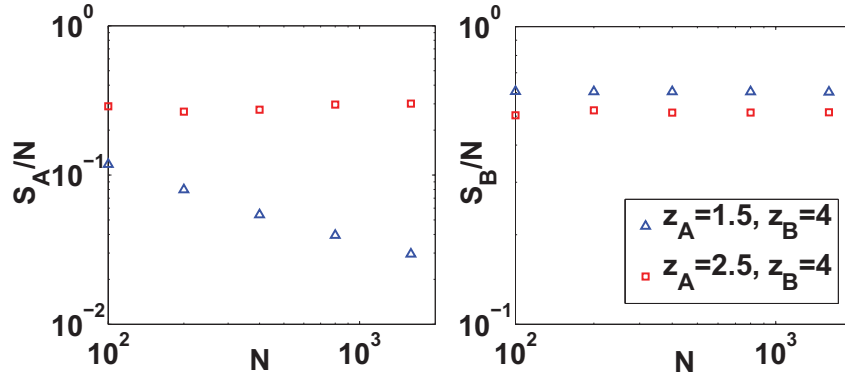


FIGURE 4.16: We represent the fraction of nodes in the giant component S_A of network A and in the giant component S_B of network B in different regions of the phase space. In region II ($z_A = 1.5, z_B = 4$) the giant component in network A (S_A) disappears in the thermodynamic limit while in region IV ($z_A = 2.5, z_B = 4$) it remains constant. The giant component in network B remains constant in the thermodynamic limit both in region II and region IV. Each data point is simulated for the two networks for N nodes and averaged 200 times.

- *Region (I) in Figure 4.15:* The boundary of this region is defined by $z_A < 1, z_B < 1$. In this region both giant components in network A (S_A) and network B (S_B) are zero, $S_A = 0, S_B = 0$, and therefore essentially agents never vote.
- *Region (II) in Figure 4.15:* In this region the giant component in network B emerges, $S_B > 0, S_A = 0$.
- *Region (III) in Figure 4.15:* In this region the giant component in network A emerges, $S_A > 0, S_B = 0$.
- *Region (IV) in Figure 4.15:* In this region we have the pluralism solution of the opinion dynamics and both giant component in network A and B are different from zero, $S_A > 0, S_B > 0$.

In Regions II (III) the active agents in party B (party A) percolate the system while agents in party A (party B) remain concentrated in disconnected clusters. Nevertheless, if the average connectivity of the two antagonistic parties is comparable (Region IV), the system can sustain an effective pluralism of opinions with both parties percolating in the system. Therefore, we find the interesting result that if the connectivity of the two parties is large enough, i.e. we are in region IV of the phase diagram (Figure 4.15B) the pluralism can be preserved in the model and there will be two parties with a high number of votes. In order for a party to win the election, it is necessary that the active agents percolate in the corresponding network. The election outcome, nevertheless, depends crucially on the total number of votes in network A, m_A and the total number of votes in network B, m_B . In Figure 4.17 we plot the difference between the number of votes in

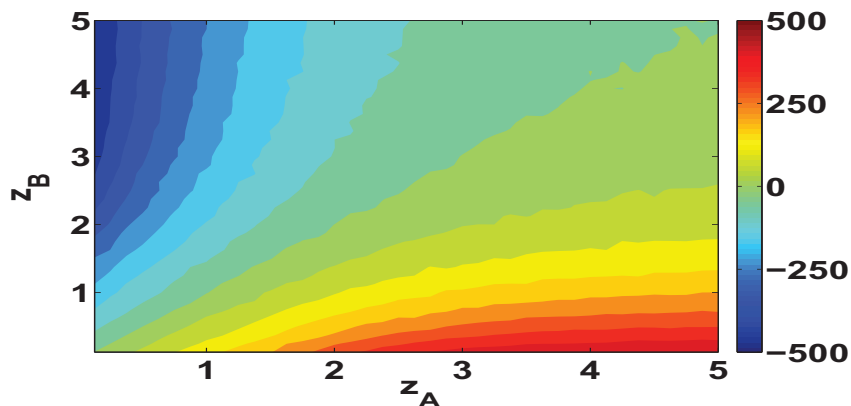


FIGURE 4.17: The contour plot for the difference between the total number of votes m_A in party A (total number of agents active in network A) and the total number of votes m_B in party B (total number of agents active in network B). The data is simulated for two networks for $N = 500$ nodes and averaged 90 times. It is clear that the larger the difference in average connectivity of the two networks, the larger the advantage of the more connected political party.

network A and the number of votes in network B. Very interestingly, we observe that the more connected party (network) has the majority of the votes. It is also worth noting that the final outcome of the election does not depend on the initial conditions. Overall, this result supports the intuition that if a party has a supporting network that is more connected it will win the elections, and is coherent with recent results concerning the role of densely connected social networks on the adoption of a behavior [157].

4.5.4 Committed agents

Very recently, different models have focused on the role of committed agents in opinion dynamics [154, 155]. Here to consider the role of committed agents in the network during the election campaign, we perform a simulated annealing algorithm where a fraction of the nodes always remain active in one of the two networks, never changing their opinion. Figure 4.18 shows that in Region IV a small fraction of agents $f \simeq 0.1$ in the less connected network can reverse the outcome of the election, indeed the probability distribution $P = P(m_A - m_B)$ of different realization of the dynamics is shifted towards the committed minority party. Interestingly this finding fits perfectly with the results of the radically different models proposed in [154, 155]. Thus the best strategy to win the election is to build a well connected network and at the same time to have committed agents to the party.

The opinion dynamics has a rich phase diagram. The results are that in the thermodynamic limit the most connected network wins the election independent of the initial

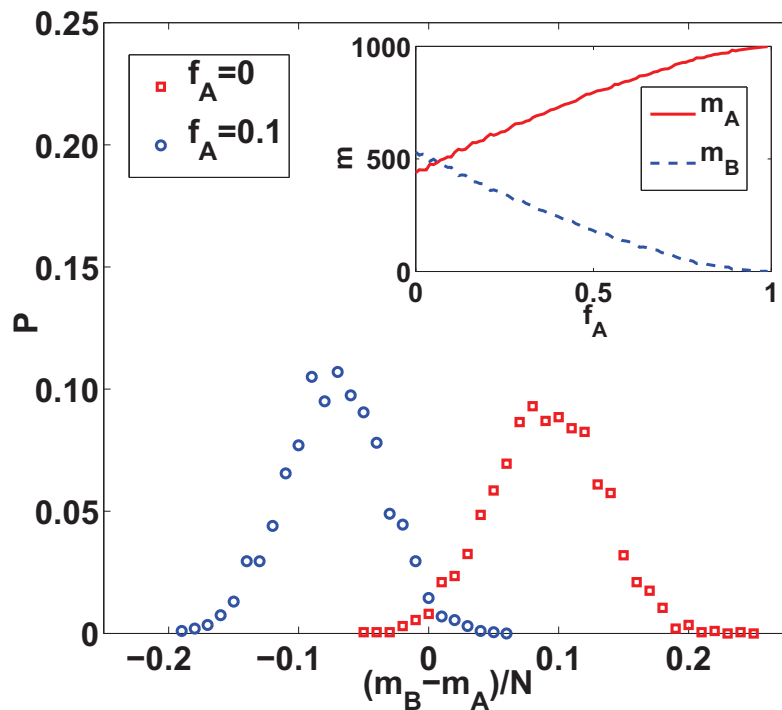


FIGURE 4.18: We represent the role of a fraction f of committed agents in reverting the outcome of the election. In particular we plot the histogram of the difference between the fraction of agents m_B/N voting for party B and the fraction of agents m_A/N voting for party A for a fraction f_A of committed agents to party A , with $f_A = 0$ and $f_A = 0.1$ and average connectivities of the networks $z_A = 2.5, z_B = 4$. The histogram is performed for 1000 realizations of two networks of size $N = 1000$. In the inset we show the average number of agents in network A (m_A) and agents in network B (m_B) as a function of the fraction of committed agents f_A . A small fraction of agents ($f_A \simeq 0.1$) is sufficient to reverse the outcome of the elections. The data in the inset is simulated for two networks for $N = 1000$ nodes and averaged 10 times.

condition of the system, in agreement with recent results on the persuasive role of a densely connected social network [157]. However, for a large region of the parameters the voting results of the two parties are very close and small perturbations could alter the results. In this context, we observe that a small minority of committed agents can reverse the outcome of the election result, thus confirming the results obtained in very recent and different models [154, 155].

4.6 Conclusion

In this chapter, we first have investigated how much antagonistic interactions modify the phase diagram of the percolation transition. The introduction of antagonistic interactions between interacting networks introduces show important new physics in the percolation problem. In fact the percolation process in this case show a bistability of

the solutions. This implies that depending on the details of the percolation dynamics, the steady state of the system might change. In particular we have demonstrated the bistability of the percolation solution for the percolation problem on two antagonistic Poisson networks, or two antagonistic networks with different topology: a Poisson network and a scale-free network. Moreover, in the percolation transition between two scale-free antagonistic networks and in the percolation transition between two antagonistic networks with a Poisson network and a scale-free networks, we found a region in the phase diagram in which both networks are percolating, despite the presence of antagonistic interactions.

In addition, we have investigated how much interdependencies and incompatibilities modify the stability of complex networks and change the phase diagram of the percolation transition. We found that interdependent networks are robust against antagonistic interactions, and that we need a fraction $q > q_c = 2/3$ of antagonistic interactions for reducing significantly the phase diagram region in which both networks are percolating. Nevertheless, we observe that even a small fractions of antagonistic nodes $0 < q < 0.4$ might induce a bistability of the percolation solutions in same regions of the phase space.

Finally we have put forth a simple model for the opinion dynamics taking place during an election campaign. We have modeled parties (or opinions) in terms of a social networks, and individuals in terms of nodes belonging to these social networks and connecting them. We have considered the case of antagonistic agents who have to decide for a single party, or for none of them. We have described the quenching of the opinions preceding the voting moment as a simulated annealing process where the temperature is progressively lowered till the voting moment, when the individuals minimize the number of conflicts with their neighbors. We have shown that there is a wide region in the phase diagram where two antagonistic parties survive gathering a finite fraction of the votes, and therefore the existence of pluralism in the election system. Moreover, we have pointed out that a key quantity to get a finite share of the overall votes is the connectivity of the networks corresponding to a different parties. Nevertheless connectivity is not sufficient to win the elections, since a small fraction of committed agents is sufficient to invert the results of the voting process. Though deliberately basic, this model provides insights into different aspects of the election dynamics.

We believe that this chapter opens new perspectives in the percolation problem on interdependent networks, which might include both interdependencies and antagonistic interactions eventually combined in a boolean rule. In an increasingly interconnected world understanding how much these different types of interactions affect percolation transition is becoming key to answer fundamental question about the robustness of interdependent networks.

Chapter 5

Summary

In this thesis, we have focused on statistical mechanics of temporal and interacting networks, a new topic in network science with wide applications and significant impact in a large variety of disciplines, from social science, to economy and biology. In this final chapter, we summarize our work as follows.

In Chapter 2, we have investigated the modeling of temporal social networks. In particular, we have focused on modeling the human social interactions in short-time scale, from face-to-face interactions to phone-call communication. By analyzing a large dataset of mobile-phone communication, we have showed that the contact durations of mobile-phone calls are distributed in a Weibull distribution, differing in this respect from the power-law distribution observed in the contact durations of face-to-face interactions. Therefore we have concluded that human social interactions are bursty and adaptive. We have proposed a general model to capture the bursty and adaptive feature in human social interactions based on a reinforcement dynamics. We believe that this chapter will shed light on methodological analysis of large dataset on human contacts and phenomenological modelling of human social dynamics.

In Chapter 3, we have investigated the entropy of temporal networks and growing networks. First, we have introduced the entropy of temporal social networks formed by human social interactions, providing a way to extract information from temporal social networks. By applying entropy measures to a dataset of mobile-phone communication, we have shown that the entropy of the mobile-phone calls depends on the circadian rhythms. Furthermore, we have evaluated how the entropy of the phenomenological model of human social interactions proposed in Chapter 2 changes according to a parametrization of the duration of contacts mimicking the adaptability of human social interactions. We have shown that the entropy of temporal social networks is able to quantify the information encoded in human social interactions, e.g. to capture the

circadian rhythms and adaptability in human social interactions. Second, we have introduced the entropy rate of growing trees that quantifies the number of typical graphs generated by the growing network models. We have investigated the entropy rate of a variety of classical growing network models and non-equilibrium growing network models showing structural phase transitions. We have shown that when a growing network model has a phase transition, the entropy rate changes its scaling with the system size indicating the disorder-to-order transition. Therefore in this chapter we have presented new frameworks to evaluate the complexity of temporal networks and growing networks and also to quantify the information encoded in these networks.

In Chapter 4, we have introduced the antagonistic interactions between interacting networks. We have shown that the percolation process on antagonistic networks has bistable solutions, indicating that the steady state of the system strongly depends on the details of the percolation dynamics. In particular, we have investigated the percolation problem on two antagonistic networks. For two antagonistic Poisson networks, and two antagonistic networks with different topology: a Poisson network and a scale-free network, we have demonstrated the bistability of the percolation solution. For two scale-free antagonistic networks, and two antagonistic networks with different topology: a Poisson network and a scale-free network, we have found a region in the phase diagram in which both networks are percolating despite the presence of antagonistic interactions. Moreover, we have investigated how much interdependencies and incompatibilities modify the stability of complex networks and change the phase diagram of the percolation transition. We have found that interdependent networks are robust against antagonistic interactions, and a fraction $q > q_c = 2/3$ of antagonistic interactions is needed for reducing significantly the phase diagram region in which both networks are percolating. Nevertheless, we have observed that even a small fractions of antagonistic nodes $0 < q < 0.4$ might induce a bistability of the percolation solutions in some regions of the phase space. Finally we have proposed a simple model for the opinion dynamics of political election based on the percolation dynamics of antagonistic networks. We believe that this chapter opens new perspectives in the percolation problem on interacting networks.

In conclusion this thesis is aimed at characterizing the evolution of temporal networks, the level of information present in these networks and some examples of critical phenomena in interacting systems. On one side new phenomena are observed in these systems that extend the results obtained on single networks. For example it is interesting to notice that in order to model temporal social networks we have used a reinforcement dynamics that is in spirit related to the preferential attachment in the BA model. Moreover, in order to characterize the information present in temporal and growing network we can always use entropy measures but we need to specifically address the temporal

nature of the networks. On the other side, we observed a totally new phenomenology on the percolation problem when introducing antagonistic interactions between interacting networks. In particular we have shown that the percolation steady state can be bistable. This is in line with recent findings on the percolation transition that have shown how the percolation transition, believed until now to be always continuous, can be strongly affected when defined on interacting networks, becoming first order. We believe that the work presented in this thesis offers good insight in the wide variety of new questions that are raised in the emerging field of temporal and interacting complex networks.

Appendix A

Solution to the model of face-to-face interactions

A.1 Self-consistent solution of the pairwise model

In this section we give the details of the self-consistent calculation that is able to solve for the mean-field dynamics of the pairwise interaction model. As explained in Chapter 2, the rate equations Eqs. (2.4) for this model are solved together with the definition of the transition rates $\pi_{21}(t)$ and $\pi_{12}(t)$ given by Eqs. (2.6) by making the self-consistent assumption Eqs.(2.7). For convenience here we recall the rate equations Eqs. (2.4)

$$\begin{aligned}\frac{\partial N_1(t, t')}{\partial t} &= -2\frac{N_1(t, t')}{N}f_1(t, t') + \pi_{21}(t)\delta_{tt'}, \\ \frac{\partial N_2(t, t')}{\partial t} &= -2\frac{N_2(t, t')}{N}f_2(t, t') + \pi_{12}(t)\delta_{tt'},\end{aligned}\tag{A.1}$$

the transition equations Eqs. (2.6)

$$\begin{aligned}\pi_{21}(t) &= \frac{2}{N} \sum_{t'=1}^t f_2(t, t')N_2(t, t'), \\ \pi_{12}(t) &= \frac{2}{N} \sum_{t'=1}^t f_1(t, t')N_1(t, t'),\end{aligned}\tag{A.2}$$

and the self-consistent assumption Eqs.(2.7)

$$\begin{aligned}\pi_{21}(t) &= \tilde{\pi}_{21} \left(\frac{t}{N} \right)^{-\alpha_1}, \\ \pi_{12}(t) &= \tilde{\pi}_{12} \left(\frac{t}{N} \right)^{-\alpha_2}.\end{aligned}\tag{A.3}$$

Inserting in the definition of $\pi_{21}(t)$ and $\pi_{12}(t)$ given by Eqs. (A.2) the structure of the solution of the mean-field dynamical Eq. (2.5) and the self-consistent assumption Eqs.(A.3), we get

$$\pi_{21}(t) = 2\tilde{\pi}_{12} \frac{b_2}{N} \sum_{t'=1}^{t-1} \left(\frac{t'}{N} \right)^{-\alpha_2} \left(1 + \frac{t-t'}{N} \right)^{-2b_2-1}.\tag{A.4}$$

For large N we can evaluate (A.4) by going to the continuous limit. Therefore in Eq. (A.4) we substitute the sum over time steps t' with an integral over the variable $y' = t'/N$. The transition rate $\pi_{21}(y) = N\pi_{21}(t)$, that is, the average number of agents that shift from state $1 \rightarrow 0$ in the unit time $y = t/N$, can be evaluated by the following integral:

$$\begin{aligned}\pi_{21}(y) &= 2N\tilde{\pi}_{12}b_2y^{-\alpha_2-2b_2} \int_0^1 x^{-\alpha_2}(1+y^{-1}-x)^{-2b_2-1} dx \\ &= 2N\tilde{\pi}_{12}b_1y^{-\alpha_2} f(\alpha_2, 2b_2 + 1, y),\end{aligned}\tag{A.5}$$

where $f(a, b, y)$ is given by

$$f(a, b, y) = y^{-(b-1)} \int_0^1 x^{-a}(1+y^{-1}-x)^{-b} dx.\tag{A.6}$$

The asymptotic expansion of $f(a, b, y)$ for $y \gg 1$ is given by

$$f(a, b, y) = \frac{1}{b-1} + B(1-b, 1-a)y^{1-b} + O\left(\frac{1}{y} + y^{-b}\right),\tag{A.7}$$

where B is the β function. Inserting (A.7) into (A.5) we get

$$\pi_{21}(y) = N\tilde{\pi}_{12}y^{-\alpha_2}.\tag{A.8}$$

This expression proves that the self consistent assumption given by Eq. (A.3) is valid. In particular since we have assumed

$$\pi_{21}(y) = N\tilde{\pi}_{21}y^{-\alpha_1}\pi_{12}(y) = N\tilde{\pi}_{12}y^{-\alpha_2}$$

these relations are consistent with the result of Eq. (A.8) obtained in the limit $N \rightarrow \infty, y \gg 1$ if

$$\begin{aligned}\alpha_1 &= \alpha_2 = \alpha \\ \tilde{\pi}_{21} &= \tilde{\pi}_{12} = \tilde{\pi}.\end{aligned}\tag{A.9}$$

In order to find the expression for α and $\tilde{\pi}$ we use the conservation of the total number of agents. Indeed we have

$$\sum_{t'} \left[N_1(t, t') + N_2(t, t') \right] = N \tag{A.10}$$

Using the Eqs. (2.5), (A.8) and (A.9) and substituting in Eq. (A.10) the sum over t' with an integral over the variable $x = y'/y$, we get, in the limit $N \gg 1$

$$\begin{aligned}N\tilde{\pi}y^{-\alpha} &\left[y^{-(2b_1-1)} \int_0^1 x^{-\alpha} (1+y-x)^{-2b_1} dx \right. \\ &\left. + y^{-(2b_2-1)} \int_0^1 x^{-\alpha} (1+y-x)^{-2b_2} dx \right] = N \quad ,\end{aligned}\tag{A.11}$$

which yields

$$\tilde{\pi}y^{-\alpha} (f(\alpha, 2b_1, y) + f(\alpha, 2b_2, y)) = 1 \tag{A.12}$$

Finally using the asymptotic expansion Eq. (A.7) we get the solution given by the Eqs. (2.8) that we rewrite here for convenience

$$\begin{aligned}\alpha &= \max(0, 1 - 2b_2, 1 - 2b_1) \\ \tilde{\pi} &= \frac{\sin[2\pi \min(b_1, b_2)]}{\pi} [1 - \delta(\alpha, 0)] \\ &\quad + \frac{(2b_1 - 1)(2b_2 - 1)}{2(b_1 + b_2 - 1)} \delta(\alpha, 0).\end{aligned}\tag{A.13}$$

A.2 Self-consistent solution of the general model

In this appendix we solve the general model in which groups of different size are allowed and the parameter λ is arbitrary. The strategy that leads to the solution of the mean-field equation of this dynamics is essentially the same as in the pairwise model but a new phase transition occurs when $\lambda < 0.5$. The dynamical Eqs. (2.11) can be solved as a function of the variables $\pi_{mn}(t)$ by Eqs. (2.13) and Eqs. (2.15) assuming self-consistently that that $\epsilon(t) = \hat{\epsilon}$ in the large time limit. In order to find the analytic solution of the mean-field dynamics it therefore important to determine the relations between the transition rates $\pi_{mn}(t)$ and the variables $N_n(t, t')$. These relations are

given by

$$\begin{aligned}
 \pi_{2,1}(t) &= 2\lambda \sum_{t'} \frac{N_2(t, t')}{N} f_2(t, t') \\
 \pi_{n,1}(t) &= \lambda \sum_{t'} \frac{N_n(t, t')}{N} f_2(t, t'), \quad n \geq 3 \\
 \pi_{n+1,n}(t) &= n\lambda \sum_{t'} \frac{N_{n+1}(t, t')}{N} f_2(t, t'), \quad n \geq 2 \\
 \pi_{1,2}(t) &= 2 \sum_{t'} \frac{N_1(t, t')}{N} f_1(t, t') \\
 \pi_{1,n}(t) &= (1 - \lambda) \sum_{t'} \frac{N_{n-1}(t, t')}{N} f_2(t, t'), \quad n \geq 3 \\
 \pi_{n,n+1}(t) &= n(1 - \lambda) \sum_{t'} \frac{N_n(t, t')}{N} f_1(t, t'), \quad n \geq 2.
 \end{aligned} \tag{A.14}$$

The coupled Eqs. (2.13), (2.15) and (A.14) can be solved by making the additional self-consistent assumptions on the transition rates $\pi_{mn}(t)$ given by

$$\pi_{mn}(y) = N \tilde{\pi}_{mn} y^{-\alpha_{mn}} \tag{A.15}$$

where $y = t/N$ and $\pi_{mn}(y) = N\pi_{mn}(t)$.

Applying the same technique as in Appendix A.1 we can prove that all the exponents $\alpha_{m,n}$ are equal and given by $\alpha_{m,n} = \alpha$. Performing straightforward calculations we get the following relations

$$\begin{aligned}
 n\tilde{\pi}_{n,1} &= \lambda[\tilde{\pi}_{n-1,n} + \tilde{\pi}_{n+1,n} + \tilde{\pi}_{1,n}] \quad \text{for } n \geq 3 \\
 \tilde{\pi}_{2,1} &= \lambda[\tilde{\pi}_{2,1} + \tilde{\pi}_{3,2}] \\
 \tilde{\pi}_{n,1} &= (1 - \lambda)\tilde{\pi}_{n-1,1} + \lambda\tilde{\pi}_{n+1,1} \quad \text{for } n \geq 4 \\
 \tilde{\pi}_{3,1} &= \frac{1 - \lambda}{2}\tilde{\pi}_{2,1} + \lambda\tilde{\pi}_{4,1} \\
 \tilde{\pi}_{2,1} &= \lambda\tilde{\pi}_{2,1} + 2\lambda\tilde{\pi}_{3,1}.
 \end{aligned} \tag{A.16}$$

Therefore if the self-consistent assumption is valid, the number of agents $N_n(t, t')$ in state n since time t' , is given at time t by

$$\begin{aligned} N_1(t, t') &= \frac{\pi_{2,1}(t')}{K} \left(1 + \frac{t-t'}{N}\right)^{-b_1[2+(1-\lambda)\hat{\epsilon}]} \\ N_2(t, t') &= \frac{\pi_{2,1}(t')}{\lambda} \left(1 + \frac{t-t'}{N}\right)^{-2b_2} \\ N_n(t, t') &= \frac{n\pi_{n,1}(t')}{\lambda} \left(1 + \frac{t-t_0}{N}\right)^{-nb_2} \end{aligned} \quad (\text{A.17})$$

where the variable K is defined by

$$K = \frac{\tilde{\pi}_{2,1}}{\sum_{n \geq 2} \tilde{\pi}_{n,1}}. \quad (\text{A.18})$$

Using the relations given by Eqs. (A.16) we find

$$\tilde{\pi}_{n,1} = \frac{1}{2} \tilde{\pi}_{2,1} \left(\frac{1-\lambda}{\lambda}\right)^{n-2} \quad \text{for } n \geq 3. \quad (\text{A.19})$$

Substituting Eq. (A.19) in the definition of K , Eq. (A.18), we find that K is only defined for $\lambda > 0.5$. For $\lambda < 0.5$ the summation in Eq. (A.18) is in fact divergent and there is a breakdown of the self-consistent assumption Eq. (A.15). For $\lambda > 0.5$ we can perform the summation and we get

$$\begin{aligned} K &= \frac{2(2\lambda - 1)}{3\lambda - 1} \\ \hat{\epsilon} &= \frac{1}{2\lambda - 1}. \end{aligned} \quad (\text{A.20})$$

Finally the value of α and $\tilde{\pi}_{1,0}$ are found by enforcing the conservation law of the number of agent N

$$\sum_{t'=1}^t \sum_n N_n(t, t') = N. \quad (\text{A.21})$$

Therefore, in the large y limit $y \gg 1$ we get the solution

$$\alpha = \max\left(0, 1 - b_1 \frac{3\lambda - 1}{2\lambda - 1}, 1 - 2b_2\right). \quad (\text{A.22})$$

The value of $\tilde{\pi}_{2,1}$ depends on the value assumed by α .

(1) For $\alpha = 0$, the value of $\tilde{\pi}_{2,1}$ is given by

$$\tilde{\pi}_{2,1} = \left[\frac{1}{2(b_1 - \frac{2\lambda-1}{3\lambda-1})} + \frac{1}{2\lambda} \sum_{n \geq 2} \frac{n}{nb_2 - 1} \left(\frac{1-\lambda}{\lambda} \right)^{n-2} \right]^{-1}. \quad (\text{A.23})$$

(2) For $\alpha = 1 - b_1 \frac{3\lambda-1}{2\lambda-1}$, the value of $\tilde{\pi}_{2,1}$ is given by

$$\tilde{\pi}_{2,1} = \frac{2(2\lambda-1)}{3\lambda-1} \frac{1}{B(1 - b_1 \frac{3\lambda-1}{2\lambda-1}, b_1 \frac{3\lambda-1}{2\lambda-1})}, \quad (\text{A.24})$$

where $B(a, b)$ indicates the Beta function.

(3) For $\alpha = 1 - 2b_2$, the value of $\tilde{\pi}_{2,1}$ is given by

$$\tilde{\pi}_{2,1} = \frac{\lambda}{B(1 - 2b_2, 2b_2)} \quad (\text{A.25})$$

where $B(a, b)$ indicates the Beta function.

The average coordination number is defined by

$$\langle n \rangle = \sum_{t'}^t \sum_{n=1}^N n N_n(t, t'). \quad (\text{A.26})$$

Substituting Eqs. (A.17) to the definition of $\langle n \rangle$, Eq. (A.26) and applying the same transformation in Eq. (A.5) to evaluate the integral over t , we get

$$\langle n \rangle = 1 + \sum_{n=2}^N \frac{\tilde{\pi}_{n1}}{\lambda} (n - \delta_{n,2}) y^{-\alpha} f(\alpha, nb_2, y) \quad (\text{A.27})$$

where $y = t/N$ and $f(a, b, y)$ is defined in Eq. (A.6). Substituting the asymptotic expansion Eq. (A.7) into (A.27), we get

$$\begin{aligned} \langle n \rangle = & 1 + \sum_{n=2}^N \frac{\tilde{\pi}_{n1}}{\lambda} (n - \delta_{n,2}) y^{-\alpha} \left[\frac{1}{nb_2 - 1} \right. \\ & \left. + B(1 - nb_2, 1 - \alpha) y^{1-nb_2} \right]. \end{aligned} \quad (\text{A.28})$$

where $B(a, b)$ indicates the Beta function. In the asymptotic limit $y \rightarrow \infty$, using Eqs. (A.19), (A.23)-(A.25) and counting only the leading terms in Eq. (A.28) to compute $\langle n \rangle$ for different value of α , we can recover Eqs. (2.19)-(2.21).

A.3 Self-consistent solution of the heterogeneous model for $\lambda = 1$

In this appendix we show the self-consistent calculations that solve analytically the heterogeneous model with pairwise interactions.

We assume self-consistently that the transition rate $\pi_{21}^\eta(t)$ and $\pi_{12}^{\eta,\eta'}$ decay in time as a power-law, i.e. we assume

$$\begin{aligned}\pi_{21}^\eta(t) &= \Delta\eta\tilde{\pi}_{21}^\eta\left(\frac{t}{N}\right)^{-\alpha(\eta)} \\ \pi_{12}^{\eta,\eta'}(t) &= \Delta\eta\Delta\eta'\tilde{\pi}_{12}^{\eta,\eta'}\left(\frac{t}{N}\right)^{-\alpha(\eta,\eta')}\end{aligned}\quad (\text{A.29})$$

Inserting this self-consistent assumption and the structure of the solution given by Eqs. (2.24) in Eqs. (2.25) we can evaluate $\tilde{\pi}^{\eta,\eta'}$ in the limit $N \rightarrow \infty$. Therefore we get,

$$\begin{aligned}\tilde{\pi}_{12}^{\eta,\eta'} y^{-\alpha(\eta,\eta')} &= \frac{2N}{C(y)}\eta\tilde{\pi}_{21}^\eta y^{-\alpha(\eta)} f(\alpha(\eta), 2\eta + 1, y) \\ \eta'\tilde{\pi}_{21}^{\eta'} y^{-\alpha(\eta')} &= f(\alpha(\eta'), 2\eta' + 1, y)\end{aligned}\quad (\text{A.30})$$

where $f(a, b, y)$ is given by

$$f(a, b, y) = y^{-(b-1)} \int_0^1 x^{-a} (1 + y^{-1} - x)^{-b} dx. \quad (\text{A.31})$$

The asymptotic expansion to $f(a, b, y)$ for $y \gg 1$ is given by

$$f(a, b, y) = \frac{1}{b-1} + B(1-b, 1-a)y^{1-b} + O\left(\frac{1}{y} + y^{-b}\right) \quad (\text{A.32})$$

where B is the Beta function. Inserting (A.32) into (A.30), we get in the limit $y \gg 1$

$$\tilde{\pi}_{12}^{\eta,\eta'} y^{-\alpha(\eta,\eta')} = \frac{N}{2C(y)}\tilde{\pi}_{21}^\eta y^{-\alpha(\eta)}\tilde{\pi}_{21}^{\eta'} y^{-\alpha(\eta')} \quad (\text{A.33})$$

Similarly, inserting (A.29) into the definition of $C(y)$ given by Eq. (2.26) we get, in the limit $y \gg 1$

$$C(y) = \frac{N}{2} \int_0^1 y^{-\alpha(\eta)} \tilde{\pi}_{21}^\eta d\eta \quad (\text{A.34})$$

where we make use of the asymptotic expansion (A.32). In the limit $y \gg 1$, the integral above can be calculated approximately by the saddle point method if $\tilde{\pi}_{21}^\eta$ changes with η much slower than $y^{-\alpha(\eta)}$. Therefore we have

$$\frac{2C(y)}{N} = \tilde{\pi}_{21}^{\eta^*} y^{-\gamma} \quad (\text{A.35})$$

where γ and η^* are given by

$$\begin{aligned}\gamma &= \min_{\eta} \alpha(\eta) \\ \eta^* &= \operatorname{argmin}_{\eta} \alpha(\eta).\end{aligned}\tag{A.36}$$

By comparing both sides of Eq. (A.33) and using Eq. (A.35) we get

$$\begin{aligned}\tilde{\pi}_{12}^{\eta\eta'} &= \frac{1}{\tilde{\pi}_{21}^{\eta^*}} \tilde{\pi}_{21}^{\eta} \tilde{\pi}_{21}^{\eta'} \\ \alpha(\eta, \eta') &= \alpha(\eta) + \alpha(\eta') + \gamma.\end{aligned}\tag{A.37}$$

Finally, in order to fully solve the problem we impose the conservation laws of this heterogeneous model. In particular the total number of agent with value $\eta_i \in (\eta, \eta + \Delta\eta)$ is given by the following relation,

$$\sum_{t'} [N_1(t, t', \eta) + \sum_{\eta'} N_2(t, t', \eta, \eta')] = N\Delta(\eta).\tag{A.38}$$

Inserting the self-consistent ansatz Eq. (A.29) for $\pi_{12}(t)$ and Eq. (A.33) into Eq. (A.38) we get, in the continuous limit approximation valid for $N \gg 1$,

$$\begin{aligned}\tilde{\pi}_{21}^{\eta} y^{-\alpha(\eta)} &= \left[\frac{\theta(2\eta - 1)}{2\eta - 1} + \theta(1 - 2\eta) \right. \\ &\quad \left. \times B(1 - 2\eta, 1 - \alpha(\eta)) y^{1-2\eta} + I(\eta) \right]^{-1}\end{aligned}\tag{A.39}$$

where

$$\begin{aligned}I(\eta) &= \frac{N}{2C(y)} \int_0^1 \left[\frac{\theta(1 - \eta - \eta')}{1 - \eta - \eta'} + \theta(\eta + \eta' - 1) \right. \\ &\quad \left. \times B(\eta + \eta' - 1, 1 - \alpha(\eta')) y^{\eta+\eta'-1} \right] \\ &\quad \times \pi_{21}^{\eta'} y^{-\alpha(\eta')} d\eta'.\end{aligned}\tag{A.40}$$

We compute $I(\eta)$ defined in Eq. (A.40) by counting the leading term only. Therefore we find

$$\alpha(\eta) = \max(0, 1 - 2\eta, \eta - 1 + \gamma + D)\tag{A.41}$$

with D given by

$$D = \max_{\eta} [\eta - \alpha(\eta)].\tag{A.42}$$

Solving the Eqs. (A.41) and (A.42) we get $\gamma = 0$ and $D = \frac{1}{2}$ and $\eta^* = 1/2$. Therefore we can determine the exponent $\alpha(\eta)$ and $\alpha(\eta, \eta')$ that are given by

$$\begin{aligned}\alpha(\eta) &= \max\left(1 - 2\eta, \eta - \frac{1}{2}\right) \\ \alpha(\eta, \eta') &= \alpha(\eta) + \alpha(\eta').\end{aligned}\tag{A.43}$$

Moreover the constants $\tilde{\pi}_{21}^\eta$ are given, in the limit $N \gg 1$ and $y \gg 1$, by

$$\tilde{\pi}_{21}^\eta = \begin{cases} \frac{\rho(\eta)}{B(1-2\eta, 2\eta)} & \eta \leq \frac{1}{2} \\ \frac{\rho(\eta)}{B(\eta-\frac{1}{2}, 1)} & \eta \geq \frac{1}{2}. \end{cases}\tag{A.44}$$

Solving equation (A.46), let $\gamma + D \leq \frac{1}{2}$, then

$$\alpha(\eta) = \begin{cases} 1 - 2\eta & \eta \leq \frac{1}{2} \\ 0 & \frac{1}{2} \leq \eta \leq 1 - \gamma - D \\ \eta - 1 + \gamma + D & \eta \geq 1 - \gamma - D \end{cases}\tag{A.45}$$

and

$$\eta - \alpha(\eta) = \begin{cases} 3\eta - 1 & \eta \leq \frac{1}{2} \\ \eta & \frac{1}{2} \leq \eta \leq 1 - \gamma - D \\ 1 - \gamma - D & \eta \geq 1 - \gamma - D \end{cases}\tag{A.46}$$

obviously, $\gamma = 0$ and D is reached either at $\eta = \frac{1}{2}$ or $\eta = 1 - \gamma - D$, so

$$D = \max\left(\frac{1}{2}, 1 - D\right)\tag{A.47}$$

The only solution to the above expression is $D = \frac{1}{2}$. Similarly, for $\gamma + D \geq \frac{1}{2}$,

$$\alpha(\eta) = \begin{cases} 1 - 2\eta & \eta \leq \frac{2-\gamma-D}{3} \\ \eta - 1 + \gamma + D & \eta \geq \frac{2-\gamma-D}{3} \end{cases}\tag{A.48}$$

$$\eta - \alpha(\eta) = \begin{cases} 3\eta - 1 & \eta \leq \frac{2-\gamma-D}{3} \\ 1 - \gamma - D & \eta \geq \frac{2-\gamma-D}{3} \end{cases}\tag{A.49}$$

Both γ and D are reached at $\eta = \frac{2-\gamma-D}{3}$, so

$$\begin{cases} \gamma = 1 - \frac{2(2-\gamma-D)}{3} \\ D = (2 - \gamma - D) - 1 \end{cases}\tag{A.50}$$

Appendix B

Solution to the model of cellphone communication

B.1 Dynamical social network for pairwise communication

We consider a system consisting of N agents representing the mobile phone users. The agents are interacting in a social network G representing social ties such as friendships, collaborations or acquaintances. The network G is weighted with the weights indicating the strength of the social ties between agents. To model the mechanism of cellphone communication, the agents can call their neighbors in the social network G forming groups of interacting agents of size two. Since at any given time a call can be initiated or terminated the network is highly dynamical. We assign to each agent $i = 1, 2, \dots, N$ a coordination number n_i to indicate his/her state. If $n_i = 1$ the agent is non-interacting, and if $n_i = 2$ the agent is in a mobile phone connection with another agent. The dynamical process of the model at each time step t can be described explicitly by the following algorithm:

- (1) An agent i is selected randomly at time t .
- (2) The subsequent action of agent i depends on his/her current state (i.e. n_i):
 - (i) If $n_i = 1$, he/she will call one of his/her non-interacting neighbors j of G with probability $f_1(t_i, t)$ where t_i denotes the last time at which agent i has changed his/her state. Once he/she decides to call, agent j will be chosen randomly in between the neighbors of i with probability proportional to $f_1(t_j, t)$, therefore the coordination numbers of agent i and j are updated according to the rule $n_i \rightarrow 2$ and $n_j \rightarrow 2$.

- (ii) If $n_i = 2$, he/she will terminate his/her current connection with probability $f_2(t_i, t|w_{ij})$ where w_{ij} is the weight of the link between i and the neighbor j that is interacting with i . Once he/she decides to terminate the connection, the coordination numbers are then updated according to the rule $n_i \rightarrow 1$ and $n_j \rightarrow 1$.
- (3) Time t is updated as $t \rightarrow t + 1/N$ (initially $t = 0$) and the process is iterated until $t = T_{max}$.

B.2 General solution to the model

In order to solve the model analytically, we assume the quenched network G to be annealed and uncorrelated. Therefore we assume that at each time the network is rewired keeping the degree distribution $p(k)$ and the weight distribution $p(w)$ constant. Moreover we solve the model in the continuous time limit. Therefore we always approximate the sum over time-steps of size $\delta t = 1/N$ by integrals over time. We use $N_1^k(t_0, t)dt_0$ to denote the number of agents with degree k that at time t are not interacting and have not interacted with another agent since time $t' \in (t_0, t_0 + 1/N)$. Similarly we denote by $N_2^{k,k',w}(t_0, t)dt_0$ the number of connected agents (with degree respectively k and k' and weight of the link w) that at time t are interacting in phone call started at time $t' \in (t_0, t_0 + 1/N)$. Consistently with the annealed approximation the probability that an agent with degree k is called is proportional to its degree. Therefore the rate equations of the model are given by

$$\begin{aligned} \frac{\partial N_1^k(t_0, t)}{\partial t} &= -N_1^k(t_0, t)f_1(t_0, t) - ckN_1^k(t_0, t)f_1(t_0, t) + N\pi_{21}^k(t)\delta_{tt_0} \\ \frac{\partial N_2^{k,k',w}(t_0, t)}{\partial t} &= -2N_2^{k,k',w}(t_0, t)f_2(t_0, t|w) + N\pi_{12}^{k,k',w}(t)\delta_{tt_0} \end{aligned} \quad (\text{B.1})$$

where the constant c is given by

$$c = \frac{\sum_{k'} \int_0^t dt_0 N_1^{k'}(t_0, t) f_1(t_0, t)}{\sum_{k'} k' \int_0^t dt_0 N_1^{k'}(t_0, t) f_1(t_0, t)}. \quad (\text{B.2})$$

In Eqs. (B.1) the rates $\pi_{pq}(t)$ indicate the average number of agents changing from state $p = 1, 2$ to state $q = 1, 2$ at time t . These rates can be also expressed in a self-consistent way as

$$\begin{aligned} \pi_{21}^k(t) &= \frac{2}{N} \sum_{k',w} \int_0^t dt_0 f_2(t_0, t|w) N_2^{k,k',w}(t_0, t) \\ \pi_{12}^{k,k',w}(t) &= \frac{P(w)}{CN} \int_0^t dt_0 \int_0^t dt'_0 N_1^k(t_0, t) N_1^{k'}(t'_0, t) f_1(t_0, t) f_1(t'_0, t) (k + k') \end{aligned} \quad (\text{B.3})$$

where the constant C is given by

$$C = \sum_{k'} \int_0^t dt_0 k' N_1^{k'}(t_0, t) f_1(t_0, t). \quad (\text{B.4})$$

The solution to Eqs. (B.1) is given by

$$\begin{aligned} N_1^k(t_0, t) &= N \pi_{21}^k(t_0) e^{-(1+ck) \int_{t_0}^t f_1(t_0, t) dt} \\ N_2^{k,k',w}(t_0, t) &= N \pi_{12}^{k,k',w}(t_0) e^{-2 \int_{t_0}^t f_2(t_0, t|w) dt} \end{aligned} \quad (\text{B.5})$$

which must satisfy the self-consistent constraints Eqs. (B.3) and the conservation of the number of agents with different degree

$$\int dt_0 [N_1^k(t_0, t) + \sum_{k',w} N_2^{k,k',w}(t_0, t)] = N p(k). \quad (\text{B.6})$$

In the following we will denote by $P_1^k(t_0, t)$ the probability distribution that an agent with degree k is non-interacting for a period from t_0 to t and by $P_2^w(t_0, t)$ the probability that a connection of weight w at time t is active since time t_0 . It is immediate to see that these distributions are given by the number of individual in a state $n = 1, 2$ multiplied by the probability of having a change of state, i.e.

$$\begin{aligned} P_1^k(t_0, t) &= (1 + ck) f_1(t_0, t) N_1^k(t_0, t) \\ P_2^w(t_0, t) &= 2 f_2(t_0, t|w) \sum_{k,k'} N_2^{k,k',w}(t_0, t). \end{aligned} \quad (\text{B.7})$$

B.3 Stationary solution with specific $f_1(t_0, t)$ and $f_2(t_0, t)$

In order to capture the behavior of the empirical data with a realistic model, we have chosen

$$\begin{aligned} f_1(t_0, t) &= f_1(\tau) = \frac{b_1}{(1 + \tau)^\beta} \\ f_2(t_0, t|w) &= f_2(\tau|w) = \frac{b_2 g(w)}{(1 + \tau)^\beta} \end{aligned} \quad (\text{B.8})$$

with parameters $b_1 > 0$, $b_2 > 0$, $0 \leq \beta \leq 1$ and arbitrary positive function $g(w)$. In Eqs. (B.8), τ is the duration time elapsed since the agent has changed his/her state for the last time (i.e. $\tau = t - t_0$). The functions of $f_1(\tau)$ and $f_2(\tau|w)$ are decreasing function of their argument τ reflecting the reinforcement dynamics discussed in the main body of the paper. The function $g(w)$ is generally chosen as a decreasing function of w , indicating that connected agents with a stronger weight of link interact typically for a longer time.

We are especially interested in the stationary state solution of the dynamics. In this regime we have that for large times $t \gg 1$ the distribution of the number of agents is only dependent on τ . Moreover the transition rates $\pi_{pq}(t)$ also converge to a constant independent of t in the stationary state. Therefore the solution of the stationary state will satisfy

$$\begin{aligned} N_1^k(t_0, t) &= N_1^k(\tau) \\ N_2^{k,k',w}(t_0, t) &= N_2^{k,k',w}(\tau) \\ \pi_{pq}(t) &= \pi_{pq}. \end{aligned} \quad (\text{B.9})$$

The necessary condition for the stationary solution to exist is that the summation of self-consistent constraints given by Eq. (B.2) and Eq. (B.2) together with the conservation law Eq. (B.6) converge under the stationary assumptions Eqs. (B.9). The convergence depends on the value of the parameters b_0 , b_1 , β and the choice of function $g(w)$. In particular, when $0 \leq \beta < 1$, the convergence is always satisfied. In the following subsections, we will characterize further the stationary state solution of this model in different limiting cases.

B.3.1 Case $0 < \beta < 1$

The expression for the number of agent in a given state $N_1^k(\tau)$ and $N_2^{k,k',w}(\tau)$ can be obtained by substituting Eqs. (B.8) into the general solution Eqs. (B.5), using the stationary conditions Eqs. (B.9). In this way we get the stationary solution given by

$$\begin{aligned} N_1^k(\tau) &= N\pi_{21}^k e^{\frac{b_1(1+c_k)}{1-\beta}[1-(1+\tau)^{1-\beta}]} = N\pi_{21}^k m_1^k(\tau) \\ N_2^{k,k',w}(\tau) &= N\pi_{12}^{k,k',w} e^{\frac{2b_2g(w)}{1-\beta}[1-(1+\tau)^{1-\beta}]} = N\pi_{12}^{k,k',w} m_2^w(\tau). \end{aligned} \quad (\text{B.10})$$

To complete the solution is necessary to determine the constants π_{21}^k and $\pi_{12}^{k,k',w}$ in a self-consistent type of solution. To find the expression of $\pi_{12}^{k,k',w}$ as a function of π_{21}^k we substitute Eqs. (B.10) in Eq.(B.3) and we get

$$\begin{aligned} \pi_{12}^{k,k',w}(t) &= \frac{1}{C}\pi_{21}^k P(w) \left[k \int_0^t dt_0 m_1^k(t_0, t) f_1(t_0, t) \int_0^t dt'_0 N_1^{k'}(t'_0, t) f_1(t'_0, t) \right. \\ &\quad \left. + k' \int_0^t dt_0 m_1^k(t_0, t) f_1(t_0, t) \int_0^t dt'_0 N_1^{k'}(t'_0, t) f_1(t'_0, t) \right]. \end{aligned} \quad (\text{B.11})$$

Finally we get a closed equation for π_{21}^k by substituting Eq.(B.11) in Eq.(B.6) and using the definition of c and C , given respectively by Eq. (B.2) and Eq. (B.2). Therefore we

get

$$\begin{aligned} \pi_{21}^k & \left[\int_0^\infty m_1^k(\tau) d\tau + \int_{w_{min}}^{w_{max}} P(w) \int_0^\infty m_2^w(\tau) d\tau dw \right. \\ & \left. \times \left(ck \int_0^\infty m_1^k(\tau) f_1(\tau) d\tau + \int_0^\infty m_1^k(\tau) f_1(\tau) d\tau \right) \right] = p(k). \end{aligned} \quad (B.12)$$

Performing explicitly the last two integrals using the dynamical solution given by Eqs. (B.10), this equation can be simplified as

$$\pi_{21}^k = \left[\int_0^\infty m_1^k(\tau) d\tau + \int_{w_{min}}^{w_{max}} P(w) \int_0^\infty m_2^w(\tau) d\tau dw \right]^{-1} p(k). \quad (B.13)$$

Finally the self-consistent solution of the dynamics is solved by expressing Eq. (B.2) by

$$c = \frac{\sum_k \pi_{21}^k (1 + ck)^{-1}}{\sum_k \pi_{21}^k k (1 + ck)^{-1}}. \quad (B.14)$$

Therefore we can use Eqs. (B.13) and (B.14) to compute the numerical value of π_{21}^k and c . Inserting in these equations the expressions for $f_1(\tau)$, $f_2(\tau|w)$ given by Eqs. (B.8) and the solutions $N_1^k(\tau)$, $N_2^{k,k',w}(\tau)$ given by Eqs. (B.10) we get

$$\begin{aligned} P_1^k(\tau) & \propto \frac{b_1(1 + ck)}{(1 + \tau)^\beta} e^{-\frac{b_1(1+ck)}{1-\beta}(1+\tau)^{1-\beta}} \\ P_2^w(\tau) & \propto \frac{2b_2g(w)}{(1 + \tau)^\beta} e^{-\frac{2b_2g(w)}{1-\beta}(1+\tau)^{1-\beta}}. \end{aligned} \quad (B.15)$$

The probability distributions $P_1^k(\tau)$ and $P_2^w(\tau)$, can be manipulating performing a data collapse of the distributions, i.e.

$$\begin{aligned} \tau_1^*(k) P_1^k \left(x_1 = \frac{\tau}{\tau_1^*(k)} \right) & = A_1 x_1^{-\beta} e^{-\frac{x_1^{1-\beta}}{1-\beta}} \\ \tau_2^*(w) P_2^w \left(x_2 = \frac{\tau}{\tau_2^*(w)} \right) & = A_2 x_2^{-\beta} e^{-\frac{x_2^{1-\beta}}{1-\beta}} \end{aligned} \quad (B.16)$$

with $\tau_1^*(k)$ and $\tau_2^*(w)$ defined as

$$\begin{aligned} \tau_1^*(k) & = [b_1(1 + ck)]^{-\frac{1}{1-\beta}} \\ \tau_2^*(w) & = [2b_2g(w)]^{-\frac{1}{1-\beta}} \end{aligned} \quad (B.17)$$

where A_1 and A_2 are the normalization factors. The data collapse defined by Eqs. (B.16) of the curves $P_1^k(\tau)$, $P_2^w(\tau)$ and are both described by Weibull distributions.

B.4 Comparisons with quenched simulations

To check the validity of our annealed approximation versus quenched simulations, we performed a computer simulation according to the dynamical process on a quenched network. In Figure B.1 we compare the results of the simulation with the prediction of the analytical solution. In particular in the reported simulation we have chosen $\beta = 0.5$, $b_1 = 0.02$, $b_2 = 0.05$ and $g(w) = w^{-1}$, the simulation is based on a number of agent $N = 2000$ and for a period of $T_{max} = 10^5$, finally the data are averaged over 10 realizations and the network is Poisson with average $\langle k \rangle = 6$ and weight distribution $p(w) \propto w^{-2}$. In Figure B.1, we show evidence that the Weibull distribution and the data collapse of $P_2^w(\tau)$ well capture the empirical behavior observed in the mobile phone data (Figure 2.2). The distribution of the non-interaction periods $P_1^k(\tau)$ in the model is by construction unaffected by circadian rhythms but follow a similar data collapse as observed in the real data (Figure 2.4). The simulated data are also in good agreement with the analytical prediction predicted in the annealed approximation for the parameter chosen in the figure. As the network becomes more busy and many agents are in a telephone call, the quenched simulation and the annealed prediction of $P_1^k(\tau)$ differs more significantly.

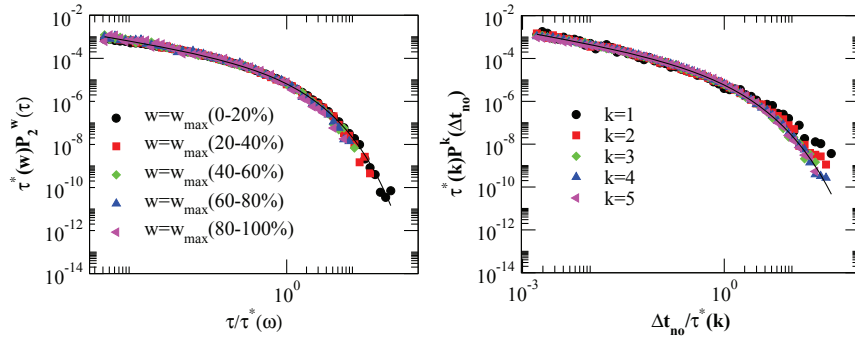


FIGURE B.1: Data collapse of the simulation of the proposed model for cell phone communication. In the panel (A) we plot the probability $P_2^w(\tau)$ that in the model a pair of agents with strength w are interacting for a period τ and in the panel (B) we plot the probability $P_1^k(\tau)$ that in the model an agent of degree k is non-interacting for a period τ . The simulation data on a quenched network are compared with the analytical predictions (solid lines) in the annealed approximation. The collapse of data of $P_2^w(\tau)$ is described by a Weibull distribution in agreement with the empirical results found in the mobile phone data.

B.4.1 Case $\beta = 0$

For $\beta = 0$ the functions $f_1(\tau)$ and $f_2(\tau|w)$ given by Eqs.(B.8) reduce to constants, therefore the process of creation of an interaction is a Poisson process and no reinforcement

dynamics is taking place in the network. Assigning $\beta = 0$ to Eqs. (B.5), we get the solution

$$\begin{aligned} N_1^k(\tau) &= N\pi_{21}^k e^{-b_1(1+ck)\tau} \\ N_2^{k,k',w}(\tau) &= N\pi_{12}^{k,k',w} e^{-2b_2g(w)\tau}. \end{aligned} \quad (\text{B.18})$$

and consequently the distributions of duration of given states Eqs. (B.7) are given by

$$\begin{aligned} P_1^k(\tau) &\propto e^{-b_1(1+ck)\tau} \\ P_2^w(\tau) &\propto e^{-2b_2g(w)\tau}. \end{aligned} \quad (\text{B.19})$$

Therefore the probability distributions $P_1^k(\tau)$ and $P_2^w(\tau)$ are exponentials as expected in a Poisson process.

B.4.2 Case $\beta = 1$

In this section, we discuss the case for $\beta = 1$ such that $f_1^k(\tau) \propto (1+\tau)^{-1}$ and $f_2^w(\tau|w) \propto (1+\tau)^{-1}$. Using Eqs. (B.1) we get the solution

$$\begin{aligned} N_1^k(\tau) &= N\pi_{21}^k (1+\tau)^{-b_1(1+ck)} \\ N_2^{k,k',w}(\tau) &= N\pi_{12}^{k,k',w} (1+\tau)^{-2b_2g(w)}. \end{aligned} \quad (\text{B.20})$$

and consequently the distributions of duration of given states Eqs. (B.7) are given by

$$\begin{aligned} P_1^k(\tau) &\propto \pi_{21}^k (1+\tau)^{-b_1(1+ck)-1} \\ P_2^w(\tau) &\propto \pi_{12}^{k,k',w} (1+\tau)^{-2b_2g(w)-1}. \end{aligned} \quad (\text{B.21})$$

The probability distributions are power-laws. This result remains valid for every value of the parameters $b_1, b_2, g(w)$ nevertheless the stationary condition is only valid for

$$\begin{aligned} b_1(1+ck) &> 1 \\ 2b_2g(w) &> 1. \end{aligned} \quad (\text{B.22})$$

Indeed this condition ensures that the self-consistent constraints Eqs. (B.2), (B.2) and the conservation law Eq. (B.6) have a stationary solution.

B.5 Solution of the mean-field model on a fully connected network

Finally, we discuss the mean-field limit on the model in which every agent can interact with every other agent. In this case, social network is a fully connected network. Therefore we use $N_1(t_0, t)$ and $N_2(t_0, t)$ to denote the number of agents of the two different states respectively and the rate equations are then revised to

$$\begin{aligned}\frac{\partial N_1(t_0, t)}{\partial t} &= -2N_1(t_0, t)f_1(t_0, t) + N\pi_{21}(t)\delta_{tt_0} \\ \frac{\partial N_2(t_0, t)}{\partial t} &= -2N_2(t_0, t)f_2(t_0, t) + N\pi_{12}(t)\delta_{tt_0}\end{aligned}\quad (\text{B.23})$$

Since we will refer to this model only in the framework of a null model, we will only discuss the case in which the dynamics of the network is Poissonian, i.e. when

$$\begin{aligned}f_1(t_0, t) &= b_1 \\ f_2(t_0, t) &= b_2.\end{aligned}\quad (\text{B.24})$$

The stationary solution of this model is given by exponentials, i.e.

$$\begin{aligned}N_1(\tau) &= N\pi_{21}e^{-2b_1\tau} \\ N_2(\tau) &= N\pi_{12}e^{-2b_2\tau}.\end{aligned}\quad (\text{B.25})$$

Finally the distributions of duration of given states expressed by Eqs. (B.7) are given by

$$\begin{aligned}P_1(\tau) &\propto e^{-2b_1\tau} \\ P_2(\tau) &\propto e^{-2b_2\tau},\end{aligned}\quad (\text{B.26})$$

which are exponential distributions as expected in a Poisson process.

Appendix C

Calculations of the entropy of temporal social networks

C.1 Entropy of the temporal social networks of pairwise communication

The definition of the entropy of temporal social networks of a pairwise communication model, is given by Eq. (3.6) of the main body of the article that we repeat here for convenience,

$$\begin{aligned} S = & - \sum_i P(g_i(t) = 1 | \mathcal{S}_t) \log P(g_i(t) = 1 | \mathcal{S}_t) \\ & - \sum_{ij} a_{ij} P(g_{ij}(t) = 1 | \mathcal{S}_t) \log P(g_{ij}(t) = 1 | \mathcal{S}_t) \end{aligned} \quad (C.1)$$

In this equation the matrix a_{ij} is the adjacency matrix of the social network and $g_{ij}(t) = 1$ indicates that at time t the agents i and j are interacting while $g_i(t) = 1$ indicates that agent i is non-interacting. Finally $\mathcal{S}_t = \{g_i(t'), g_{ij}(t') \quad \forall t' < t\}$ indicates the dynamical evolution of the social network. In this section, we evaluate the entropy of temporal social networks in the framework of the annealed model of pairwise communication explained in detail in Chapter 2 and Appendix B. To evaluate the entropy of dynamical social network explicitly, we have to carry out the summations in Eq. (C.1). These sums, will in general depend on the particular history of the dynamical social network, but in the framework of the model we study, in the large network limit will be dominated by their average value. In the following therefore we perform these sum in the large network limit. The first summation in Eq. (C.1) denotes the average loglikelihood of finding at time t a non-interacting agent given a history \mathcal{S}_t . We can distinguish between two

eventual situations occurring at time t : (i) the agent has been non-interacting since a time $t - \tau$, and at time t remains non-interacting; (ii) the agent has been interacting with another agent since time $t - \tau$, and at time t the conversation is terminated by one of the two interacting agents. In order to characterize situation (i) we indicate by $P_{1 \rightarrow 1}^k(\tau)$ the probability that a non-interacting agent with degree k in the social network, that has not interacted since a time τ , doesn't change state. Similarly, in order to characterize situation (ii), we indicate by $P_{2 \rightarrow 1}^{k,k',w}(\tau)$ the probability that a connected pair of agents (with degrees k and k' respectively, and weight of the link w) have interacted since time τ and terminate their conversation at time t . Given the stationary solution of the pairwise communication model, performed in the annealed approximation, the rates $P_{1 \rightarrow 1}^k(\tau)$ and $P_{2 \rightarrow 1}^{k,k',w}(\tau)$ are given by

$$\begin{aligned} P_{1 \rightarrow 1}^k(\tau) &= 1 - \frac{f_1(\tau)}{N} - \frac{k f_1(\tau)}{NC} \sum_{k'} \int N_1^{k'}(\tau') f_1(\tau') d\tau' \\ &= 1 - (1 + ck) \frac{f_1(\tau)}{N} \\ P_{2 \rightarrow 1}^{k,k',w}(\tau) &= \frac{2f_2(\tau|w)}{N} \end{aligned} \quad (\text{C.2})$$

where the constant C is given by

$$C = \sum_{k'} \int k' N_1^{k'}(\tau') f_1(\tau') d\tau' \quad (\text{C.3})$$

and $f_1(\tau)$ and $f_2(\tau|w)$ are given in Chapter 2. The variable $N_1^k(\tau)$ indicates the number of agents of connectivity k noninteracting since a time τ . This number can in general fluctuate but in the large network limit it converges to its mean-field value given by Eq. (B.10). The second term in the right hand side of Eq. (C.1), denotes the average loglikelihood of finding two agents in a connected pair at time t given a history \mathcal{S}_t . There are two possible situations that might occur for two interacting agents at time t : (iii) these two agents have been non-interacting, and to time t one of them decides to form a connection with the other one; (iv) the two agents have been interacting with each other since a time $t - \tau$, and they remain interacting at time t . To describe the situation (iii), we indicate by $P_{1 \rightarrow 2}^{k,k'}(\tau, \tau')$ the probability that two non interacting agents, isolated since time $t - \tau$ and $t - \tau'$ respectively, interact at time t . In order to describe situation (iv), we denote by $P_{2 \rightarrow 2}^{k,k',w}(\tau)$ the probability that two interacting agents, in interaction since a time $t - \tau$, remain interacting at time t . In the framework of the stationary annealed approximation of the dynamical network these probabilities are given by

$$\begin{aligned} P_{1 \rightarrow 2}^{k,k'}(\tau, \tau') &= \frac{f_1(\tau) f_1(\tau')}{NC} (k + k') \\ P_{2 \rightarrow 2}^{k,k',w}(\tau) &= 1 - \frac{2f_2(\tau|w)}{N}. \end{aligned} \quad (\text{C.4})$$

Therefore, the entropy of temporal social networks given by Eq. (C.1) can be evaluated in the thermodynamic limit, and in the annealed approximation, according to the expression

$$\begin{aligned}
\mathcal{S} = & - \sum_k \int_0^\infty N_1^k(\tau) P_{1 \rightarrow 1}^k(\tau) \log P_{1 \rightarrow 1}^k(\tau) d\tau \\
& - \sum_{k,k',w} \int_0^\infty N_2^{k,k',w}(\tau) P_{2 \rightarrow 1}^{k,k',w}(\tau) \log P_{2 \rightarrow 1}^{k,k',w}(\tau) d\tau \\
& - \frac{1}{2} \sum_{k,k'} \int_0^\infty \int_0^\infty N_1^k(\tau) N_1^{k'}(\tau') P_{1 \rightarrow 2}^{k,k'}(\tau, \tau') \log P_{1 \rightarrow 2}^{k,k'}(\tau, \tau') d\tau d\tau' \\
& - \frac{1}{2} \sum_{k,k',w} \int_0^\infty N_2^{k,k',w}(\tau) P_{2 \rightarrow 2}^{k,k',w}(\tau) \log P_{2 \rightarrow 2}^{k,k',w}(\tau) d\tau, \tag{C.5}
\end{aligned}$$

with $N_1^k(\tau)$ and $N_2^{k,k',w}(\tau)$ given in the large network limit by Eqs. (B.10) in Appendix B.

C.2 Entropy of the null model

To understand the impact of the distribution of duration of the interactions and of the distribution of non-interaction periods, we have compared the entropy S of the pairwise communication model with the entropy S_R of a null model. Here we use the exponential mean-field model described in Section B.5 as our null model. In this model the agents are embedded in a fully connected networks and the probability of changing the agent state does not include the reinforcement dynamics. In fact we have that the transition rates are independent of time ($\beta = 0$) and given by $f_1^R(\tau) = b_1^R$ and $f_2^R(\tau) = b_2^R$. Following the same steps for evaluating S in the model of pairwise communication on the networks, it can be easily proved that the entropy S_R of the dynamical null model is given by

$$\begin{aligned}
S_R = & - \int_0^\infty N_1^R(\tau) \left[1 - \frac{2b_1^R}{N} \right] \log \left[1 - \frac{2b_1^R}{N} \right] d\tau \\
& - \int_0^\infty N_2^R(\tau) \frac{2b_2^R}{N} \log \frac{2b_2^R}{N} d\tau \\
& - \frac{1}{2} \int_0^\infty \int_0^\infty N_1^R(\tau) N_1^R(\tau') \frac{2b_1^R}{NC^R} \log \frac{2b_1^R}{NC^R} d\tau d\tau' \\
& - \frac{1}{2} \int_0^\infty N_2^R(\tau) \left[1 - \frac{2b_2^R}{N} \right] \log \left[1 - \frac{2b_2^R}{N} \right] d\tau \tag{C.6}
\end{aligned}$$

where the constant C^R is given by

$$C^R = \int_0^\infty N_1^R(\tau) d\tau, \tag{C.7}$$

and where N_1, N_2 are given, in the large network limit by their mean-field value given by Eq.(B.25). In order to build an appropriate null model for the pairwise communication model parametrized by (β, b_1, b_2) , we take the parameters of the null model b_1^R and b_2^R such that the proportion of the total number of agents in the two states (interacting or non-interacting) is the same in the pairwise model of social communication and in the null model. In order to ensure this condition we need to satisfy the following relation

$$\frac{\sum_k \int_0^\infty N_1^k(\tau) d\tau}{\sum_{k,k',w} \int_0^\infty N_2^{k,k',w}(\tau) d\tau} = \frac{\int_0^\infty N_1^R(\tau) d\tau}{\int_0^\infty N_2^R(\tau) d\tau}. \quad (C.8)$$

In particular we have chosen $b_1^R = b_1$ and we have used Eq. (C.8) to determine b_2^R .

C.3 Measurement of the entropy of a typical week-day of cell-phone communication from the data

In this section we discuss the method of measuring the dynamical entropy from empirical cellphone data as a function of time t in a typical weekday. This analysis gave rise to the results presented in Figure 3.2 in Chapter 3. We have analyzed the call sequence of subscribers of a major European mobile service provider. We considered calls between users who at least once called each other during the examined 6 months period in order to examine calls only reflecting trusted social interactions. The resulted event list consists of 633,986,311 calls between 6,243,322 users. For the entropy calculation we selected 562,337 users who executed at least one call per a day during a working week period. Since the network is very large we have assumed that the dynamical entropy can be evaluate in the mean-field approximation. We measured the following quantities directly from the sample:

- $N_1(\tau, t)$ the number of agents in the sample that at time t are not in a conversation since time $t - \tau$;
- $N^{calls}(\tau, t)$ the number of agents in the sample that are not in a conversation since time $t - \tau$ and make a call at time t ;
- $N^{called}(\tau, t)$ the number of agents in the sample that are not in a conversation since time $t - \tau$ and are called at time t ;
- $M^{in}(\tau, t)$ the number of agents that at time t are in a conversation of duration τ with another agent in the sample;
- $M^{out}(\tau, t)$ the number of agents that at time t are in a conversation of duration τ with another agent outside the sample;

- $M^{end}(\tau, t)$ the number of calls of duration τ that end at time t .

Using the above quantities, we estimated the probability $p^{calls}(\tau, t)$ that an agent makes a call at time t after a non-interaction period of duration τ , the probability $p^{called}(\tau, t)$ that an agent is called at time t after a non-interaction period of duration τ and the probability $\pi(\tau, t)$ that a call of duration τ ends at time t , according to the following relations

$$\begin{aligned} p^{calls}(\tau, t) &= \frac{N^{calls}(\tau, t)}{N_1(\tau, t)} \\ p^{called}(\tau, t) &= \frac{N^{called}(\tau, t)}{N_1(\tau, t)} \\ \pi(\tau, t) &= \frac{M^{end}(\tau, t)}{M^{in}(\tau, t)/2 + M^{out}(\tau, t)}. \end{aligned} \quad (\text{C.9})$$

Since the sample of 562,337 users we are considering is a subnetwork of the whole dataset constituted by 6,243,322 users, in our measurement, an agent can be in one of three possible states

- *state 1*: the agent is non-interacting;
- *state 2*: the agent is in a conversation with another agent of the sample;
- *state 3*: the agent is in a conversation with an agent outside the sample.

Therefore, to evaluate the entropy of the data, we can modify Eq.(C.1) into

$$\begin{aligned} \mathcal{S}(t) = & - \sum_i P(g_i(t) = 1 | \mathcal{S}_t) \log P(g_i(t) = 1 | \mathcal{S}_t) \\ & - \sum_{ij} a_{ij} P(g_{ij}(t) = 1 | \mathcal{S}_t) \log P(g_{ij}(t) = 1 | \mathcal{S}_t) \\ & - \sum_i P(g'_i(t) = 1 | \mathcal{S}_t) \log P(g'_i(t) = 1 | \mathcal{S}_t) \end{aligned} \quad (\text{C.10})$$

where a_{ij} is the adjacency matrix of the quenched social network, $g_i(t) = 1$ indicates that the agent i is in state 1, $g_{ij}(t) = 1$ indicates that the agent is in state 2 interacting with agent j and $g'_i(t) = 1$ indicates the agent i is in state 3. Finally $\mathcal{S}_t = \{g_i(t'), g_{ij}(t') g'_i(t) \ \forall t' < t\}$ indicates the dynamical evolution of the social network. To explicitly evaluate Eq. (C.10) in the large network limit where we assume that the dependence on the particular history are vanishing, we sum over the loglikelihood of all transitions between different states using the same strategy in the last section, which

is

$$\begin{aligned}
\mathcal{S}(t) = & - \sum_{\tau} N_1(\tau, t) P_{1 \rightarrow 1}(\tau, t) \log P_{1 \rightarrow 1}(\tau, t) \\
& - \sum_{\tau} M^{in}(\tau, t) P_{2 \rightarrow 1}(\tau, t) \log P_{2 \rightarrow 1}(\tau, t) \\
& - \sum_{\tau} M^{out}(\tau, t) P_{3 \rightarrow 1}(\tau, t) \log P_{3 \rightarrow 1}(\tau, t) \\
& - \frac{1}{2} \sum_{\tau, \tau'} N_1(\tau, t) N_1(\tau', t) P_{1 \rightarrow 2}(\tau, \tau', t) \log P_{1 \rightarrow 2}(\tau, \tau', t) \\
& - \frac{1}{2} \sum_{\tau} M^{in}(\tau, t) P_{2 \rightarrow 2}(\tau, t) \log P_{2 \rightarrow 2}(\tau, t) \\
& - \sum_{\tau} N_1(\tau, t) P_{1 \rightarrow 3}(\tau, t) \log P_{1 \rightarrow 3}(\tau, t) \\
& - \sum_{\tau} M^{out}(\tau, t) P_{3 \rightarrow 3}(\tau, t) \log P_{3 \rightarrow 3}(\tau, t). \tag{C.11}
\end{aligned}$$

where the probabilities of transitions between different states are given by

$$\begin{aligned}
P_{1 \rightarrow 1}(\tau, t) &= 1 - p^{calls}(\tau, t) - p^{called}(\tau, t) \\
P_{2 \rightarrow 1}(\tau, t) &= P_{3 \rightarrow 1}(\tau, t) = \pi(\tau, t) \\
P_{1 \rightarrow 2}(\tau, \tau', t) &= \frac{(1 - \gamma)}{C} \left[p^{calls}(\tau, t) p^{called}(\tau', t) + p^{calls}(\tau', t) p^{called}(\tau, t) \right] \\
P_{2 \rightarrow 2}(\tau, t) &= P_{3 \rightarrow 3}(\tau, t) = 1 - \pi(\tau, t) \\
P_{1 \rightarrow 3}(\tau, t) &= \gamma \left[p^{calls}(\tau, t) + p^{called}(\tau, t) \right] \tag{C.12}
\end{aligned}$$

and where C is given by

$$C = \sum_{\tau} N_1(\tau, t) p^{called}(\tau, t). \tag{C.13}$$

Finally in C.12 we have introduced a parameter $\gamma \in [0, 1]$ to denote the portion of the calls occurring between an agent in the sample and an agent out of the sample. For simplicity, we assume that γ is a constant. Substituting Eq.(C.12) into Eq.(C.11), we have performed the summation over τ to obtain the value of entropy as a function of t presented in Figure 3.2 in Chapter 3 where we have taken $\gamma = 0.8$, consistently with the data.

Bibliography

- [1] C. Cattuto, W. V. d. Broeck, A. Barrat, V. Colizza, J. F. Pinton, and A. Vespignani, “Dynamics of person-to-person interactions from distributed rfid sensor networks,” *PloS one*, p. e11596, 2010.
- [2] S. N. Dorogovtsev, J. F. F. Mendes, and A. N. Samukhin, “Structure of growing networks with preferential linking,” *Physical Review Letters*, vol. 85, no. 21, pp. 4633–4636, 2000.
- [3] P. L. Krapivsky, S. Redner, and F. Leyvraz, “Connectivity of growing random networks,” *Physical Review Letters*, vol. 85, pp. 4629–4632, 2000.
- [4] P. L. Krapivsky and S. Redner, “Organization of growing random networks,” *Physical Review E*, vol. 63, no. 6, p. 066123, 2001.
- [5] G. Bianconi and A.-L. Barabási, “Bose-einstein condensation in complex networks,” *Physical Review Letters*, vol. 86, no. 24, pp. 5632–5635, 2001.
- [6] S. N. Dorogovtsev and J. F. F. Mendes, “Evolution of networks with aging of sites,” *Physical Review E*, vol. 62, no. 2, p. 1842, 2000.
- [7] R. Albert and A.-L. Barabási, “Statistical mechanics of complex networks,” *Review of Modern Physics*, vol. 74, pp. 47–97, 2002.
- [8] S. N. Dorogovtsev and J. F. F. Mendes, *Evolution of networks: From biological nets to the Internet and WWW*. Oxford University Press, 2003.
- [9] M. E. J. Newman, “The structure and function of complex networks,” *SIAM Review*, vol. 45, pp. 167–256, 2003.
- [10] R. Pastor-Satorras and A. Vespignani, *Evolution and structure of the Internet: A statistical physics approach*. Cambridge University Press, 2004.
- [11] S. Boccaletti, V. Latora, Y. Moreno, M. Chavez, and D.-U. Hwang, “Complex networks: Structure and dynamics,” *Physics Reports*, vol. 424, no. 4-5, pp. 175–308, 2006.

-
- [12] A. Barrat, M. Barthélemy, and A. Vespignani, *Dynamical processes on complex networks*. Cambridge University Press, 2008.
- [13] M. E. J. Newman, *Networks: An introduction*. Oxford University Press, 2010.
- [14] S. N. Dorogovtsev, A. V. Goltsev, and J. F. F. Mendes, “Critical phenomena in complex networks,” *Review of Modern Physics*, vol. 80, p. 1275, 2008.
- [15] P. Holme and J. Saramäki, “Temporal networks,” *Physics Reports*, vol. 519, pp. 97–125, 2012.
- [16] A.-L. Barabási, “The origin of bursts and heavy tails in humans dynamics,” *Nature*, vol. 435, pp. 207–211, 2005.
- [17] S. V. Buldyrev, R. Parshani, G. Paul, H. E. Stanley, and S. Havlin, “Catastrophic cascade of failures in interdependent networks,” *Nature*, vol. 464, no. 7291, pp. 1025–1028, 2010. 10.1038/nature08932.
- [18] A. Vespignani, “Complex networks: The fragility of interdependency,” *Nature*, vol. 464, no. 7291, pp. 984–985, 2010. 10.1038/464984a.
- [19] J. L. Moreno, “Who shall survive?,” 1953.
- [20] S. Milgram, “The small world problem,” *Psychology today*, vol. 2, no. 1, pp. 60–67, 1967.
- [21] D. J. Watts and S. S. H., “Collective dynamics of a small-world networks,” *Nature*, vol. 393, pp. 440–442, 1998.
- [22] A.-L. Barabási and R. Albert, “Emergence of scaling in random networks,” *Science*, vol. 286, pp. 509–512, 1999.
- [23] G. Bianconi and A. L. Barabási, “Competition and multiscaling in evolving networks,” *Europhysics Letters*, vol. 54, no. 4, p. 436, 2001.
- [24] B. Bollobás, *A probabilistic proof of an asymptotic formula for the number of labelled regular graphs*. Matematisk Inst., Univ., 1979.
- [25] J. Tang, S. Scellato, M. Musolesi, C. Mascolo, and V. Latora, “Small-world behavior in time-varying graphs,” *Physical Review E*, vol. 81, p. 055101, 2010.
- [26] J. M. Kumpula, J.-P. Onnela, J. Saramäki, K. Kaski, and J. Kertész, “Emergence of communities in weighted networks,” *Physical review letters*, vol. 99, no. 22, p. 228701, 2007.

- [27] N. F. Johnson, C. Xu, Z. Zhao, N. Ducheneaut, N. Yee, G. Tita, and P. M. Hui, "Human group formation in online guilds and offline gangs driven by a common team dynamic," *Physical Review E*, vol. 79, no. 6, p. 066117, 2009.
- [28] G. Palla, A.-L. Barabási, and T. Vicsek, "Quantifying social group evolution," *Nature*, vol. 446, no. 664-667, 2007.
- [29] J. Davidsen, H. Ebel, and S. Bornholdt, "Emergence of a small world from local interactions: Modeling acquaintance networks," *Physical review letters*, vol. 88, p. 128701, 2002.
- [30] M. Marsili, F. Vega-Redondo, and F. Slanina, "The rise and fall of a networked society: A formal model," *Proceedings of the National Academy of Sciences of USA*, vol. 101, pp. 1439–1442, 2004.
- [31] P. Holme and M. E. J. Newman, "Nonequilibrium phase transition in the coevolution of networks and opinions," *Physical Review E*, vol. 74, p. 05108, 2006.
- [32] F. Vazquez, V. M. Eguíluz, and M. S. Miguel, "Generic absorbing transition in coevolution dynamics," *Physical review letters*, vol. 100, no. 10, p. 108702, 2008.
- [33] C. Nardini, B. Kozma, and A. Barrat, "Whos talking first? consensus or lack thereof in coevolving opinion formation models," *Physical review letters*, vol. 100, no. 15, p. 158701, 2008.
- [34] B. Kozma and A. Barrat, "Consensus formation on adaptive networks," *Physical Review E*, vol. 77, no. 1, p. 016102, 2008.
- [35] T. Gross and H. Sayama, *Adaptive networks*. Springer, 2009.
- [36] G. Chowell, J. M. Hyman, S. Eubank, and C. Castillo-Chavez, "Scaling laws for the movement of people between locations in a large city," *Physical Review E*, vol. 68, no. 6, p. 066102, 2003.
- [37] A. De Montis, M. Barthélemy, A. Chessa, and A. Vespignani, "The structure of inter-urban traffic," *Environmental Planning Journal B*, vol. 34, pp. 905–924, 2007.
- [38] A. Barrat, M. Barthelemy, R. Pastor-Satorras, and A. Vespignani, "The architecture of complex weighted networks," *Proceedings of the National Academy of Sciences of the United States of America*, vol. 101, no. 11, pp. 3747–3752, 2004.
- [39] D. Brockmann, L. Hufnagel, and T. Geisel, "The scaling laws of human travel," *Nature*, vol. 439, pp. 462–465, 2006.

- [40] A. Gautreau, A. Barrat, and M. Barthélemy, “Microdynamics in stationary complex networks,” *Proceedings of the National Academy of Sciences*, vol. 106, no. 22, pp. 8847–8852, 2009.
- [41] D. Balcan, V. Colizza, B. Gonçalves, H. Hu, J. J. Ramasco, and A. Vespignani, “Multiscale mobility networks and the spatial spreading of infectious diseases,” *Proceedings of the National Academy of Sciences*, vol. 106, no. 51, pp. 21484–21489, 2009.
- [42] M. C. González, C. A. Hidalgo, and A.-L. Barabási, “Understanding individual human mobility patterns,” *Nature*, vol. 453, pp. 779–782, 2008.
- [43] C. Song, Z. Qu, N. Blumm, and A. L. Barabási, “Limits of predictability in human mobility,” *Science*, vol. 327, pp. 1018–1021, 2010.
- [44] P. Hui, A. Chaintreau, J. Scott, R. Gass, J. Crowcroft, and C. Diot, “Pocket switched networks and human mobility in conference environments,” *Proceedings of the 2005 ACM SIGCOMM workshop on Delay-tolerant networking*, pp. 244–251, 2005.
- [45] N. Eagle and A. S. Pentland, “Reality mining: Sensing complex social systems,” *Personal and Ubiquitous Computing*, vol. 10, pp. 255–268, 2006.
- [46] E. O'Neill, V. Kostakos, T. Kindberg, A. Penn, D. S. Fraser, T. Jones, *et al.*, “Instrumenting the city: Developing methods for observing and understanding the digital cityscape,” in *UbiComp 2006: Ubiquitous Computing*, pp. 315–332, Springer, 2006.
- [47] A. S. Pentland and S. Pentland, *Honest signals: how they shape our world*. MIT press, 2008.
- [48] M. Salathé, M. Kazandjieva, J. W. Lee, P. Levis, M. W. Feldman, and J. H. Jones, “A high-resolution human contact network for infectious disease transmission,” *Proceedings of the National Academy of Sciences*, vol. 107, no. 51, pp. 22020–22025, 2010.
- [49] <http://www.sociopatterns.org>.
- [50] H. Alani, M. Szomszor, C. Cattuto, W. Van den Broeck, G. Correndo, and A. Barrat, “Live social semantics,” in *The Semantic Web-ISWC 2009*, pp. 698–714, Springer, 2009.
- [51] L. Isella, J. Stehlé, A. Barrat, C. Cattuto, J.-F. Pinton, and W. Van den Broeck, “What’s in a crowd? analysis of face-to-face behavioral networks,” *Journal of theoretical biology*, vol. 271, no. 1, pp. 166–180, 2011.

- [52] J. P. Eckmann, E. Moses, and D. Sergi, “Entropy of dialogues creates coherent structures in e-mail traffic,” *Proceedings of the National Academy of Sciences of USA*, vol. 101, p. 14333, 2004.
- [53] G. Kossinets and D. J. Watts, “Empirical analysis of an evolving social network,” *Science*, vol. 311, no. 5757, pp. 88–90, 2006.
- [54] S. A. Golder, D. M. Wilkinson, and B. A. Huberman, “Rhythms of social interaction: Messaging within a massive online network,” in *Communities and Technologies 2007*, pp. 41–66, Springer, 2007.
- [55] J. Leskovec and E. Horvitz, “Planetary-scale views on a large instant-messaging network,” in *Proceedings of the 17th international conference on World Wide Web*, pp. 915–924, ACM, 2008.
- [56] D. Rybski, S. V. Buldyrev, S. Havlin, F. Liljeros, and H. A. Makse, “Scaling laws of human interaction activity,” *Proceedings of the National Academy of Sciences of USA*, vol. 106, pp. 12640–12645, 2009.
- [57] R. D. Malmgren, D. B. Stouffer, A. S. L. O. Campanharo, and L. A. Nunes Amaral, “On universality in human correspondence activity,” *Science*, vol. 325, pp. 1696–1700, 2009.
- [58] J. F. Padgett and C. K. Ansell, “Robust action and the rise of the medici, 1400–1434,” *American journal of sociology*, pp. 1259–1319, 1993.
- [59] M. J. Lubbers, J. L. Molina, J. Lerner, U. Brandes, J. Ávila, and C. McCarty, “Longitudinal analysis of personal networks. the case of argentinean migrants in spain,” *Social Networks*, vol. 32, no. 1, pp. 91–104, 2010.
- [60] A. Scherrer, P. Borgnat, E. Fleury, J.-l. Guillaume, and C. Robardet, “Description and simulation of dynamic mobility networks,” *Computer Networks*, vol. 52, no. 15, pp. 2842–2858, 2008.
- [61] P. Holme, “Network reachability of real-world contact sequences,” *Physical Review E*, vol. 71, p. 046119, 2005.
- [62] A. Vazquez, B. Rácz, A. Lukács, and A. L. Barabási, “Impact of non-poissonian activity patterns on spreading processes,” *Physical Review Letters*, vol. 98, no. 15, p. 158702, 2007.
- [63] J.-P. Onnela, J. Saramäki, G. Szabó, D. Lazer, K. Kaski, J. Kertész, and A.-L. Barabási, “Structure and tie strengths in mobile communication networks,” *Proceedings of the National Academy of Sciences of USA*, vol. 104, no. 18, pp. 7332–7336, 2007.

- [64] R. Parshani, M. Dickison, R. Cohen, H. E. Stanley, and S. Havlin, "Dynamic networks and directed percolation," *Europhysics Letter*, vol. 90, p. 38004, 2010.
- [65] A. Mowshowitz and M. Dehmer, "Entropy and the complexity of graphs revisited," *Entropy*, vol. 14, no. 3, pp. 559–570, 2012.
- [66] J. Körner, "Coding of an information source having ambiguous alphabet and the entropy of graphs," *6th Prague Conference on Information Theory*, pp. 411–425, 1973.
- [67] M. Dehmer and A. Mowshowitz, "A history of graph entropy measures," *Information Sciences*, vol. 181, no. 1, pp. 57–78, 2011.
- [68] G. Simonyi, "Graph entropy: a survey," *Combinatorial Optimization*, vol. 20, p. 399–441, 1995.
- [69] G. Bianconi, "The entropy of randomized network ensembles," *Europhysics Letter*, vol. 81, p. 28005, 2008.
- [70] G. Bianconi, "The entropy of network ensembles," *Physical Review E*, vol. 79, p. 036114, 2009.
- [71] K. Anand and G. Bianconi, "Entropy measures for networks: Toward an information theory of complex topologies," *Physical Review E*, vol. 80, p. 045102, 2009.
- [72] K. Anand and G. Bianconi, "Gibbs entropy of network ensembles by cavity methods," *Physical Review E*, vol. 82, no. 1, p. 011116, 2010.
- [73] K. Anand, G. Bianconi, and S. Severini, "Shannon and von neumann entropy of random networks with heterogeneous expected degree," *Physical Review E*, vol. 83, p. 036109, 2011.
- [74] M. E. Newman, S. H. Strogatz, and D. J. Watts, "Random graphs with arbitrary degree distributions and their applications," *Physical Review E*, vol. 64, no. 2, p. 026118, 2001.
- [75] M. Molloy and B. Reed, "A critical point for random graphs with a given degree sequence," *Random Structures and Algorithms*, vol. 6, p. 161, 1995.
- [76] R. Cohen, K. Erez, D. Ben-Avraham, and S. Havlin, "Resilience of the internet to random breakdowns," *Physical Review Letters*, vol. 85, p. 4626, 2000.
- [77] S.-W. Son, G. Bizhani, C. Christensen, P. Grassberger, and M. Paczuski, "Percolation theory on interdependent networks based on epidemic spreading," *EPL (Europhysics Letters)*, vol. 97, no. 1, p. 16006, 2012.

- [78] R. Parshani, S. V. Buldyrev, and S. Havlin, “Interdependent networks: Reducing the coupling strength leads to a change from a first to second order percolation transition,” *Physical review letters*, vol. 105, no. 4, p. 048701, 2010.
- [79] S.-W. Son, P. Grassberger, and M. Paczuski, “Percolation transitions are not always sharpened by making networks interdependent,” *Physical Review Letters*, vol. 107, no. 19, p. 195702, 2011.
- [80] G. Baxter, S. Dorogovtsev, A. Goltsev, and J. Mendes, “Bootstrap percolation on complex networks,” *Physical Review E*, vol. 82, no. 1, p. 011103, 2010.
- [81] S. Dorogovtsev, A. Goltsev, and J. Mendes, “k-core architecture and k-core percolation on complex networks,” *Physica D: Nonlinear Phenomena*, vol. 224, no. 1, pp. 7–19, 2006.
- [82] D. Achlioptas, R. M. D’Souza, and J. Spencer, “Explosive percolation in random networks,” *Science*, vol. 323, no. 5920, pp. 1453–1455, 2009.
- [83] K. Zhao and G. Bianconi, “Social interactions model and adaptability of human behavior,” *Frontiers in Physiology*, vol. 2, 2011.
- [84] K. Zhao, M. Karsai, and G. Bianconi, “Entropy of dynamical social networks,” *PloS one*, vol. 6, no. 12, p. e28116, 2011.
- [85] K. Zhao, J. Stehlé, G. Bianconi, and A. Barrat, “Social network dynamics of face-to-face interactions,” *Physical Review E*, vol. 83, no. 5, p. 056109, 2011.
- [86] K. Zhao, M. Karsai, and G. Bianconi, *Temporal Networks*, ch. Models, entropy and information of temporal social networks. Springer, 2013.
- [87] G. Caldarelli, *Scale-free networks*. Oxford University Press, 2007.
- [88] C. Castellano, S. Fortunato, and V. Loreto, “Statistical physics of social dynamics,” *Review of Modern Physics*, vol. 81, pp. 591–646, 2009.
- [89] Y. Y. Ahn, J. P. Bagrow, and S. Lehmann, “Link communities reveal multiscale complexity in networks,” *Nature*, vol. 466, pp. 761–764, 2010.
- [90] G. Bianconi, P. Pin, and M. Marsili, “Assessing the relevance of node features for network structure,” *Proceedings of the National Academy of Sciences of USA*, vol. 106, no. 28, pp. 11433–11438, 2009.
- [91] G. Bianconi, “Mean field solution of the ising model on a barabási-albert network,” *Physics Letters A*, vol. 303, no. 2, pp. 166–168, 2002.

- [92] S. Bradde, F. Caccioli, L. Dall’Asta, and G. Bianconi, “Critical fluctuations in spatial complex networks,” *Physical review letters*, vol. 104, no. 21, p. 218701, 2010.
- [93] M. Granovetter, “The strength in weak ties,” *American Journal of Sociology*, vol. 78, pp. 1360–1380, 1973.
- [94] S. Wasserman and K. Faust, *Social network analysis: Methods and applications*. Cambridge University Press, 1994.
- [95] A. Vázquez, J. G. Oliveira, Z. Dezsó, K.-I. Goh, I. Kondor, and A.-L. Barabási, “Modeling bursts and heavy tails in human dynamics,” *Physical Review E*, vol. 73, p. 036127, 2006.
- [96] J. Stehlé, A. Barrat, and G. Bianconi, “Dynamical and bursty interactions in social networks,” *Physical Review E*, vol. 81, no. 3, pp. 1–4, 2010.
- [97] M. Karsai, K. Kaski, A.-L. Barabási, and J. Kertész, “Universal features of correlated bursty behaviour,” *Scientific Reports*, vol. 2, p. 397, 2012.
- [98] H.-H. Jo, M. Karsai, J. Kertész, and K. Kaski, “Circadian pattern and burstiness in mobile phone communication,” *New Journal of Physics*, vol. 14, p. 013055, 2012.
- [99] M. Karsai, M. Kivelä, R. K. Pan, K. Kaski, J. Kertész, A. L. Barabási, and J. Saramäki, “Small but slow world: how network topology and burstiness slow down spreading,” *Physical Review E*, vol. 83, p. 025102, 2011.
- [100] K. Zhao, A. Halu, S. Severini, and G. Bianconi, “Entropy rate of nonequilibrium growing networks,” *Physical Review E*, vol. 84, no. 6, p. 066113, 2011.
- [101] G. Bisson, G. Bianconi, and V. Torre, “The dynamics of group formation among leeches,” *Frontiers in Physiology*, vol. 3, 2012.
- [102] C. Anteneodo and D. R. Chialvo, “Unraveling the fluctuations of animal motor activity,” *Chaos*, vol. 19, p. 033123, 2009.
- [103] E. G. Altmann, J. B. Pierrehumbert, and A. E. Motter, “Beyond word frequency: Bursts, lulls, and scaling in the temporal distributions of words,” *PloS one*, vol. 4, p. e7678, 2009.
- [104] D. Quercia, R. Lambiotte, D. Stillwell, M. Kosinski, and J. Crowcroft, *The personality of popular facebook users*, vol. 12. ACM CSCW, 2012.
- [105] R. Lambiotte, V. D. Blondel, C. D. Kerchove, E. Huens, C. Prieur, Z. Smoreda, and P. V. Dooren, “Geographical dispersal of mobile communication networks,” *Physica A*, vol. 387, no. 21, p. 17, 2008.

- [106] R. V. Solé and S. Valverde, *Information Theory of Complex Networks: On Evolution and Architectural Constraints*. Springer, Berlin, 2004.
- [107] G. Bianconi, A. Coolen, and C. J. P. Vicente, “Entropies of complex networks with hierarchical constraint topologies,” *Physical Review E*, vol. 78, p. 016114, 2008.
- [108] A. Annibale, A. C. C. Coolen, L. P. Fernandes, F. Fraternali, and J. Kleinjung, “Tailored graph ensembles as proxies or null models for real networks i: tools for quantifying structure,” *Journal of Physics A: Mathematical and Theoretical*, vol. 42, p. 485001, 2009.
- [109] E. S. Roberts, T. Schlitt, and A. C. C. Coolen, “Tailored graph ensembles as proxies or null models for real networks ii: results on directed graphs,” *Journal of Physics A: Mathematical and Theoretical*, vol. 44, no. 27, p. 5002, 2011.
- [110] S. Johnson, J. J. Torres, J. Marro, and M. A. Muñoz, “Entropic origin of disassortativity in complex networks,” *Physical Review Letters*, vol. 104, p. 108702, 2010.
- [111] A. E. Teschendorff and S. Severini, “Increased entropy of signal transduction in the cancer metastasis phenotype,” *BMC Systems Biology*, vol. 4, p. 104, 2010.
- [112] S. L. Braunstein, S. Ghosh, T. Mansour, S. Severini, and R. C. Wilson, “Some families of density matrices for which separability is easily tested,” *Physical Review A*, vol. 73, no. 012320, pp. 1–10, 2006.
- [113] S. Braunstein, S. Ghosh, and S. Severini, “A basic combinatorial approach to separability of mixed states,” *Annals of Combinatorics*, vol. 10, pp. 291–317, 2006.
- [114] S. Garnerone, P. Giorda, and P. Zanardi, “Bipartite quantum states and random complex networks,” *arxiv:1103.5989v1*, 2011.
- [115] J. Gomez-Gardenes and V. Latora, “Entropy rate of diffusion processes on complex networks,” *Physical Review E*, vol. 78, p. 065102, 2008.
- [116] R. Sinatra, J. Gómez-Gardeñes, R. Lambiotte, V. Nicosia, and V. Latora, “Maximal-entropy random walks in complex networks with limited information,” *Physical Review E*, vol. 83, no. 3, p. 030103, 2011.
- [117] Z. Burda, J. Duda, J. M. Luck, and B. Waclaw, “The various facets of random walk entropy,” *arXiv:1004.3667*, 2010.
- [118] M. E. J. Newman, “The structure of scientific collaboration networks,” *Proceedings of the National Academy of Sciences of USA*, vol. 98, pp. 404–409, 2001.
- [119] J. M. Kleinberg, “Navigation in a small world,” *Nature*, vol. 406, p. 845, 2000.

- [120] M. Muñoz, R. Juhász, C. Castellano, and G. ódor, “Griffiths phases on complex networks,” *Physical review letters*, vol. 105, p. 128701, 2010.
- [121] S. N. Dorogovtsev, *Lectures on complex networks*. Oxford University Press, 2010.
- [122] C. I. D. Genio, H. Kim, Z. Toroczkai, and K. E. Bassler, “Efficient and exact sampling of simple graphs with given arbitrary degree sequence,” *PloS one*, vol. 5, p. e10012, 2010.
- [123] C. I. Del Genio, T. Gross, and K. E. Bassler, “All scale-free networks are sparse,” *Physical Review Letters*, vol. 107, no. 17, p. 178701, 2011.
- [124] C. Godrèche, H. Grandclaude, and J. Luck, “Finite-time fluctuations in the degree statistics of growing networks,” *Journal of Statistical Physics*, vol. 137, p. 1117, 2009.
- [125] K. Zhao and G. Bianconi, “Percolation on interacting, antagonistic networks,” *arXiv preprint arXiv: 1210.7498*, 2012.
- [126] K. Zhao and G. Bianconi, “Percolation on interdependent networks with a fraction of antagonistic interactions,” *arXiv preprint arXiv:1304.3597*, 2013.
- [127] A. Halu, K. Zhao, A. Baronchelli, and G. Bianconi, “Connect and win: The role of social networks in political elections,” *Europhysics Letters*, vol. 102, p. 16002, 2013.
- [128] R. Cohen, K. Erez, D. Ben-Avraham, and S. Havlin, “Breakdown of the internet under intentional attack,” *Physical Review Letters*, vol. 86, no. 3682, 2001.
- [129] S. N. Dorogovtsev, A. V. Goltsev, and J. F. F. Mendes, “Ising model on networks with an arbitrary distribution of connections,” *Physical Review E*, vol. 66, p. 016104, 2002.
- [130] M. Leone, A. Vázquez, A. Vespignani, and R. Zecchina, “Ferromagnetic ordering in graphs with arbitrary degree distribution,” *The European Physical Journal B*, vol. 28, no. 2, pp. 191–197, 2002.
- [131] R. Pastor-Satorras and A. Vespignani, “Epidemic spreading in scale-free networks,” *Physical Review Letters*, vol. 86, p. 3200, 2001.
- [132] S. Eubank, H. Guclu, V. S. A. Kumar, M. V. Marathe, A. Srinivasan, Z. Toroczkai, and N. Wang, “Modelling disease outbreaks in realistic urban social networks,” *Nature*, vol. 429, p. 180, 2004.
- [133] A. E. Motter, C. Zhou, and J. Kurths, “Network synchronization, diffusion, and the paradox of heterogeneity,” *Physical Review E*, vol. 71, p. 016116, 2005.

- [134] T. Nishikawa, A. E. Motter, Y.-C. Lai, and F. C. Hoppensteadt, “Heterogeneity in oscillator networks: Are smaller worlds easier to synchronize?,” *Physical Review Letters*, vol. 91, p. 014101, 2003.
- [135] M. Barahona and L. M. Pecora, “Synchronization in small-world systems,” *Physical review letters*, vol. 89, p. 054101, 2002.
- [136] A. Arenas, A. Díaz-Guilera, J. Kurths, Y. Moreno, and C. Zhou, “Synchronization in complex networks,” *Physics Reports*, vol. 469, pp. 93–153, 2008.
- [137] Z. Toroczkai and K. E. Bassler, “Jamming is limited in scale-free systems,” *Nature*, vol. 428, p. 716, 2004.
- [138] P. Echenique, J. Gómez-Gardeñes, and Y. Moreno, “Dynamics of jamming transitions in complex networks,” *Europhysics Letters*, vol. 71, no. 2, p. 325, 2005.
- [139] D. De Martino, L. Dall’Asta, G. Bianconi, and M. Marsili, “Congestion phenomena on complex networks,” *Physical Review E*, vol. 79, no. 1, p. 015101, 2009.
- [140] G. Bianconi, “Superconductor-insulator transition on annealed complex networks,” *Physical Review E*, vol. 85, no. 6, p. 061113, 2012.
- [141] A. Halu, L. Ferretti, A. Vezzani, and G. Bianconi, “Phase diagram of the bose-hubbard model on complex networks,” *Europhysics Letters*, vol. 99, p. 18001, 2012.
- [142] G. Bianconi, “Enhancement of t_c in the superconductor–insulator phase transition on scale-free networks,” *Journal of Statistical Mechanics: Theory and Experiment*, vol. 2012, no. 07, p. P07021, 2012.
- [143] F. Radicchi and S. Fortunato, “Explosive percolation: A numerical analysis,” *Physical Review E*, vol. 81, no. 3, p. 036110, 2010.
- [144] R. A. da Costa, S. N. Dorogovtsev, A. V. Goltsev, and J. F. F. Mendes, “Explosive percolation transition is actually continuous,” *Physical Review Letters*, vol. 105, no. 25, p. 255701, 2010. PRL.
- [145] O. Riordan and L. Warnke, “Explosive percolation is continuous,” *Science*, vol. 333, no. 6040, pp. 322–324, 2011.
- [146] J. Gao, S. V. Buldyrev, S. Havlin, and H. E. Stanley, “Robustness of a network of networks,” *Physical Review Letters*, vol. 107, no. 19, p. 195701, 2011.
- [147] R. Parshani, S. V. Buldyrev, and S. Havlin, “Critical effect of dependency groups on the function of networks,” *Proceedings of the National Academy of Sciences of USA*, vol. 108, no. 3, pp. 107–1010, 2011.

-
- [148] G. J. Baxter, S. N. Dorogovtsev, A. V. Goltsev, and J. F. F. Mendes, “Avalanche collapse of interdependent network,” *arXiv:1207.0448*, 2012.
- [149] S. Gomez, A. Diaz-Guilera, J. Gomez-Gardeñes, C. J. Perez-Vicente, Y. Moreno, and A. Arenas, “Diffusion dynamics on multiplex networks,” *arXiv:1207.2788*, 2012.
- [150] E. Cozzo, A. Arenas, and Y. Moreno, “Stability of boolean multilevel networks,” *Physical Review E*, vol. 86, p. 036115, 2012.
- [151] A. Bashan, R. P. Bartsch, J. W. Kantelhardt, S. Havlin, and P. C. Ivanov, “Network physiology reveals relations between network topology and physiological function,” *Nat Commun*, vol. 3, p. 702, 2012. 10.1038/ncomms1705.
- [152] A. Baronchelli, M. Felici, V. Loreto, E. Caglioti, and L. Steels, “Sharp transition towards shared vocabularies in multi-agent systems,” *Journal of Statistical Mechanics: Theory and Experiment*, vol. 2006, no. 06, p. P06014, 2006.
- [153] A. Baronchelli, L. Dall’Asta, A. Barrat, and V. Loreto, “Nonequilibrium phase transition in negotiation dynamics,” *Physical Review E*, vol. 76, no. 5, p. 051102, 2007.
- [154] S. A. Marvel, H. Hong, A. Papush, and S. H. Strogatz, “Encouraging moderation: Clues from a simple model of ideological conflict,” *Physical Review Letters*, vol. 109, no. 11, p. 118702, 2012.
- [155] J. Xie, S. Sreenivasan, G. Korniss, W. Zhang, C. Lim, and B. Szymanski, “Social consensus through the influence of committed minorities,” *Physical Review E*, vol. 84, no. 1, p. 011130, 2011.
- [156] D. S. Hillygus, “The evolution of election polling in the united states,” *Public opinion quarterly*, vol. 75, no. 5, pp. 962–981, 2011.
- [157] D. Centola, “An experimental study of homophily in the adoption of health behavior,” *Science*, vol. 334, no. 6060, pp. 1269–1272, 2011.